

Distribution Agreement

In presenting this thesis or dissertation as a partial fulfillment of the requirements for an advanced degree from Emory University, I hereby grant to Emory University and its agents the non-exclusive license to archive, make accessible, and display my thesis or dissertation in whole or in part in all forms of media, now or hereafter known, including display on the world wide web. I understand that I may select some access restrictions as part of the online submission of this thesis or dissertation. I retain all ownership rights to the copyright of the thesis or dissertation. I also retain the right to use in future works (such as articles or books) all or part of this thesis or dissertation.

Signature:

Sarah Daniel

Date

**Cell Types in the Bed Nucleus of the Stria Terminalis: Effectors for Stress
Modulation of Anxiety**

By

Sarah E. Daniel
Doctor of Philosophy

Graduate Division of Biological and Biomedical Science
Neuroscience

Donald G. Rainnie
Advisor

Thomas Kash
Committee Member

Kerry Ressler
Committee Member

David Walker
Committee Member

Larry Young
Committee Member

Accepted:

Lisa A. Tedesco, Ph.D.
Dean of the James T. Laney School of Graduate Studies

Date

**Cell Types in the Bed Nucleus of the Stria Terminalis: Effectors for Stress
Modulation of Anxiety**

By

Sarah E. Daniel
B.A., Barnard College at Columbia University, 2009

Advisor: Donald G. Rainnie, PhD

An abstract of
A dissertation submitted to the Faculty of the
James T. Laney School of Graduate Studies of Emory University
in partial fulfillment of the requirements for the degree of
Doctor of Philosophy in the Graduate Division of Biological and Biomedical Science
Neuroscience
2016

Abstract

Cell Types in the Bed Nucleus of the Stria Terminalis: Effectors for Stress Modulation of Anxiety

By: Sarah E. Daniel

The anterolateral group of the bed nucleus of the stria terminalis (BNST_{ALG}) is a complex brain structure that plays a crucial role in regulating anxiety. It contains multiple sub-regions composed of neurons expressing a range of neuropeptides and receptors. The heterogeneous nature of the BNST_{ALG}, in which sub-regions such as the oval BNST (ovBNST) and anterodorsal BNST (adBNST) modulate anxiety in opposing ways, creates two opposing circuits. Understanding the intrinsic circuitry of the BNST_{ALG} and how this circuitry may be affected by stress will be key to understanding anxiety in both a normal and pathological state. Previous work has defined three distinct cell types in the BNST_{ALG}, namely Type I, Type II, and Type III cells, based on their electrophysiological response to hyperpolarizing and depolarizing current injections and mRNA expression profile. However, little is known about how these neurons contribute to the opposing pathways that facilitate and attenuate anxiety behavior. In this dissertation, we extend the characterization of the cell types in the BNST_{ALG} with the goal of learning how these groups of neurons act together to affect anxiety behavior.

First, we explore differences in electrophysiological cell types across species and regions in the BNST_{ALG}. Type I-III cells were first described in rats, but no study has examined the electrophysiological properties of the cells in the mouse or primate BNST_{ALG}. To this end, we compare the electrophysiological and morphological properties of BNST_{ALG} neurons in the mouse, rat, and rhesus macaque. The mouse and primate BNST_{ALG} contain cells that closely fit the description of Type I-III cells in the rat, however they are observed in significantly different proportions and do not all fit into these classification schemes. These data suggest there may be significant differences in the organization of the BNST_{ALG} across species, however future studies will need to examine these differences further. The BNST_{ALG} is composed of multiple regions, including the ovBNST and adBNST that have differential effects on anxiety. In the third chapter, we compare the cell types found in these two regions and show differential expression of cell types and electrophysiological properties between the ovBNST and adBNST.

Finally, the fourth chapter seeks to explore the effects of chronic shock stress on the cell types in the BNST_{ALG}. Although different cell types are thought to play opposing roles in the anxiety circuit, the effects of stress are often investigated with out an attempt to distinguish separate cell types. Here, we show multiple effects of stress on the electrophysiological and mRNA expression profile of cells in the BNST_{ALG}, however, no effect of stress was observed in all cell types. Specifically Type III cells represent a population of corticotropin releasing factor (CRF) neurons that are uniquely sensitive to chronic stress. These results support the study of individual cell types to gain a better understanding of the circuits within the BNST_{ALG}. We can then use the understanding of these circuits to explore better therapeutic interventions for pathological anxiety.

**Cell Types in the Bed Nucleus of the Stria Terminalis: Effectors for Stress
Modulation of Anxiety**

By

Sarah E. Daniel
B.A., Barnard College at Columbia University, 2009

Advisor: Donald G. Rainnie, PhD

A dissertation submitted to the Faculty of the
James T. Laney School of Graduate Studies of Emory University
in partial fulfillment of the requirements for the degree of
Doctor of Philosophy in the Graduate Division of Biological and Biomedical Science
Neuroscience
2016

Acknowledgements

First, I would like to thank the National Institute of Health for awarding me a Predoctoral Ruth L. Kirschstein National Research Service Award (NRSA; Fall 2012 – Summer 2015).

Second, there are many people, without whom this dissertation would not have been completed, and I would like to take a moment to acknowledge their encouragement and support:

To my many teachers; particularly, to my first mentor in neuroscience, Professor Bauer, who introduced me to the complexities of the BNST, to Professor Wallenfang, whose courses inspired me to think beyond the text book, and to the members of my thesis committee for their patience, guidance, and encouragement along the way; to the past and present members of the Rainnie lab, including Teresa Madsen, David Ehrlich, Steve Ryan, Tom Hennessey, Jeffrey Hsu, Brendan O’Flaherty, JiDong Guo, Rimi Hazra, Joanna Dabrowska, Chenchen Li, Aurélie Menigoz, and Shivani Seth, for teaching me that science is not done alone; to my friends, especially Sarah Burns and Karyn Heavenrich, who have endured listening to ramblings about the BNST far too often; to all of my friends at Veritas Church, who have given me endless support, love, and encouragement, without which graduate school would have been a much lonelier place; and to my family, especially my husband, Thomas, who never ceases to remind me of my intelligence even when I am in doubt, and my mom and dad, who have supported me every step of the way. And finally, to my advisor Tig Rainnie, a conversation with whom never fails to renew my excitement for science and who always inspires me to do my best.

Thank you.

Table of Contents

Chapter 1: Stress modulation of opposing circuits in the bed nucleus of the stria terminalis	1
Abstract	1
Introduction	2
Interaction of Stress with Neuromodulators	4
Corticotropin Releasing Factor	4
Norepinephrine.....	15
Dopamine	24
Serotonin	32
Stress Modulation of Synaptic Plasticity	44
Clinical Implications	52
Future Research Directions	54
Chapter 2: Comparison of neurons in the BNST_{ALG} in the mouse, rat, and rhesus macaque	57
Introduction	58
Methods	60
Animal Subjects	60
Preparation of BNST slices	61
General patch clamp recording procedures	62
Neuronal morphology	64
Statistical Analysis	65
Results	66
Comparison of this rat sample with previous published samples	66
Distribution of cell types in the mouse	69
Distribution of cell types in the rhesus macaque	71
Type I cells	74
Type II cells.....	75
Type III cells	77
Morphology and Input Resistance	78
Discussion	80
Chapter 3: Comparison of cell types in the oval and anterodorsal BNST	87
Introduction	88
Methods	89
Animal Subjects	89
Preparation of BNST slices	90
General patch clamp recording procedures	90
Neuronal morphology	93
Single cell RT-PCR.....	94
Test of Thy1-Cre mouse line.....	95
Statistical analysis	96
Results	97
Comparison of cell types in the oval and anterodorsal BNST in the rat	97
Characterization of a novel subpopulation of neurons in <i>Thy1</i> -YFP transgenic mice.....	101
Discussion	107

Chapter 4: Chronic stress differentially affects Type III neurons in the bed nucleus of the stria terminalis	121
Introduction	122
Methods	124
Animal Subjects	124
Chronic stress and behavioral testing	124
Electrophysiology	128
Single-cell quantitative PCR	134
Statistical Analysis	137
Results	138
Context fear and anxiety-like behavior	139
Effect of stress on other electrophysiological properties of BNST neurons	140
AMPA-to-NMDA ratio and AMPA rectification	144
Effect of stress on CP-AMPA receptors in Type III and non-Type III cells	145
Effect of stress on gene expression	147
Discussion	151
Effect of CSS on context fear and anxiety-like behavior	152
Effect of stress on electrophysiological properties and genetic expression in Type III cells	154
AMPA-to-NMDA ratio	160
AMPA Rectification and CP-AMPA receptors	161
Differences in expression of NMDA receptor subunits	164
Conclusion	166
Chapter 5: Conclusion and Future Directions	169
Literature Cited	181

List of Figures

Figure 1.1	2
Figure 1.2.....	13
Figure 2.1.....	61
Figure 2.2.....	68
Figure 2.3.....	70
Figure 2.4.....	72
Figure 2.5.....	74
Figure 2.6.....	80
Figure 3.1.....	97
Figure 3.2.....	98
Figure 3.3.....	100
Figure 3.4.....	102
Figure 3.5.....	103
Figure 3.6.....	105
Figure 3.7.....	106
Figure 3.8.....	109
Figure 4.1.....	139

Figure 4.2.....	141
Figure 4.3.....	143
Figure 4.4.....	145
Figure 4.5.....	146
Figure 4.6.....	147
Figure 4.7.....	149
Figure 4.8.....	151
Figure 4.9.....	162

List of Tables

Table 1.1.....	6
Table 1.2.....	15
Table 1.3.....	33
Table 1.4.....	42
Table 2.1.....	67
Table 3.1.....	99
Table 3.2.....	103
Table 3.3.....	104
Table 4.1.....	134

Supplementary Material

Supplementary Table 4.1.....	168
-------------------------------------	------------

Chapter 1: Stress modulation of opposing circuits in the bed nucleus of the stria terminalis

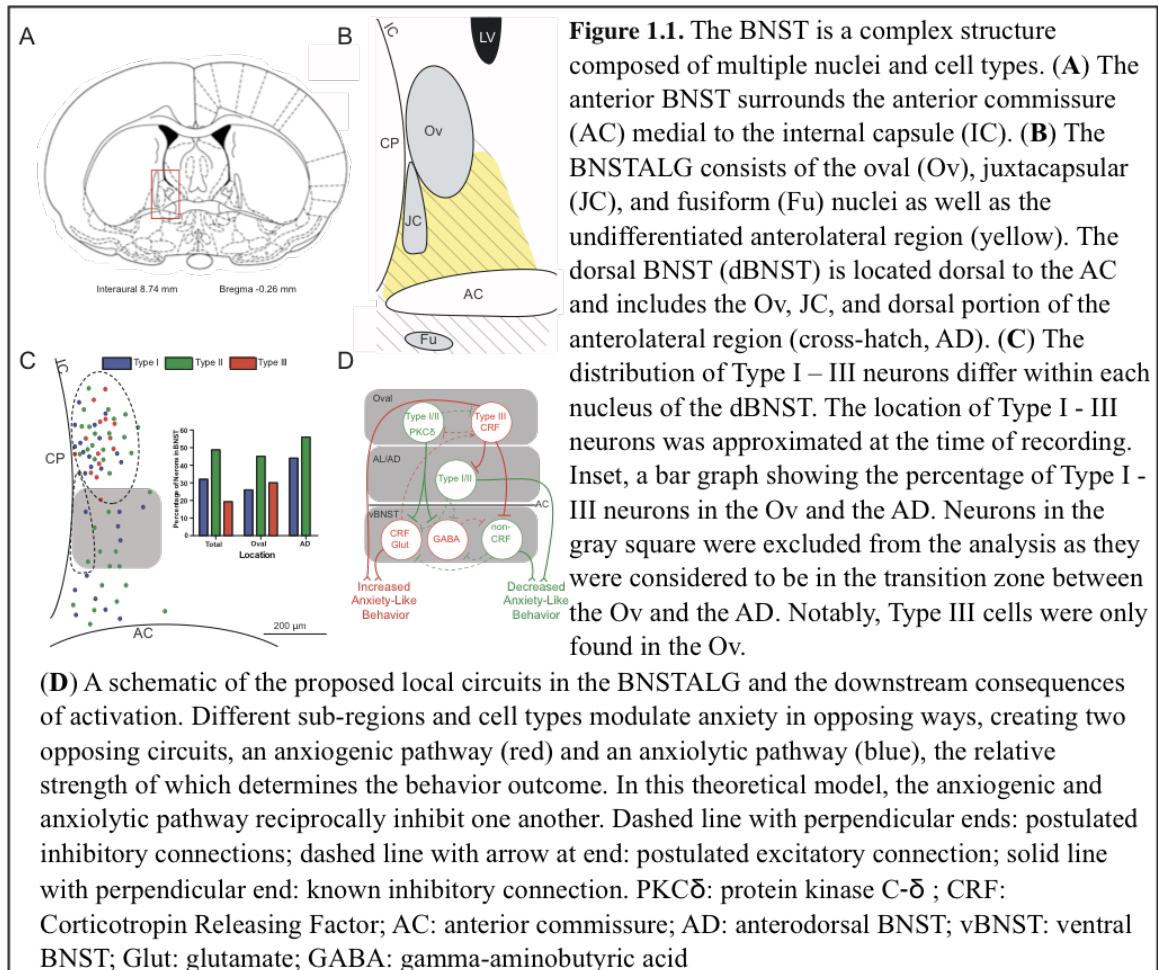
Content shown in Chapter 1 previously published as:

Daniel, S. E. & Rainnie, D. G. Stress Modulation of Opposing Circuits in the Bed Nucleus of the Stria Terminalis. *Neuropsychopharmacology* **41**, 103–125 (2015).

Abstract

The anterior bed nucleus of the stria terminalis (BNST) has been recognized as a critical structure in regulating trait anxiety, contextual fear memory, and appetitive behavior, and is known to be sensitive to stress manipulations. As one of the most complex structures in the central nervous system, the intrinsic circuitry of the BNST is largely unknown; however, recent technological developments have allowed researchers to begin to untangle the internal connections of the nucleus. This research has revealed the possibility of two opposing circuits, one anxiolytic and one anxiogenic, within the BNST, the relative strength of which determines the behavioral outcome. The balance of these pathways is critical in maintaining a normal physiological and behavioral state; however, stress and drugs of abuse can differentially affect the opposing circuitry within the nucleus to shift the balance to a pathological state. In this review, we will examine how stress interacts with the neuromodulators, corticotropin-releasing factor, norepinephrine, dopamine, and serotonin to affect the circuitry of the BNST as well as how synaptic plasticity in the BNST is modulated by stress, resulting in long-lasting changes in the circuit and behavioral state.

Introduction



A growing body of evidence suggests that the bed nucleus of the stria terminalis (BNST) plays a crucial role in regulating trait anxiety as well as contextual fear memory formation (Davis and Walker, 2014; Duvarci *et al*, 2009; Fox *et al*, 2010; Hott *et al*, 2012; Kalin *et al*, 2005; Oler *et al*, 2009; Sink *et al*, 2013; Somerville *et al*, 2010; Straube *et al*, 2007; Sullivan *et al*, 2004; Walker and Davis, 2008; Yassa *et al*, 2012; Zimmerman and Maren, 2011). However, the BNST can be subdivided into at least 16 unique sub-regions and has been reported to be one of the most complex structures in the entire central nervous

system (Bota *et al*, 2012; Dong and Swanson, 2004; Dong *et al*, 2001b; Ju *et al*, 1989; Larriva-Sahd, 2006). Indeed, recent evidence suggests that the BNST is involved in regulating appetitive as well as aversive behavior. Consequently, understanding the intrinsic circuitry of the BNST and how this circuitry may be affected by stress hormones and neurotransmitters will be key to understanding anxiety in both a normal and pathological state. The heterogeneous nature of the BNST, in which different sub-regions and cell types modulate anxiety in opposing ways, creates two opposing circuits, the relative strength of which determines the behavioral outcome. Stress can differentially affect the opposing circuitries within the BNST to shift the balance from an anxiolytic to an anxiogenic state.

In this review we will focus our attention on the anterior lateral group of the BNST (BNST_{ALG}) as it is densely connected with the hypothalamus, amygdala, midbrain, and lower brainstem regions associated with autonomic function, emotional processing, reward, and pain (Dong and Swanson, 2004; Dong *et al*, 2001b). The BNST_{ALG}, as defined by Dong and Swanson (2004), consists of the oval, juxtacapsular, fusiform, and rhomboid (not pictured) nuclei, as well as the undifferentiated region surrounding these nuclei termed the anterolateral area (BNST_{AL}; **Figure 1.1B**). Many studies also discuss the dorsal and ventral BNST (dBNST and vBNST) separately, defined as the regions dorsal and ventral to the anterior commissure. The BNST regions receive different afferents (for review see McDonald *et al*, 1999 and Dong *et al*, 2001a) and have distinct projections (Dong *et al*, 2001b; Dong *et al*, 2000). Additionally, there is a large amount of connectivity in and between the smaller BNST nuclei (Dong and Swanson, 2004; Turesson *et al*, 2013; Dong *et al*, 2000; Dong *et al*, 2001b). The vast majority of the neurons in the BNST use *gamma*-

aminobutyric acid (GABA) as the primary neurotransmitter, however there are also a small number of glutamatergic neurons primarily located in the vBNST (Csáki *et al*, 2000; Jalabert *et al*, 2009; Jennings *et al*, 2013b; Turesson *et al*, 2013). Finally, the neurons in the BNST also express a vast array of neuropeptides including corticotropin releasing factor (CRF), enkephalin (ENK), neuropeptide Y (NPY), neurotensin, and somatostatin (SOM) (Walter *et al*, 1991). In this review, we will explore how neuromodulators affect the circuitry of the BNST_{ALG} and interact with stress to provide dynamic control over the system. We will then discuss how stress modulates synaptic plasticity in the BNST_{ALG} resulting in long lasting changes in the circuit and behavioral state.

Interaction of Stress with Neuromodulators

Corticotropin Releasing Factor

Corticotropin releasing factor (CRF) is a stress hormone that both acts in the BNST_{ALG} to affect anxiety behavior and is produced by BNST_{ALG} neurons (Lee and Davis, 1997; Dabrowska *et al*, 2013a; Cummings *et al*, 1983). The BNST_{ALG} has been shown to be an important site of action for CRF's role in potentiating anxiety-like behavior and the stress response. CRF infused into the lateral cerebral ventricle increases startle, which could be blocked with either lesions of the lateral BNST or micro-infusion of a CRF antagonist into the BNST_{ALG} (Lee and Davis, 1997). Additionally, intra-BNST infusion of CRF increases anxiety-like behaviors in the elevated plus maze (Sahuque *et al*, 2006), increases retention in an inhibitory avoidance task (Liang *et al*, 2001), produces a conditioned-place aversion (Sahuque *et al*, 2006), and induces reinstatement of cocaine seeking (Erb and Stewart, 1999). The CRF-related peptides, urocortin 1, 2, and 3, may also contribute to CRF signaling in the BNST (Bale and Vale, 2004; Kormos and Gaszner,

2013; Koob, 2010). Not only does CRF act in the BNST_{ALG} to affect anxiety-like behaviors and responses to stress, but the BNST_{ALG} also contains CRF producing neurons that are responsive to stress (Cummings *et al*, 1983; Dabrowska *et al*, 2013a; Day *et al*, 1999; Ju *et al*, 1989). CRF mRNA in the BNST_{ALG} increases after exposure to corticosterone (Makino *et al*, 1994), acute foot-shock, and the alpha-2 adrenoreceptor antagonist, yohimbine, a pharmacological stressor (Funk *et al*, 2006). Hence, it is evident that CRF plays a crucial part in the role of the BNST_{ALG} in modulating stress and anxiety.

Importantly, CRF acts pre-synaptically to enhance glutamatergic transmission in the dorsal lateral BNST_{ALG}, effectively tuning the BNST_{ALG} to whichever inputs are carrying the CRFR1 receptor. Application of CRF onto the BNST_{ALG} *in vitro* increases the frequency of spontaneous excitatory post-synaptic currents (sEPSCs); an effect that is blocked by application of the selective CRF receptor 1 antagonist, NBI27914 (NBI) (Kash *et al*, 2008). Moreover, withdrawal from chronic intermittent ethanol (CIE) exposure, a potent stressor, has been shown to enhance glutamatergic tone onto BNST neurons that project to the Ventral Tegmental Area (VTA) (Silberman *et al*, 2013). Notably, the CIE effect was blocked with pre-treatment of NBI, indicating that with CIE withdrawal, CRF acts through a CRFR1-dependent mechanism *in vivo* to enhance glutamatergic input onto BNST_{ALG} neurons. Although it seems as though glutamatergic input is increased by CRF throughout the BNST_{ALG} (including regions both dorsal and ventral to the commissure), it is unknown which specific inputs are being modulated by CRF transmission and/or if all of the inputs are equally affected by stress. More targeted optogenetic manipulations may begin to address this issue. Interestingly, CRF has been reported to depolarize a subset of

neurons in the dBNST that are thought to be local interneurons, potentially counter-acting the increase in glutamatergic input into the system (Ide *et al*, 2013).

Although it is clear that CRF acts in the BNST_{ALG} to affect anxiety-like behavior, the origin of CRF is unknown, as the BNST_{ALG} contains both CRF-containing neurons and CRF fibers. The lateral division of the central nucleus of the amygdala (CeA_L) also produces CRF (Day *et al*, 1999) and contributes to the CRF-immunoreactive fibers found in the dBNST (Sakanaka *et al*, 1986). It has been proposed that it is CRF from the CeA_L that acts in the BNST to produce the BNST-dependent effects of CRF (Walker *et al*, 2009). Indeed, there is evidence for a serial flow of activation from the CeA to the BNST; morphine withdrawal induces c-fos expression in the BNST and CeA, and lesions of the CeA reduce c-fos expression in the BNST whereas lesions of the BNST have no effect on c-Fos expression in the CeA (Nakagawa *et al*, 2005). In a study using a cross-lesion design to examine the CRF-containing pathway from the CeA to the BNST in stress-induced reinstatement of cocaine seeking, tetrodotoxin infused into the CeA of one hemisphere and CRF antagonist infused into the BNST of the opposite hemisphere reduced stress-induced reinstatement compared to the unilateral manipulation, indicating that CRF's actions in the BNST are, at least in part, dependent on CeA activity (Erb *et al*, 2001). Similarly, a

	Footshock	Slow-release CORT (60 days)	High CORT (14 days)	Yohimbine	Footshock +Heroin Withdrawal	Chronic Mild Stress	Social Defeat	Hyper-tonic Saline
Dorsal BNST	+	+++	+	+	+	+	n.c.	-
Ventral BNST	+	+	n.c.	n.c.	n.c.	n.c.	+	+

Table 1.1. A summary of the studies showing the effect of a variety of stressors on CRF mRNA in the dorsal and ventral BNST (Funk *et al*, 2006; Makino *et al*, 1994; Shalev *et al*, 2001; Watts *et al*, 1995; Kim *et al*, 2006). Physical and pharmacological stressors increase CRF mRNA in the BNST (+), however this change is not always equal across the dorsal and ventral BNST. Some stressors that increase CRF mRNA in one region (+) have no effect on the level of CRF mRNA in the other (no change; n.c.) or display a greater increase in CRF mRNA (++).

unilateral lesion of the amygdala and CRF antagonist infused into the contralateral BNST reduced, but did not block, social defeat in Syrian hamsters (Jasnow *et al*, 2004). Importantly, in both studies, the bilateral manipulation did not block reinstatement completely, suggesting that although the CeA is one source of CRF in the BNST_{ALG}, it is not the only source.

Recently, evidence is growing for a role in local CRF release affecting the excitability of the BNST_{ALG}. Hence, dopamine release in the BNST has been reported to enhance excitatory transmission through an indirect action at CRFR1 receptors (Kash *et al*, 2008). Although it is possible that dopamine acts on CRF terminals from the CeA to increase CRF release in the BNST, there is also likely a direct action of dopamine on CRF neurons. A subpopulation of BNST_{ALG} neurons are significantly depolarized in response to dopamine application (Kash *et al*, 2008). Significantly, preliminary single cell RT-PCR data from our lab shows that mRNA for the D1-receptor is expressed exclusively in CRF cells dorsal to the commissure. Together, these data indicate that dopamine may be acting on CRF neurons in the oval nucleus of the BNST to increase local CRF release, thereby enhancing excitatory transmission. Additionally, the beta-adrenergic receptor agonist, isoproterenol enhances excitatory transmission in the BNST through a CRFR-1 dependent mechanism (Nobis *et al*, 2011). In fact, using a CRF-tomato mouse line to visualize CRF cells, *in vitro* patch-clamp recordings showed both dopamine and isoproterenol depolarize CRF neurons in the BNST (Silberman *et al*, 2013). This physiological evidence along with the cross-lesion studies described above indicate that both CRF from the CeA_L and the BNST act in the BNST to affect anxiety behavior and the response to stress. Future studies

should begin to determine if CRF from the CeA_L and the BNST work together, or if they are differentially activated by specific stressors.

There are at least two distinct populations of CRF neurons in the BNST_{ALG}: those found in the oval nucleus dorsal to the anterior commissure, and those found in the fusiform nucleus ventral to the commissure (Cummings *et al*, 1983; Ju *et al*, 1989). Intriguingly stress can cause an increase in the expression of CRF mRNA in these nuclei, however, not every stressor causes a change in mRNA expression in both populations of CRF neurons, implying that they are functionally distinct cell populations. Dorsal and ventral CRF mRNA both increase after an intermittent foot-shock stressor, but are differentially affected by social defeat and yohimbine, with social defeat only increasing CRF mRNA in the vBNST and yohimbine only increasing that of the dBNST (Funk *et al*, 2006). CRF mRNA in the dBNST but not vBNST increased after chronic mild stress (Kim *et al*, 2006). Similarly, high levels of subcutaneous corticosterone over 14 days resulted in increased levels of CRF mRNA in the dorsal but not ventral BNST (Makino *et al*, 1994). In another study, no change in CRF mRNA was observed after foot-shock alone, but an increase in CRF mRNA in the dBNST but not vBNST was observed after foot-shock in animals that have been extinguished from self-administration of heroin (Shalev *et al*, 2001). Finally, following hyper-tonic saline injection, the amount of CRF mRNA in the oval nucleus decreased whereas it increased in the fusiform nucleus of the BNST (Watts *et al*, 1995) (see **Table 1.1** for summary of these results). Beyond differences in responding to stress, the CRF neurons of the oval and fusiform nuclei may be distinct on a more fundamental level. The CRF neurons in the oval nucleus are known to be GABAergic, unlike the CRF neurons of the PVN that co-express glutamate (Dabrowska *et al*, 2013a). However, it is

still unknown if the CRF neurons in the fusiform nucleus are glutamatergic or GABAergic. In fact, there has been significant confusion in the literature on this topic (Choi *et al*, 2007; Radley *et al*, 2009). Nevertheless, these data suggest that the CRF neurons of the oval and fusiform nucleus are distinct cell populations that differentially respond to stress.

At least three different types of neurons in the dorsal BNST_{ALG} of the rat have been recognized based on their spiking and rectification properties and rebound depolarization in response to hyperpolarizing and depolarizing current injection: Type I (Regular Spiking), Type II (Low-threshold Bursting), and Type III (Fast Inward Rectifiers) (Hammack *et al*, 2007; Rodríguez-Sierra *et al*, 2013). The electrophysiological profile of neurons in the BNST_{ALG} may be indicative of what proteins are being expressed by that cell, including CRF. In addition to the different electrophysiological properties of these neurons, single cell RT-PCR revealed that the different cell types expressed the mRNA for distinct complements of ion channels (Hazra *et al*, 2011) and serotonin receptors (Hazra *et al*, 2012). Importantly, nearly all of the Type III cells express the mRNA for CRF (Dabrowska *et al*, 2013a). In a transgenic mouse line in which GFP is exclusively expressed in CRF-containing neurons (Martin *et al*, 2010), we have preliminary data showing that the GFP cells in the BNST share many of the same electrophysiological characteristics as Type III neurons in the rat. Another transgenic mouse line, a CRF-*tomato* reporter line, has also been used to record from CRF neurons in the BNST (Silberman *et al*, 2013). In this mouse, the CRF neurons in the BNST were not of a consistent electrophysiological profile, but rather, based on the voltage responses to hyperpolarizing and depolarizing current injections, there were some CRF neurons that fit into each cell type classification as well as some that did not fit into any of the predefined cell types. This

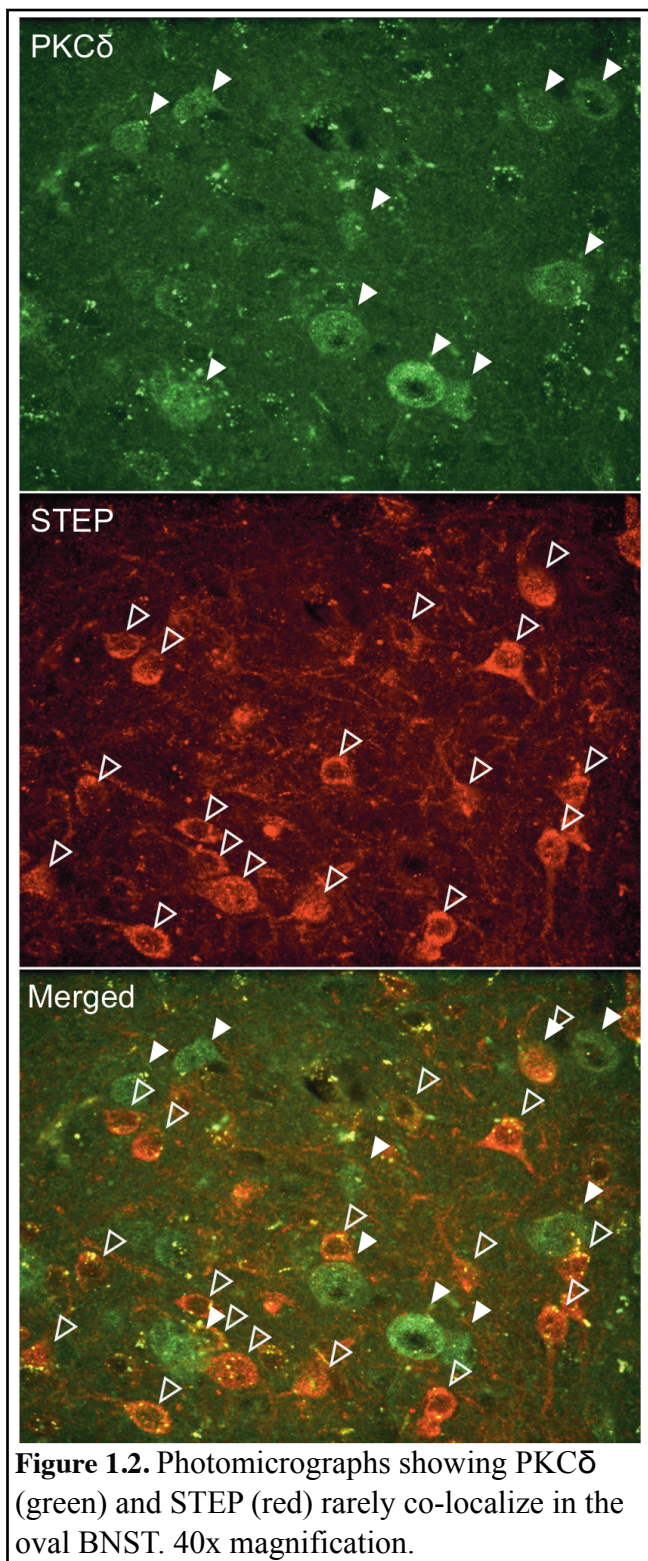
inconsistency brings up multiple questions regarding the use of cell type classification and transgenic reporter mice. First, the cell types that were defined in the rat BNST have not been confirmed to exist in the mouse. We have observed all three cell types in the mouse, but in a different proportion from what is seen in the rat BNST, as well as some cells that do not fit into the any of the predefined cell types (unpublished observation). Therefore, we must use caution when we apply concepts shown in one species to another. Additionally, it is possible that a CRF transgenic reporter line could inadvertently label more neurons than ones that express functional levels of the CRF peptide. Many cells express low (or even high levels) of an mRNA transcript without functionally expressing the corresponding protein (Tropea *et al*, 2001), however the hypothalamic field has relied on measuring CRF mRNA as a proxy for CRF peptide and found these measures to be reliable (Imaki *et al*, 1991; Swanson and Simmons, 1989). In a reporter line, the fluorescent protein is created regardless of whether, or not, the CRF mRNA is translated into functional protein. Hence, the apparent disparity in the electrophysiological phenotype of CRF neurons may be attributed to ectopic expression in the reporter line used by Silberman *et al* (2013). Indeed the expression of the *tomato* fluorescence seems to extend beyond the oval nucleus where immunohistochemical studies have localized CRF cells (Silberman *et al*, 2013; Sawchenko and Swanson, 1985; Swanson *et al*, 1983). However, immunohistochemistry is not without its faults and may be underrepresenting CRF protein expression in the BNST. In this case the GFP reporter line may not label all CRF neurons in the BNST. Regardless, in the rat 95% of Type III cells express the mRNA for CRF (Dabrowska *et al*, 2013a). Furthermore, Type III neurons are only found in the region of the oval nucleus of the rat BNST, where CRF neurons are located, and not in the

undifferentiated anterolateral region (**Figure 1.1C**, unpublished observation, details in chapter 3). Together these data indicate that Type III neurons in the dBNST express CRF.

CRF neurons in the dBNST also express distinct receptors and proteins. For example, in the oval nucleus striatal-enriched protein tyrosine phosphatase (STEP; also called Ptpn5)-immunoreactivity has almost total colocalization with CRF-immunoreactivity, and all Type III neurons express the mRNA for STEP (Dabrowska *et al*, 2013b). STEP is known to regulate long term potentiation in the amygdala (Paul *et al*, 2007; Yang *et al*, 2012) and its role in synaptic plasticity in CRF neurons in the BNST will be discussed later on in this review. Preliminary evidence from our lab suggests the D1 subtype of the dopamine receptor is also specifically expressed in Type III CRF cells in the BNST. This is supported by the finding that dopamine directly depolarizes CRF neurons in the dBNST, presumably by acting through the G_s-coupled D1 receptor (Silberman *et al*, 2013). Determining more biochemical/molecular ways in which CRF neurons in the BNST are distinct from other cell types has the potential to lead to the discovery of drugable targets that could isolate these neurons and modulate a crucial component of anxiety behavior.

Although studies have shown that CRF neurons in the BNST are responsive to stress manipulations as mentioned above, new technologies that allow us to target specific groups of cells are going to be critical in determining the role of BNST CRF neurons in anxiety behavior. A recent study has shown that distinct sub-regions of the BNST can have opposing actions in modulating anxiety (Kim *et al*, 2013). In this study, the oval nucleus was targeted with the injection of a Cre-dependent enhanced form of the halorhodopsin (eNpHR3.0) virus into the BNST of mice that express Cre in cells that express the D1

receptor (*Drd1a::cre*). Unsurprisingly, since CRF neurons express the D1 receptor and are localized in the oval nucleus, this mouse line shows eNpHR3.0 expression restricted to the oval nucleus of the BNST. Optogenetically inhibiting the oval CRF neurons in the BNST resulted in a decrease in anxiety-like behavior in the elevated-plus maze and open-field test as well as a decrease in respiratory rate, consistent with an anxiogenic role for the oval CRF neurons (Kim *et al*, 2013). These CRF neurons were also shown to send an inhibitory projection to the undifferentiated anterodorsal (AD) region of the BNST. Conversely, optogenetically inhibiting the AD region of the BNST resulted in an increase in anxiety-like behavior and respiratory rate, suggesting an anxiolytic role of this region. These data indicate that the oval CRF neurons could directly promote anxiety by release of CRF and indirectly by inhibiting the anxiolytic projection from the AD region of the BNST. In fact, in another study chemogenetically inhibiting CRF neurons using the designer receptor exclusively activated by designer drugs (DREADD) system caused a reduction in anxiety-like behavior (Pleil *et al*, 2015). CRF neurons in the BNST are thought to make both local connections as well as project out of the nucleus to regions involved in emotion processing including the periventricular nucleus of the hypothalamus (PVN), ventral tegmental area (VTA), periaqueductal gray (PAG), dorsal portion of the dorsal raphe (DRD) and locus coeruleus (LC) (Dabrowska *et al*, 2011; Dabrowska & Rainnie, 2014; Meloni *et al*, 2006; Rodaros *et al*, 2007; Silberman *et al*, 2013; Van Bockstaele *et al*, 1999). These projections could contribute to the anxiogenic role of the BNST CRF neurons and/or activate a



compensatory mechanism, such as a negative feedback loop, to put a brake on the anxiety response. Isolating the projections, inputs, and function of the different CRF cell populations in the BNST and how they are affected by stress will be an important step to understanding the circuit.

The oval CRF neurons that project out of the oval nucleus to promote anxiety-like behavior are sitting within a predominantly GABAergic nucleus, suggesting that local interneurons could provide an inhibitory control over the output of the CRF neurons. A microcircuitry for modulation of CRF neurons by local GABA neurons has recently been described in the CeA_L (Haubensak *et al*, 2010; Sakanaka *et al*, 1986). The CRF neurons in the

CeA_L are a distinct population from neurons expressing the neuronal marker, PKC- δ

(Haubensak *et al*, 2010). These PKC- δ^+ neurons form local and reciprocal inhibitory connections with the PKC- δ^- cells in the CeA_L (Haubensak *et al*, 2010). Additionally, electrically inhibiting the PKC- δ^+ cells was shown to enhance fear. Similarly, PKC- δ is also expressed in the oval nucleus of the BNST, and a PKC- δ antibody labels a population of cells largely separate from those labeled by the STEP antibody (**Figure 1.2**). As STEP has been shown to co-localize with CRF cells in the BNST (Dabrowska *et al*, 2013b), we can infer that PKC- δ neurons in the BNST are a separate population of neurons from the CRF neurons in the oval nucleus. In fact, our recent single cell RT-PCR data showed that only Type II cells in the BNST expressed the mRNA for PKC- δ (unpublished observation). As the BNST is in many ways an extension of the central amygdala (Alheid and Heimer, 1988), it is reasonable to hypothesize the local circuitry in the BNST may mirror that of the CeA, with PKC- δ^+ and CRF neurons reciprocally inhibiting one another. Whereas PKC- δ^+ neurons in the CeA_L represent “fear off” neurons (Haubensak *et al*, 2010), perhaps Type II PKC- δ^+ cells represent “anxiety off” neurons in the BNST (**Figure 1.1D**). In addition to inhibition via local GABAergic connections, CRF action and CRF neurons themselves are opposed by NPY (Ide *et al*, 2013; Kash and Winder, 2006; Pleil *et al*, 2015). In fact, NPY in the BNST has been shown to block CRF-induced- place aversion (Ide *et al*, 2013). More studies on peptides and the local circuitry involved in the regulation of CRF neuron activity are needed to better understand how the BNST modulates anxiety.

Norepinephrine

Receptor	Behavioral Role	Physiological Action
β -AR	<ul style="list-style-type: none"> Stress-induced reinstatement of drug seeking (Leri <i>et al</i>, 2002). Symptoms of opiate withdrawal including withdrawal-induced place aversion (Aston-Jones <i>et al</i>, 1999). Anxiety-like behavior after an acute stressor (Cecchi <i>et al</i>, 2002). 	<ul style="list-style-type: none"> G_s-coupled receptors. Depolarize CRF neurons in dBNST (Silberman <i>et al</i>, 2013). Facilitation of GABA transmission in vBNST in acute withdrawal (Dumont and Williams, 2004).
β_1 -AR	<ul style="list-style-type: none"> Expression of context fear (Hott <i>et al</i>, 2012). Symptoms of opiate withdrawal (Cecchi <i>et al</i>, 2007). 	<ul style="list-style-type: none"> Enhance glutamatergic transmission through CRFR1 (Nobis <i>et al</i>, 2011).
β_2 -AR	<ul style="list-style-type: none"> Stress-induced reinstatement of drug seeking (Mantsch <i>et al</i>, 2014). 	<ul style="list-style-type: none"> Increase excitatory transmission in dBNST (Egli <i>et al</i>, 2004).
α_1 -AR	<ul style="list-style-type: none"> Expression of context fear (Hott <i>et al</i>, 2012). Anxiety-like behavior and HPA axis activation after an acute stressor (Cecchi <i>et al</i>, 2002). 	<ul style="list-style-type: none"> G_q-coupled receptor. Depolarize subpopulation of BNST cells; increase GABAergic transmission in vBNST (Dumont and Williams, 2004) LTD in dBNST and vBNST (McElligott <i>et al</i>, 2007; McElligott <i>et al</i>, 2010). Increase NE release (Forray <i>et al</i>, 1999; Park <i>et al</i>, 2009)
α_2 -AR	<ul style="list-style-type: none"> Blocks stress-induced reinstatement of drug seeking, expression of fear, and other NE actions (Fendt <i>et al</i>, 2005; Shaham <i>et al</i>, 2000). 	<ul style="list-style-type: none"> G_i-coupled receptor. Presynaptic autoreceptor; inhibits NE release (Forray <i>et al</i>, 1999; Park <i>et al</i>, 2009).

Table 1.2. A summary of the behavioral role and physiological actions of the different adrenergic receptor subtypes in the BNST.

The BNST receives dense noradrenergic input from the ventral noradrenergic bundle (VNB) and lighter input from the dorsal noradrenergic bundle (DNB) (Park *et al*, 2009). The NE terminals are densest in the vBNST (Egli *et al*, 2004; Phelix *et al*, 1994) however NE also acts in the dBNST to affect synaptic transmission and behavior (Hott *et al*, 2012; Leri *et al*, 2002a; McElligott *et al*, 2010; Nobis *et al*, 2011; Silberman *et al*, 2013). The A1 cell group in the caudal ventrolateral medulla contributes to the VNB and is the strongest source of NE in the vBNST (Banihashemi and Rinaman, 2006; Forray *et al*, 2000; Park *et al*, 2009; Shin *et al*, 2008). The nucleus of the solitary tract (A2 cell group) also provides

a strong NE input through the VNB (Banhashemi and Rinaman, 2006; Forray *et al*, 2000). Finally, there is a potential small NE input from the LC through the DNB, however, the support for this connection is weak and unlike the inputs from the VNB, inputs from the LC are not involved in stress-induced reinstatement of drug-seeking (Aston-Jones *et al*, 1999; Forray *et al*, 2000; Park *et al*, 2009; Shaham *et al*, 2000).

Norepinephrine has both a tonic and phasic control over the BNST_{ALG}. There is a rise in NE release in the vBNST as a result of aversive stimuli including immobilization stress, being exposed to a context that was previously associated with a foot-shock, tail pinch, and an aversive tastant (Cecchi *et al*, 2002; Onaka and Yagi, 1998; Park *et al*, 2012; 2015). NE is also released into the BNST when a rewarding stimulus is not received when expected (Park *et al*, 2013). Additionally, there is evidence that NE is released into the BNST in basal conditions to modulate glutamatergic transmission (Forray *et al*, 1999). Together these data suggest that NE in the BNST tonically modulates input into the BNST and participates in the response to aversive stimuli, including the lack of an anticipated reward.

NE acts in the BNST to promote fear and anxiety-like behavior as well as stress-induced reinstatement of drug-seeking and symptoms of opiate withdrawal (Cecchi *et al*, 2002; 2007; Fendt *et al*, 2005; Hott *et al*, 2012; Leri *et al*, 2002b; Mantsch *et al*, 2014; Vranjkovic *et al*, 2012). Rodents are innately afraid of the odor of predators, such as the fox. Exposure to a component of fox odor, trimethylthiazoline (TMT) increases cFos expression in the oval BNST, LC, and nucleus of the solitary tract (NTS), indicating that both norepinephrine and the BNST are involved in the fear response (Day *et al*, 2004). Indeed, NE release increases in the vBNST during TMT exposure (Fendt *et al*, 2005).

Clonidine, an α_2 -AR agonist, acts on the presynaptic α_2 -AR autoreceptors to inhibit NE release into the vBNST, thereby blocking the rise in NE caused by exposure to TMT. This treatment also blocks the fear-behavior induced by TMT exposure, indicating that NE transmission in the vBNST is critical for the fear behavior (Fendt *et al*, 2005).

NE can act on four subtypes of adrenoceptors in the BNST: β_1 -AR, β_2 -AR, α_1 -AR, or α_2 -AR. Specific agonists and antagonists to these receptors have helped to elucidate the unique role of each receptor variant in the BNST. The behavioral and physiological mechanism of NE action in the BNST is summarized in **Table 1.2**. As mentioned previously, the α_2 -AR primarily acts as a presynaptic autoreceptor to inhibit the release of NE into the BNST (Forsay *et al*, 1999; Park *et al*, 2009), and is therefore able to block fear behavior towards TMT (Fendt *et al*, 2005) as well as reduce stress-induced reinstatement of drug seeking (Shaham *et al*, 2000). The other three adrenoceptors are believed to act primarily through a post-synaptic mechanism in the BNST.

The β -adrenergic receptors are involved in both anxiety-like behavior and drug withdrawal. A cocktail of β_1 -AR and β_2 -AR antagonists (betaxol+ICI118,551) in the BNST blocks anxiety-like behavior after an acute immobilization stress (Cecchi *et al*, 2002). Similarly, a non-selective β -AR antagonist, phentolamine in the BNST reduced freezing in a context previously paired with shock (Hott *et al*, 2012). A selective β_1 -AR antagonist (CGP20712), but not β_2 -AR antagonist (ICI118,551) replicated this reduction in anxiety-like behavior. From these data we can conclude that β -adrenergic signaling, primarily β_1 -adrenergic signaling in the BNST promotes anxiety-like behavior. The β adrenergic receptors are also involved in stress-induced drug reinstatement and opiate withdrawal. Hence, β -AR blockade in the BNST dose-dependently attenuates footshock-induced

reinstatement of cocaine seeking but not cocaine-induced reinstatement of cocaine seeking (Leri *et al*, 2002b), and a β_2 -AR antagonist in the BNST by itself was enough to attenuate reinstatement (Mantsch *et al*, 2014). Another study using swim stress to induce reinstatement of cocaine-seeking found there to be a cooperative role of both the β_1 -AR and β_2 -AR in reinstatement (Vranjkovic *et al*, 2012). Together this suggests that both β -ARs in the BNST facilitate stress-induced reinstatement. The β -ARs also play a role in symptoms of opiate withdrawal. Blocking both β_1 -AR and β_2 -ARs abolishes withdrawal-induced place aversion (Aston-Jones *et al*, 1999). A selective β_1 -AR antagonist in the dBNST blocks withdrawal-induced aversion and attenuates opiate-withdrawal symptoms in rats with high reactivity to novelty (Cecchi *et al*, 2007). Overall β -ARs act in the BNST to contribute to opiate-withdrawal symptoms and promote anxiety-like behavior and stress-induced reinstatement of drug-seeking.

Like the β -ARs, the α_1 -AR also promotes anxiety-like behavior. A selective α_1 -AR antagonist (WB4101), but not α_2 -AR antagonist (RX821002) in the BNST reduced freezing in a context previously paired with foot-shock (Hott *et al*, 2012). Additionally, the selective α_1 -AR antagonist, benoxathian, blocked anxiety-like behavior and reduced the plasma levels of adrenocorticotropin hormone (ACTH) after an acute stressor (Cecchi *et al*, 2002). Intriguingly, this suggests that while both the β -ARs and α_1 -AR promote anxiety-like behavior, only the α_1 -AR facilitates activation of the hypothalamic-pituitary-adrenal (HPA) axis. Furthermore, the α_1 -ARs are not involved in stress-induced drug reinstatement (Vranjkovic *et al*, 2012). The similar yet distinct roles of the α - and β -adrenergic receptors in the BNST suggest that these receptors work through distinct mechanisms activating both separate and overlapping pathways in the BNST.

Both β -ARs are metabotropic receptors generally linked to the G_s -protein and act to facilitate synaptic transmission in the BNST. Although the majority of the noradrenergic afferents are found in the vBNST, the β -ARs primarily act in the dBNST, however the lack of effect seen in the vBNST could be due to desensitization of receptors in this region (Egli *et al*, 2004). In fact, activation of β -ARs in the vBNST has been shown to mediate the negative affective component of pain in rats (Deyama *et al*, 2008). Regardless, there is no direct physiological evidence of the action of β -ARs in the vBNST at this time. In the dBNST, the nonspecific β -AR agonist, isoproterenol increases the frequency of spontaneous EPSCs (Nobis *et al*, 2011; Silberman *et al*, 2013). This effect can be blocked by application of a β_1 -AR, but not β_2 -AR, specific antagonist, suggesting that the facilitation of glutamatergic transmission occurs through the β_1 -AR (Nobis *et al*, 2011). As mentioned previously, this enhancement of excitatory transmission in the BNST acts through a CRFR-1 dependent mechanism (Nobis *et al*, 2011). Isoproterenol directly depolarizes CRF neurons in the dBNST (Silberman *et al*, 2013), potentially increasing local CRF-release that would then act on presynaptic CRFR-1 receptors to facilitate glutamatergic transmission. However, it is unknown if the β -AR is also increasing CRF release in the BNST by acting on CRF-terminals originating in the CeA. It is possible NE is increasing CRF release into the BNST by acting on CRF neurons in both the dBNST and CeA. In fact, while β -AR blockade in the BNST dose-dependently attenuates footshock-induced reinstatement of drug-seeking, β -AR blockade in the CeA completely blocks reinstatement (Leri *et al*, 2002a). Furthermore, there is evidence for a role in the CRF-projection from the CeA to the BNST in stress-induced reinstatement (Erb *et al*, 2001). If CRF from the CeA is necessary for stress-induced reinstatement, and if NE acts in the CeA

to enhance CRF release, then this could explain how β -AR blockade in the CeA completely blocks stress-induced reinstatement. In this model, β -ARs on CRF neurons in both the CeA and BNST would facilitate CRF release in the BNST, but only the CeA projection is necessary to produce stress-induced reinstatement. In contrast, local CRF release from the BNST acts to modulate the magnitude of the increase in glutamatergic transmission. Regardless of the source of the CRF input in the BNST, these studies indicate that NE interacts with CRF to increase the glutamatergic transmission in the BNST, in effect, amplifying the salient inputs into the BNST during times of stress.

In contrast, another study showed a similar effect of isoproterenol in the dBNST; the non-selective β -AR agonist enhanced excitatory transmission, however this was only blocked by the β_2 -AR specific antagonist, ICI-118,551, suggesting a β_2 -AR-dependent mechanism (Egli *et al*, 2004). It is possible that this study was actually looking at a different form of modulation of glutamatergic transmission in the dBNST that is β_2 -AR-dependent. In fact, there are important differences in the effects seen in this study and the studies done by Nobis *et al*. Egli *et al* showed no significant change in the paired-pulse ratio after isoproterenol, indicating this effect is not presynaptic (Egli *et al*, 2004). In contrast, Nobis *et al* did show a significant change in the paired-pulse ratio indicating an increase in presynaptic glutamate release (Nobis *et al*, 2011). It is possible the β_2 -AR-dependent enhancement of excitatory transmission in the dBNST is a different mechanism than the β_1 -AR and CRFR1-dependent enhancement.

Whereas β -ARs act primarily in the dBNST to facilitate excitatory transmission, activation of the α_2 -AR subtype attenuates excitatory transmission in both the dBNST and vBNST (Egli *et al*, 2004). In the vBNST, application of NE only decreases excitatory

transmission. In the dBNST however, there are two competing effects of NE: the facilitation of glutamatergic transmission through β -ARs and the inhibition of glutamatergic transmission through the α_2 -AR. In field-recordings in the dBNST, NE application resulted in a facilitation of glutamatergic transmission 62.2% of the time, however in 37.8% of the recordings, NE resulted in a long-lasting decrease of glutamatergic transmission (Egli *et al*, 2004). Because this data is from extra-cellular recordings, it is unclear if these competing processes are occurring in individual or separate cells. Interestingly, glutamatergic input from the parabrachial nucleus to the dBNST is sensitive to the α_2 -AR agonist, guanfacine, whereas glutamatergic input from the basolateral amygdala (BLA) is not, suggesting specificity in noradrenergic modulation of inputs into the BNST (Flavin *et al*, 2014). The modulation of the β and α_2 -AR pathways could tip the scale in either direction. For example, administration of α_2 -AR agonists blocks footshock-induced reinstatement of heroin seeking (Erb *et al*, 2000). In that vein, facilitation of the α_2 -AR pathway could suppress the NE-induced increase in glutamatergic transmission in the dBNST, thereby decreasing some of the behavioral actions of NE.

In addition to modulating glutamatergic transmission in the BNST, NE has also been shown to enhance GABAergic transmission in the vBNST. Neurons in the vBNST that project to the VTA, labeled with fluorescent microspheres that were injected into the VTA and retrogradely transported to the vBNST, only exhibit a small hyperpolarization in response to NE application, whereas unlabeled vBNST neurons exhibit a large depolarizing response (Dumont and Williams, 2004). However, VTA-projecting neurons show an increase in frequency of spontaneous GABA_A-IPSCs with application of NE, raising the possibility that the non-VTA-projecting neurons in the vBNST send a GABAergic-

projection to the VTA-projecting vBNST neurons. This increase in frequency of IPSCs is blocked by the α_1 -AR antagonist, prazosin, indicating it is an α_1 -AR-dependent effect. The same increase in GABA_A-IPSCs occurs in rats after withdrawal from a 5-day treatment with morphine, however this effect is attenuated by the non-selective β -AR antagonist, propranolol as well as prazosin (Dumont and Williams, 2004). Additionally, the protein kinase A (PKA)-inhibitor, H89 also attenuates this effect only in animals treated with morphine. Chronic morphine treatment can result in a hyperactive adenylyl cyclase (AC)-PKA pathway, and β -AR G_s-signaling cascade results in activation of this pathway. These data suggest that during morphine withdrawal, β -ARs are recruited into facilitating GABAergic transmission onto VTA –projecting vBNST neurons through an over-active AC-PKA pathway (Dumont and Williams, 2004). This increased inhibitory drive could come from the local GABA neurons in the vBNST and/or GABAergic neurons in the dBNST. A non-specific β -AR agonist is known to depolarize the GABAergic CRF neurons in the dBNST, however we do not know if activation of α_1 -ARs would have a similar effect (Silberman *et al*, 2013). There is a strong inhibitory connection from the dBNST to the vBNST, supporting the idea that some of the inhibitory control of VTA-projecting neurons in the vBNST originates from the dBNST (Turesson *et al*, 2013).

The α_1 -ARs are also implicated in modulating glutamatergic transmission in the BNST. In both the dorsal and ventral BNST activation of α_1 -ARs causes a G_q-receptor-dependent long term depression (LTD) of glutamatergic transmission in the BNST (McElligott and Winder, 2007; McElligott *et al*, 2010). This G_q dependent plasticity is maintained by a loss of functional calcium-permeable AMPA receptors (CP-AMPA receptors) and is modulated by stress (McElligott *et al*, 2010). After 10 days of chronic restraint stress,

which increases extracellular levels of NE in the BNST, α 1-AR LTD was blocked in the vBNST and significantly attenuated in the dBNST (McElligott *et al*, 2010). This was due to a loss of function of CP-AMPARs. Chronic restraint stress caused an increase of NE release into the BNST which acted on α 1-ARs *in vivo* resulting in LTD, thereby already decreasing the function of the CP-AMPARs by the time of the *in vitro* recordings. The authors hypothesize that, as a GABAergic nucleus, the BNST acts as a brake on the PVN and the amygdala. After stress, the LTD disengages that brake resulting in an unregulated stress axis and limbic system (McElligott *et al*, 2010). However, this interpretation must be re-examined in light of recent evidence that the different nuclei of the BNST_{ALG} have opposing roles in anxiety-like behavior (Kim *et al*, 2013). Therefore it is unlikely that the BNST as a whole acts as a brake on the PVN and amygdala. However, this long-term depression does change the set-point for the response to future incoming stimuli.

To summarize, NE is released into the BNST during stress and other aversive events. It acts in the dBNST through β -ARs to increase CRF release and facilitate the glutamatergic input into the dBNST (Egli *et al*, 2004; Nobis *et al*, 2011; Silberman *et al*, 2013). In this way, NE tunes the dBNST to possible salient inputs potentially increasing the output of the anxiogenic portion of the dBNST to increase anxiety-like behaviors (Cecchi *et al*, 2002; Hott *et al*, 2012). Although there are both anxiolytic and anxiogenic outputs in the dBNST, the predatory odor TMT which causes an increase in NE release into the BNST, specifically increases cFos expression in the oval BNST which is known to be a significant contributor to the anxiogenic pathway (Day *et al*, 2004; Fendt *et al*, 2005; Kim *et al*, 2013). NE also acts in the vBNST on α ₁-ARs, perhaps more strongly than the actions in the dBNST due to more NE release in this region (Egli *et al*, 2004; Phelix *et*

al., 1994). Here NE application results in increased local GABAergic transmission potentially inhibiting the anxiolytic projection from the vBNST (Dumont and Williams, 2004). Action on α_1 -ARs may also cause a feed-forward increase in NE release into the BNST (Forray *et al.*, 1999; Park *et al.*, 2009). The α_2 -ARs, however, act to control the effects of NE in the BNST. Activation of α_2 -ARs inhibits NE release and decreases excitatory transmission (Egli *et al.*, 2004; Forray *et al.*, 1999; Park *et al.*, 2009). After chronic stress, the prolonged NE release may cause a long-term depression of glutamatergic transmission in the dBNST and vBNST through the α_1 -ARs (McElligott *et al.*, 2010). Because chronic stress results in an increase in anxiety-like behavior, it is hypothesized that this LTD inhibits the anxiolytic-pathway in the BNST. However, although unlikely, it is also possible that this LTD is a compensatory mechanism for the increase in excitatory transmission into the BNST. More research needs to be done on the effect of chronic stress on NE's actions in the BNST. As the literature stands, it seems the β -ARs and α_1 -ARs act to potentiate the anxiogenic pathway and inhibit the anxiolytic pathway in the BNST, whereas the α_2 -AR stands alone in its ability to inhibit the anxiogenic-effects of NE release. Modulating these opposing noradrenergic pathways may be a potential target in the treatment of drug addiction and anxiety disorders.

Dopamine

The BNST receives dopaminergic input from the PAG, VTA, and, to a lesser extent, the substantia nigra pars compacta (Hasue and Shammah-Lagnado, 2002; Meloni *et al.*, 2006). Injections of the retro-grade tracer Fluoro-Gold (FG) into the dBNST combined with tyrosine hydroxylase immunofluorescence revealed that the A10dr and A10dc dopaminergic cell groups in the PAG are the strongest sources of dopaminergic afferents

in the dBNST (Meloni *et al*, 2006). Similar to NE, there is both anatomical and functional evidence that dopamine (DA) interacts with CRF in the BNST to affect stress behaviors (Day *et al*, 2002; Kash *et al*, 2008; Meloni *et al*, 2006; Phelix *et al*, 1994; Silberman *et al*, 2013), however unlike the NE projections, the DA projections are primarily in the dBNST and form synapses with the CRF neurons in the oval BNST (Freedman and Cassell, 1994; Phelix *et al*, 1994). Both DA and NE cause a direct depolarization in CRF neurons in the BNST of mice (Silberman *et al*, 2013) and an indirect increase in frequency of sEPSCs in the BNST through CRF signaling, however DA and NE are most likely facilitating distinct populations of glutamatergic synapses (Kash *et al*, 2008; Nobis *et al*, 2011; Silberman *et al*, 2013). On the other hand, there is evidence for some cross talk between systems. For example, DA has been shown to inhibit glutamatergic input into the BNST by acting on the α 2-AR (Krawczyk *et al*, 2011a). The precise circuitry affected by NE and DA-induced CRF signaling will need to be elucidated in order to better understand their differing roles.

Interestingly, there is some debate over the nature of DA receptor distribution in the dBNST with various groups reporting the presence or absence of the D1, D2, and D3 receptors in this region (Eiler *et al*, 2003; Kim *et al*, 2013; Krawczyk *et al*, 2011b; Mengod *et al*, 1992; Savasta *et al*, 1986; Scibilia *et al*, 1992). Using receptor autoradiography and immunohistochemistry there is little evidence for the presence of the D1 receptor in the dBNST in control animals (Krawczyk *et al*, 2011a; Savasta *et al*, 1986). This is intriguing given evidence that the D1 specific antagonist, SCH 23390 in the BNST dose-dependently reduces alcohol-motivated responding, whereas the D2 antagonist, eticlopride has no effect (Eiler *et al*, 2003). Additionally, the *Drd1a::cre* transgenic mouse that expresses Cre in cells in which D1 is expressed specifically labels the oval nucleus of the BNST (Kim *et al*,

2013). As discussed in a previous section of this review, preliminary single cell RT-PCR results have shown that mRNA for the D1 receptor is specifically expressed in Type III CRF neurons of the oval BNST (unpublished observation). It is possible that the mRNA for the D1 receptor is expressed in these neurons without being translated into functional protein under basal conditions. In support of this hypothesis, there is a switch from a D2-mediated response in the dBNST of drug-naïve rats to a D1-mediated response in cocaine self-administering rats (Krawczyk *et al*, 2011b). In control rats, DA was found to suppress evoked GABA transmission in the dBNST through a presynaptic D2 receptor mechanism (Krawczyk *et al*, 2011a; 2011b). However, after prolonged cocaine self-administration, DA acted on D1 receptors to increase IPSC amplitude. Importantly, this switch was not observed in rats that received cocaine passively, emphasizing DA's involvement in motivated behaviors. Perhaps self-administration of drugs of abuse triggers translation of D1 mRNA in the dBNST into functional protein to mediate drug-motivated behavior. However, if D1 receptors are not functional in drug-naïve animals, it is unclear how DA could depolarize CRF neurons in the BNST (Silberman *et al*, 2013). Both D2 and D3 receptors are G_i-coupled receptors, activation of which generally enhances G-protein coupled inwardly-rectifying potassium (GIRK) channel activity thereby hyperpolarizing the neuron and preventing synaptic release (Michaeli and Yaka, 2010). It is more likely that DA acts on the G_s-coupled D1 receptor to depolarize the CRF neurons in the BNST. More research needs to be done to clarify the functional expression of DA receptors in the BNST in both naïve and drug-exposed animals.

As the similar effects on the local circuit may suggest, DA and NE seem to be involved in similar processes, however the timing of their release indicate that they relay

related but separate and sometimes reciprocal signals. In a study looking at the release of DA and NE in response to intracranial self-stimulation (ICSS) in the region of the VTA/substantia nigra, both catecholamines were released into the BNST, however, DA was released into the dBNST in response to cues that predicted reward whereas NE was not released into the vBNST at these times. Conversely, there was a suppression of extracellular DA during extinction of a lever press being paired with ICSS and an increase in release of NE into the vBNST (Park *et al*, 2013). Similarly, in another study DA release in the dBNST increased in response to intra-orally-administered sucrose but decreased in response to the aversive tastant, quinine (Park *et al*, 2012). This indicates that DA relays information about obtaining a reward or pleasurable stimulus whereas NE relays information about the lack of an anticipated-reward.

Dopamine's involvement in reward suggests it plays an important role in drug abuse. Like in the nucleus accumbens shell, drugs of abuse increase extracellular DA in the BNST (Carboni *et al*, 2000). Cocaine, nicotine, morphine, and tetrahydrocannabinol (THC; the psychoactive component of cannabis) all increase extracellular signal-related kinase (ERK) activation in the BNST_{ALG} (Valjent *et al*, 2004). The ERK pathway plays an important role in synaptic plasticity, learning, and memory, indicating it could be a potential molecular mechanism for the long-lasting effects of drugs of abuse. Importantly, this increase in ERK activation can be blocked with an injection of the D1 receptor antagonist SCH 23390 15 minutes prior to drug administration, suggesting DA acts on D1 receptors in the BNST to increase ERK activation (Valjent *et al*, 2004). In the striatum, the ERK signaling cascade is activated with simultaneous activation of NMDA and D1-receptors (Valjent *et al*, 2005). In this way, the ERK cascade acts as a coincidence detector

and is activated during times of high glutamatergic input and dopamine release. Perhaps the same process is occurring in the BNST. Interestingly, STEP inhibits ERK activity and thereby regulates the duration of ERK-signaling (Valjent *et al*, 2005; Yang *et al*, 2012). STEP is specifically expressed in the CRF neurons of the oval BNST while ERK1/2 is found in both cells co-expressing STEP and those not expressing STEP (Dabrowska *et al*, 2013b). NMDA and DA have the potential to activate the ERK cascade in all of these neurons, but only the CRF cells contain STEP, the molecular brake for the ERK signal. However, STEP expression in the oval BNST is reduced after chronic stress causing a potential increase in ERK activation with DA present in the BNST (Dabrowska *et al*, 2013b). This may be relevant for stress-induced drug seeking, where the loss of the molecular brake on ERK signaling in CRF neurons in the dBNST could contribute to drug craving or the motivation to seek out drugs.

DA interacts with CRF signaling in the BNST to play an important role in stress behavior in other ways as well. For example, a unilateral 6-hydroxydopamine (6-OHDA) lesion causes a hemispheric asymmetry in CRF mRNA expression in the CeA and oval nucleus of the BNST (Day *et al*, 2002). This lesion selectively removes the mesostriatal dopaminergic inputs to the brain through use of the neurotoxin, 6-OHDA injected into the medial forebrain bundle. The hemisphere with the lesion exhibited reduced CRF mRNA in the oval BNST compared to the hemisphere with the mesostriatal DA system still intact (Day *et al*, 2002). Interestingly, there was no effect of the 6-OHDA lesion on ENK mRNA expression in the BNST. As CRF and ENK are expressed in separate cell populations in the BNST, this suggests that the DA system effects mRNA expression in a specific subset of cells, namely the CRF neurons. In addition to promoting CRF expression, DA is

involved in facilitating CRF-enhanced startle. The peripheral administration of the D1 antagonist, SCH 23390 attenuates CRF-enhanced startle, a behavior in which the BNST is critically involved (Lee and Davis, 1997; Meloni *et al*, 2006). This raises the possibility that CRF kicks off a feed-forward circuit between the BNST and a major source of DA input such as the PAG. In this model put forward by Meloni *et al*, CRF acts on CRFR1 to activate CRF neurons in the BNST that then send projections to the PAG (Meloni *et al*, 2006). Indeed the BNST sends strong projections to the PAG including a CRF projection from the oval nucleus (Dong and Swanson, 2004; Dong *et al*, 2001a; 2001b; Gray and Magnuson, 1992). CRF depolarizes neurons in the PAG thereby activating the dopaminergic cells to release DA in the dBNST (Bowers *et al*, 2003). DA then acts on D1 receptors in the BNST, particularly on CRF neurons, to further increase CRF release into the BNST (Silberman *et al*, 2013). CRF then facilitates glutamatergic transmission into the BNST through its action on presynaptic-CRFR1 (Kash *et al*, 2008; Silberman *et al*, 2013). In this way, DA and CRF create a feed-forward circuit that acts to increase CRF signaling and activation of the BNST pathway involved in the startle reflex. Dopamine's role in appetitive signaling and its interaction with CRF place dopamine at the intersection of stress and reward.

There is little direct evidence that DA is released into the dBNST after a stressor. Activity of DA neurons in the dorsal VTA is primarily decreased by an acute stressor such as a foot-shock (Brischoux *et al*, 2009). However a smaller group of DA neurons in the ventral VTA is activated by foot-shock, yet it is unknown if these DA neurons project to the BNST (Brischoux *et al*, 2009). Extracellular DA levels increase in the dorsal striatum and nucleus accumbens core during tail-pinch and increase in the nucleus accumbens shell

only at the termination of tail pinch (Budygin *et al*, 2012). This indicates DA is released during both aversive and rewarding stimuli, however it is still unclear where and when DA is released into the BNST. Social-defeat stress and exposure to TMT, a component of fox odor, produces increased c-Fos activation in the PAG, possibly indicating an increase in activity of PAG DA neurons that project to the BNST (Janitzky *et al*, 2014; Miczek *et al*, 1999). It is clear that DA cells throughout the brain are activated by different stimuli at different times; therefore the role of DA in the BNST is complex. DA in the BNST seems to both signal reward and facilitate the stress response. Rather than acting to suppress or enhance the anxiolytic or anxiogenic circuit within the BNST, DA seems to facilitate both pathways to modulate motivated behavior.

The BNST not only receives dopaminergic projections, but it also sends reciprocal connections to the main sources of dopaminergic input including the PAG and VTA (Dong and Swanson, 2004; Georges and Aston-Jones, 2001; 2002; Gray and Magnuson, 1992; Jalabert *et al*, 2009; Kudo *et al.*, 2012; Jennings *et al*, 2013; Kim *et al*, 2013; Silberman *et al*, 2013). Additionally, the LC and VTA are reciprocally connected, indicating that the release of each of the catecholamines can influence that of the other (Mansari *et al*, 2010). Both NE and DA cause an increase in CRF signaling that results in enhancement of glutamatergic signaling into the BNST, including onto neurons that project to the VTA (Silberman *et al*, 2013). There is evidence that VTA-projecting neurons in the BNST activate DA neurons in the VTA via an excitatory amino acid pathway (Georges and Aston-Jones, 2001; 2002), however, both glutamatergic and GABAergic neurons in the vBNST project to the VTA and form connections with medial DA neurons as well as non-DA neurons (Kudo *et al.*, 2012; Jennings *et al*, 2013). Hence, there is a complex circuit

controlling the activity of dopaminergic-VTA neurons by the vBNST through both direct and indirect excitatory and inhibitory projections (Jennings *et al*, 2013). Activation of the glutamatergic projection from the vBNST to the VTA resulted in aversive behaviors including avoidance of the chamber paired with a rewarding brain stimulation, a reduction in active reward seeking, and an increase in anxiety-like behavior in an open-field test. In contrast, activation of the GABAergic projection from the vBNST to the VTA resulted in a combination of behaviors signaling a pleasurable state including preference for the chamber in which the stimulation occurred, active reward seeking, and anxiolytic behavior in an elevated plus maze task (Jennings *et al*, 2013). Similarly, stimulation of the projections from the AD BNST to the VTA, also a GABAergic projection, produced a conditioned place preference indicating activation of this pathway is rewarding (Kim *et al*, 2013). GABAergic CRF neurons in the oval nucleus also project to the VTA (Rodaros *et al*, 2007; for a review on the control of VTA-DA neurons by the BNST see Jalabert *et al*, 2009). It is still unclear if the GABAergic and glutamatergic projections from the BNST to the VTA result in an increase or decrease in DA release to the BNST and other regions. With both excitatory and inhibitory projections synapsing on dopaminergic cells, the circuit is not made obvious. Additionally, excitatory and inhibitory projections synapse onto non-DA inhibitory interneurons in the VTA (for a review on the heterogeneity of the VTA see Walsh & Han, 2014). Indeed, not all VTA DA neurons respond the same way to reward and stress, therefore it is possible that one pathway from the BNST will increase activity of a sub-population of DA neurons and inhibit others (Brischoux *et al*, 2009). Future experiments will need to isolate the effect of the different projections from the BNST to the VTA on DA cell firing. Of equal importance, new research will need to

elucidate the role of dopamine in the BNST on motivated behavior. As the literature stands, DA is intricately involved in both reward and stress, but the precise mechanism of action is unknown.

Serotonin

The serotonin system is an important target for treatment of affective and anxiety disorders. The most commonly prescribed pharmacological treatments for depression and anxiety disorders are selective serotonin reuptake inhibitors (SSRIs) (Kent *et al*, 1998; Stokes and Holtz, 1997). Although SSRIs effectively treat depression in the long-term, the therapeutic improvement only occurs after several weeks, and there is an acute effect of SSRI treatment associated with an exacerbation of the expression of fear and anxiety behavior in animals and humans (Burghardt *et al*, 2004; Grillon *et al*, 2007; for a review on SSRI's effect on fear conditioning in rodents see Burghardt and Bauer, 2013). Intriguingly, a drug that enhances serotonin reuptake, tianeptine, has also been shown to be an effective antidepressant, specifically in patients with coexisting depression and anxiety (Wilde and Benfield, 1995). There is evidence that serotonin acts in the BNST to affect anxiety behavior in humans, non-human primates, and rodents alike. Acute tryptophan depletion, causing a reduction in serotonin levels in the brain, significantly increases long-duration anxiety-potentiated startle in humans while having no effect on short-duration fear-potentiated startle (Robinson *et al*, 2012). The possible role for

serotonin in long-duration anxiety and not the phasic fear response implicates the BNST, as it is specifically involved in long- but not short-duration responses (Walker *et al*, 2009). Additionally, serotonin transporter (5-HTT) availability in the BNST positively correlates with individual differences in anxious temperament in rhesus monkeys (Oler *et al*, 2009). This could imply that SSRIs affect anxiety in highly anxious individuals by inhibiting excess 5-HTT activity in the BNST, thereby increasing the amount of serotonin in the synapse. Indeed, serotonin fibers innervate both the dBNST and vBNST, with a denser innervation in the dBNST, and appear to make connections with the CRF cells in both of these regions (Commons *et al*, 2003; Phelix *et al*, 1992). The serotonin fibers originate in the dorsal raphe nucleus (DRN), specifically the medial to caudal aspect of the dorsal DRN (DRD) (Petit *et al*, 1995; Weller and Smith, 1982). In this region of the DRD, there is a cluster of CRF containing cells bodies, most of which show dual labeling for serotonin, indicating that both CRF and serotonin could be co-released into the BNST in some conditions (Commons *et al*, 2003). In order to understand the mechanisms behind SSRI's

Receptor	Physiological Action in the BNST	Cell Type Distribution (Hazra <i>et al</i> , 2012)			Behavioral Action	
		I	II	III	BNST	CNS
5-HT _{1A}	Hyperpolarization (GIRK Channels)	63%	32%	41%	Anxiolytic (Levita <i>et al</i> , 2004; Gomes <i>et al</i> , 2011)	Anxiolytic (Albert <i>et al</i> , 2014)
5-HT ₇	Depolarization (G _s Receptor)	55%	44%	0%	Unknown	Depressive (Mnie-Filali <i>et al</i> , 2011)
5-HT _{2C}	Depolarization (G _q Receptor)	5%	0%	59%	Anxiogenic (Heisler <i>et al</i> , 2007; Marcinkiewicz <i>et al</i> , 2015)	Anxiogenic (Heisler <i>et al</i> , 2007; Kimura <i>et al</i> , 2009)
5-HT _{1B}	Presynaptic inhibition	0%	21%	41%	Unknown	Aggression & Impulsivity (Saudou <i>et al</i> , 1994; Nautiyal <i>et al</i> , 2015)

Table 1.3. A summary of the physiological and behavioral action of the different serotonin receptor subtypes as well as their distribution in Type I, II, and III neurons.

actions and to improve pharmacological therapy, a better knowledge of serotonin's actions in the BNST and interaction with CRF is necessary.

Serotonergic neurons of the dorsal raphe are activated in response to uncontrollable stressors such as inescapable foot-shock, anxiogenic drugs, and social defeat, and CRF mediates this response (Abrams *et al*, 2005; Amat *et al*, 2005; Gardner *et al*, 2005; Hammack *et al*, 2002; Grahn *et al*, 1999; for a review on the functional neuroanatomy of defined serotonergic systems see Lowry, 2002). CRF acts on both CRFR1 and CRFR2 in the DRD to affect serotonin release (Amat *et al*, 2004; Hale *et al*, 2010; Kirby *et al*, 2000; Rice and Valentino, 2000; for a review on the interactions between CRF and serotonergic systems see Fox and Lowry, 2013). At low doses, CRF inhibits firing in the DRN, however at higher doses, CRF becomes excitatory (Rice and Valentino, 2000). The CRFR1 antagonist, antalarmin attenuates the inhibitory effect of CRF at low doses. In contrast, the CRFR2 agonist, urocortin 2 (UCN 2) increases c-Fos expression in serotonergic neurons of the DRD that project to limbic regions, including the BNST, and increases serotonin release (Amat *et al*, 2004; Hale *et al*, 2010; Staub *et al*, 2005). Because CRF has a higher binding affinity for CRFR1 than CRFR2, these data suggest that low levels of CRF inhibit the DRD through the CRFR1 receptor and high levels of CRF activate the serotonergic neurons of the DRD through the CRFR2 receptor. Interestingly, a selective CRFR2, but not CRFR1 antagonist in the DRD blocks the behavioral consequences of uncontrollable stress, indicating CRF acts on CRFR2 in the DRD to facilitate the prolonged activation of serotonergic neurons of the DRD in uncontrollable stress (Hammack *et al*, 2003). Importantly, the dBNST and vBNST provide input into the DRD, potentially contributing to the CRF projections there (Peyron *et al*, 1998).

The effects of serotonin on BNST circuitry are complex (For a summary see **Table 1.3**). Serotonin acts presynaptically in the BNST to modulate glutamatergic transmission (Guo and Rainnie, 2010). In whole-cell patch-clamp recording experiments, serotonin application reduced the amplitude of evoked EPSCs (eEPSCs), which was accompanied by an increase in paired pulse ratio. The non-selective 5-HT_{1B/D} agonist, sumatriptan, and the selective 5-HT_{1B} agonist CP93129 both mimicked the effect while the 5-HT_{1B} antagonist GR55562 attenuated the inhibitory effect of serotonin on eEPSC amplitude (Guo and Rainnie, 2010; however see Krawczyk *et al*, 2011a). In this way, serotonin release in the BNST after stress may counter-act the facilitation of glutamatergic transmission into the BNST caused by CRF. Furthermore, it is possible that 5-HT_{1B} receptor activation in the BNST limits other transmitter release into the BNST, such as CRF from the CeA, thereby providing an inhibitory control over the anxiety response after a stressor. More research on how serotonin and CRF interact to affect input into the BNST needs to be done to clarify this circuit.

The postsynaptic modulation of neurons in the BNST by serotonin is determined by the specific combination of serotonin receptor subtypes expressed in each individual neuron. The anterolateral BNST expresses mRNA transcripts for the 5-HT_{1A}, 5-HT_{1B}, 5-HT_{1D}, 5-HT_{1F}, 5-HT_{2A}, 5-HT_{2C}, 5-HT₃, 5-HT₄, 5-HT_{5A}, 5-HT₆, and 5-HT₇ receptors, and the complex response to serotonin mirrors the heterogeneous expression of serotonin receptor subtypes (Guo *et al*, 2009). Bath application of serotonin in the dBNST results in one of 4 responses: about 16% of neurons exhibit a pure hyperpolarization response (5-HT_{Hyp}), about 28% show hyperpolarization followed by a delayed depolarization response (5-HT_{Hyp-Dep}), and about 34% show only depolarization (5-HT_{Dep}). Finally, about 22% of cells

show no postsynaptic response to serotonin application (5-HT_{NR}). Because the depolarizing portion of the $5\text{-HT}_{\text{Hyp-Dep}}$ response was rarely large enough to overcome the initial hyperpolarization, the most common response to serotonin application in the dBNST is hyperpolarization, the most common response to serotonin application in the dBNST is hyperpolarization (Guo *et al*, 2009; Levita *et al*, 2004). All of the postsynaptic responses to serotonin are associated with a decrease in membrane resistance and an increase in conductance, suggesting serotonin application results in a facilitation or opening of ion channels (Levita *et al*, 2004). In about 25% of the cells that respond to serotonin with a 5-HT_{Hyp} response, the serotonin current reverses direction at -89 mV , which is close to the potassium equilibrium potential predicted by the Nernst equation. In fact, serotonin receptors can act to open GIRK channels. The hyperpolarizing response in these neurons could be blocked with a GIRK channel inhibitor, tertiapin-Q, confirming involvement of GIRK channels in the 5-HT_{Hyp} response. The other 75% of cells with a 5-HT_{Hyp} response exhibited a reversal potential around -74 mV , which most likely reflects a combined reversal of a few different serotonin receptor subtypes including those that act on GIRK channels. The hyperpolarizing response to serotonin is most likely due to activation of the $5\text{-HT}_{1\text{A}}$ receptor. Indeed the hyperpolarizing response could be blocked by the $5\text{-HT}_{1\text{A}}$ specific antagonist WAY 100635 (Levita *et al*, 2004). The 5-HT_{Dep} response and the depolarizing component of the $5\text{-HT}_{\text{Hyp-Dep}}$ response are mediated by the $5\text{-HT}_{2\text{A}}$, $5\text{-HT}_{2\text{C}}$, and/or the 5-HT_7 receptors. Neurons that exhibit a $5\text{-HT}_{\text{Hyp-Dep}}$ response only show a monophasic inward current in the presence of WAY 100635. This current can be attenuated by the $5\text{-HT}_{2\text{A}}$ antagonist MDL 100907, the $5\text{-HT}_{2\text{C}}$ antagonist RS 102221, and/or the 5-HT_7 antagonist SB 269970 indicating that any combination of these receptors can contribute to the depolarization response to serotonin (Guo *et al*, 2009).

The complicated pharmacological profile of BNST neurons to serotonin suggests an equally complicated receptor expression pattern. Single cell RT-PCR was used to screen mRNAs corresponding to the different serotonin receptor subtypes in individual dBNST neurons. Indeed, dBNST neurons exhibited a composite pattern of serotonin receptor gene expression, with some neurons expressing mRNA for one subtype and some expressing mRNA for two or three subtypes. As predicted by the primarily inhibitory nature of serotonin in the BNST, one of the most prominent receptor subtypes is 5-HT_{1A}, expressed in 41% of neurons tested. The other common receptor subtype is 5-HT₇ expressed in 46% of neurons, however 23% of those neurons that express 5-HT₇ also co-express 5-HT_{1A}, predicting a combined hyperpolarizing and depolarizing response to serotonin. Indeed the serotonin response profile predicted by the 5-HT receptor mRNA expression was not statistically different from the observed serotonin response profile of the BNST neurons (Guo *et al*, 2009). Interestingly, the three different cell types in the BNST (Type I-III) express different distributions of serotonin receptor subtypes (**Table 1.3**). In short, the Type I cells express high levels of 5-HT_{1A} mRNA, the Type II cells express high levels of 5-HT₇ and 5-HT_{1A} mRNA, and the Type III cells express high levels of 5-HT_{1A} and 5-HT_{2C} mRNA. As expected, the three cell types respond to serotonin application differently. The Type III cells also express mRNA for the 5-HT_{1B} receptor. As mentioned previously, this receptor is often expressed on axon terminals, indicating that the Type III neurons express the 5-HT_{1B} receptor on terminals in target areas to modulate neurotransmitter release (Guo *et al*, 2009). The Type III neurons may also express the 5-HT_{1B} receptor on local axon terminals allowing serotonin to modulate local synaptic transmission as well. Interestingly, serotonin has been reported to bi-directionally modulate evoked IPSC (eIPSC) amplitude

in the BNST (Krawczyk *et al* 2011a). The inhibitory effects of serotonin on eIPSCs can be mimicked by 5-HT_{1B} agonists and blocked with 5-HT_{1B} antagonists indicating that local 5-HT_{1B} expression in the BNST inhibits GABAergic transmission within the nucleus (unpublished observation). Importantly, the different serotonin receptor expression among the three cell types offers an opportunity for specific modulation of BNST neurons by serotonin ligands. As mentioned above, the type III neurons are mainly CRF neurons, hence drugs targeting the 5-HT_{2C} or 5-HT_{1B} receptor may specifically modulate CRF neurons.

The primary action of serotonin in the BNST is to inhibit neurons both through postsynaptic and presynaptic mechanisms. However, the BNST may also play a role in activating the serotonergic DRD neurons themselves. In a review on serotonin's actions in the BNST, Hammack *et al* propose a model in which the activation of the serotonin neurons of the DRD by the BNST forms a negative feedback loop to attenuate anxiety levels in the presence of a stressor (Hammack *et al*, 2009). An acute stressor activates the BNST causing an increase in CRF release in target areas including the DRD. With enough CRF, CRF acts on CRFR2 to increase serotonergic release in limbic regions including the BNST (Amat *et al*, 2004; Hale *et al*, 2010; Staub *et al*, 2005). Serotonin acts on the BNST in a primarily inhibitory manner, thereby inhibiting further CRF release and attenuating the anxiety response. However, maintaining this negative feedback loop requires the balance of serotonin receptor subtypes in the BNST to remain in favor of inhibition.

In support of this hypothesis, all cell types in the BNST express the mRNA for the 5-HT_{1A} receptor that causes a hyperpolarizing inhibitory response (Guo *et al*, 2009; Hazra *et al*, 2012). Single cell RT-PCR analysis showed that 5-HT_{1A} is expressed in 63% of Type

I, 32% of Type II, and 41% of Type III neurons in the dBNST (Hazra *et al*, 2012). In support of the negative feedback hypothesis described above, there is evidence that 5-HT_{1A} activation in the BNST results in a reduction of anxiety-like behavior. The 5-HT₁ agonist, 5-CT infused into the BNST significantly reduced the acoustic startle response in rats, indicating an anxiolytic-like effect (Levita *et al*, 2004). Consistent with this observation, cannabidiol (CBD) in the BNST attenuates expression of context fear conditioning and anxiety-like behavior (Gomes *et al*, 2011; 2012). CBD is a component of cannabis that has been shown to have antipsychotic, antidepressive, and anxiolytic effects, but does not have the psychotomimetic effects of cannabis. CBD can act as a 5-HT_{1A} agonist as well as block reuptake and degradation of the endogenous cannabinoid anandamide. CBD in the BNST attenuates freezing and fear-induced increase in heart rate and mean arterial pressure (MAP) in a context previously paired with foot-shock. Pre-treatment with the 5-HT_{1A} antagonist, WAY 100635 reduced the behavioral and cardiovascular effects of CBD, indicating that CBD acts through the 5-HT_{1A} receptor to affect the expression of contextual fear conditioning (Gomes *et al*, 2012). CBD in the BNST also decreases anxiety-like behavior in the elevated plus maze and Vogel conflict test through actions on 5-HT_{1A} receptors. Similarly, the 5-HT_{1A} receptor agonist, 8-OH-DPAT also decreased anxiety-like behavior in these tests (Gomes *et al*, 2011). CBD also acts through 5-HT_{1A} receptors in the BNST to modulate the BNST's control of the parasympathetic cardiac response (Alves *et al*, 2010; Gomes *et al*, 2013). The BNST has a tonic inhibitory influence on the parasympathetic component of the baroreflex, however during acute restraint stress, the BNST activates the parasympathetic system to modulate the heart rate increase associated with acute stress (Crestani *et al*, 2006; 2009). This suggests that the two opposing parallel

circuits in the BNST modulate the parasympathetic system in opposing ways during basal and stress states. CBD and 8-OH-DPAT facilitate baroreceptor reflex bradycardia in basal conditions, and this effect is blocked by WAY 100635 (Alves *et al*, 2010). This is in agreement with 5-HT_{1A} activation inhibiting the BNST's inhibitory influence on the parasympathetic response. Similarly, CBD acts through 5-HT_{1A} receptors in the BNST to enhance the increase in heart rate during restraint stress, consistent with 5-HT_{1A} activation inhibiting the BNST's role in activating the parasympathetic system to modulate heart rate during acute stress (Gomes *et al*, 2013; for a review on the BNST's role in modulating autonomic functions see Crestani *et al*, 2013). Although 5-HT_{1A} activation facilitating the increase in heart rate seems in contrast to its role in reducing anxiety, it suggests that individual aspects of the response to acute stress are modulated by different circuits within the BNST, and serotonin impacts multiple aspects of the circuit.

In contrast to 5-HT_{1A}, 5-HT₇ contributes to the depolarization response to serotonin in the BNST. 5-HT₇ is the most commonly expressed serotonin receptor subtype in the BNST, however it is not expressed in the Type III neurons, but is expressed in the majority of Type I and Type II cells (Guo *et al*, 2009; Hazra *et al*, 2012). This raises an intriguing question about the functional and behavioral role of the 5-HT₇ receptors in the BNST. If the Type III CRF neurons are the anxiogenic projection neurons of the dBNST, then it is likely that Type I and/or Type II cells provide an inhibitory control over the output of the CRF neurons as described previously. In this case, 5-HT₇ activation could potentially facilitate the inhibition of CRF neurons by activating the local inhibitory circuit. In fact, 5-CT is a mixed 5-HT_{1/7} agonist but acts to reduce anxiety-like behavior in the BNST (Hammack *et al*, 2009). Since Type III neurons do not express 5-HT₇, 5-CT would only

act on 5-HT_{1A} receptors resulting in a hyperpolarizing response. In contrast, perhaps 5-CT has more of a mixed response in Type I/II cells that could potentially result in depolarization due to the high prevalence of 5-HT₇ receptors. This could further facilitate the anxiolytic effect of 5-CT by activating the inhibitory control over the Type III cells. In this model, 5-HT₇ receptor activation in the BNST would be hypothesized to be anxiolytic, however elsewhere in the brain, blockade of 5-HT₇ receptors produces a fast anti-depressive effect (Mnie-Filali *et al*, 2011; for a review on 5-HT₇ and its role in nervous system disorders see Hedlund, 2009). In fact, pharmacological blockade of the 5-HT₇ receptor has been investigated as a potential antidepressant strategy. Unlike the SSRI fluoxetine, acute administration of the 5-HT₇ antagonist, SB-269970 does not increase anxiety-like behavior in the open field test. In fact, co-administration of SB-269970 with fluoxetine counteracted the anxiogenic-like effect of fluoxetine alone. Furthermore, treatment with SB-269970 significantly reduced immobility time in the forced swim test, an important predictor of a successful antidepressant (Mnie-Filali *et al*, 2011). This suggests 5-HT₇ activation in the BNST could potentially act to increase anxiety-like behavior. However, it is important to note that an anxiogenic role of a receptor in other parts of the brain does not mean it cannot play a different role in the BNST. This is a prime example of why it is crucial to better understand the local circuitry of the BNST and the role of specific receptor subtypes.

Along with the 5-HT₇ receptor, the 5-HT_{2C} receptor also acts in the BNST to depolarize neurons and affect anxiety-like behavior. 5-HT_{2C} knock-out mice are deficient in stress-induced activation of dBNST CRF neurons and show lower anxiety-like behavior relative to wild type mice, indicating 5-HT_{2C} is involved in facilitating the anxiety response

through activation of CRF neurons in the BNST (Heisler *et al*, 2007). Unlike the 5-HT₇ receptor, the 5-HT_{2C} receptor is expressed almost exclusively in the Type III putative CRF neurons in the dBNST (Guo *et al*, 2009; Hazra *et al*, 2012). There is also evidence that serotonin acts on 5-HT_{2C} receptors in the vBNST to facilitate stress-induced anxiety-like behaviors. The potent stressor, chronic intermittent ethanol (CIE) exposure, is known to increase general and social anxiety-like behavior in rodents and c-Fos expression in the vBNST. Peripheral injections of the selective 5-HT_{2C} antagonist, SB 242,084 mitigate the CIE-induced increase in social anxiety-like behavior as well as the increase in c-Fos expression in the vBNST (Marcinkiewicz *et al*, 2015). As mentioned previously, there is a CRF-dependent increase in glutamatergic input into the BNST after CIE (Silberman *et al*, 2013). Perhaps the increase in BNST activation due to CIE causes CRF to be released into

Modulator	Behavioral Role		Physiological Action
	Anxiolytic/ Rewarding	Anxiogenic/ Aversive	
CRF		1, 2, 3, 5, 7, 8, 9	<ul style="list-style-type: none"> Enhances glutamatergic input in BNST (4, 5, 6)
NE	19	10, 11, 12, 13, 14, 15, 16, 17	<ul style="list-style-type: none"> Enhances glutamatergic input in dBNST (5, 6, 18) Depolarizes CRF neurons in dBNST (5) Attenuates glutamatergic transmission in vBNST (18) Enhances GABAergic transmission in vBNST (20) Chronic stress results in LTD of glutamatergic input (21)
DA	12, 22	23	<ul style="list-style-type: none"> Enhances glutamatergic input in dBNST (5, 4) Depolarizes CRF neurons in dBNST (4)
5-HT	24, 27, 28, 29	30, 31	<ul style="list-style-type: none"> Attenuates glutamatergic input in dBNST (25) Inhibits a large portion of the dBNST and depolarizes a small portion of the dBNST (26, 27) The inhibitory/excitatory balance may shift after chronic stress (32)
<p>References: (1) Sahuque <i>et al</i>, 2006; (2) Liang <i>et al</i>, 2001; (3) Lee and Davis, 1997; (4) Kash <i>et al</i>, 2008; (5) Silberman <i>et al</i>, 2013; (6) Nobis <i>et al</i>, 2011; (7) Erb <i>et al</i>, 2001, (8) Jasnow <i>et al</i>, 2004; (9) Kim <i>et al</i>, 2013, (10) Cecchi <i>et al</i>, 2002; (11) Onaka and Yagi, 1998; (12) Park <i>et al</i>, 2012; (13) Fendt <i>et al</i>, 2005; (14) Hott <i>et al</i>, 2012; (15) Leri <i>et al</i>, 2002b; (16) Mantsch <i>et al</i>, 2014; (17) Vranjkovic <i>et al</i>, 2012; (18) Egli <i>et al</i>, 2004; (19) Erb <i>et al</i>, 2000; (20) Dumont and Williams, 2004; (21) McElligott <i>et al</i>, 2010; (22) Park <i>et al</i>, 2013; (23) Meloni <i>et al</i>, 2006; (24) Robinson <i>et al</i>, 2012; (25) Guo and Rainnie, 2010; (26) Guo <i>et al</i>, 2009; (27) Levita <i>et al</i>, 2004; (28) Gomes <i>et al</i>, 2011; (29) Gomes <i>et al</i>, 2012; (30) Heisler <i>et al</i>, 2007; (31) Marcinkiewicz <i>et al</i>, 2015; (32) Hazra <i>et al</i>, 2012</p>			
<p>Table 1.4. A summary of the behavioral and physiological action of corticotropin releasing factor (CRF), norepinephrine (NE), dopamine (DA), and serotonin (5-HT) in the BNST_{ALG}</p>			

the DRD, thereby increasing serotonin activity in the BNST. Serotonin can then act on 5-HT_{2C} receptors in the BNST (potentially specifically on CRF neurons) to further increase their activity and facilitate anxiety-like behavior. In whole-cell patch clamp recordings in the vBNST, CIE treatment increased neuronal excitability. These cells were induced to fire significantly more action potentials than neurons from animals not given CIE. This increase in firing rate was blocked with application of the 5-HT_{2C} antagonist, RS102221. Additionally, bath application of mCPP, a 5-HT_{2C} agonist depolarized cells more in the CIE treated group than control group, indicating enhancement of 5-HT_{2C} signaling after withdrawal (Marcinkiewicz *et al*, 2015). This suggests that serotonin's actions on 5-HT_{2C} receptors in the BNST can actually create a feed-forward loop to facilitate the anxiety response. However, this feed-forward increase in activity would be tempered by serotonin's ability to inhibit BNST activity through actions on 5-HT_{1A} and 5-HT_{1B} receptors. Therefore, serotonin's effect on anxiety-like behavior may be critically dependent on the balance of excitatory and inhibitory serotonin receptors in the BNST (Hammack *et al*, 2009).

Importantly, chronic stress can alter the serotonin receptor subtype expression in the BNST, thereby potentially drastically altering its effects on the circuitry of the BNST and resulting anxiety-like behavior (Hazra *et al*, 2012). After 4 days of unpredictable shock stress (USS), there was a 2.8 fold decrease in 5-HT_{1A} mRNA, 2 fold increase in 5-HT_{1B} mRNA, and 3.5 fold increase in 5-HT₇ mRNA in the BNST. Single cell RT-PCR was also used to characterize the effects of stress on serotonin receptor expression in the different cell types. There was a reduction in the number of neurons expressing 5-HT_{1A} mRNA across all cell types. Since this is the primary inhibitory serotonin receptor, this

reduction in expression may impair serotonin's ability to complete the negative feedback loop required to dampen anxiety-like behavior. However, there was also an increase in the number of Type III neurons that express the mRNA for the 5-HT_{1B} receptor after chronic USS (Hazra *et al*, 2012). The increase in 5-HT_{1B} expression in Type III neurons could potentially act to compensate for the increase in the excitability of Type III neurons after stress by inhibiting neurotransmitter release. Finally, more Type I and Type II cells expressed mRNA for the 5-HT₇ receptor after the chronic USS. If 5-HT₇ receptor activation facilitates local inhibitory connections onto the anxiogenic output of the BNST, then this increase in expression could be counteracting the loss of 5-HT_{1A} expression. On the other hand, if 5-HT₇ activation facilitates the anxiety response, then the increase in 5-HT₇ receptor expression combined with the decrease in 5-HT_{1A} expression could result in a loss of the negative feedback loop between the BNST and DRD and facilitate serotonin's ability to create a feed-forward increase in BNST activity. Overall, chronic USS seems to cause a shift from inhibitory to excitatory serotonergic control in the BNST after stress, however more research needs to be done to understand the effects of this change on BNST circuitry and the impact on anxiety-like behavior. The behavioral roles and physiological actions of the neuromodulators discussed above are summarized in **Table 1.4**.

Stress Modulation of Synaptic Plasticity

Synaptic plasticity is a mechanism by which brain circuits can use prior experience to re-structure future responses. Stress is known to cause a long-lasting increase in anxiety-like behavior, and as the BNST is a crucial structure in modulating both the stress response and anxiety behavior, it is reasonable to predict that stress would cause a long-lasting change in BNST synaptic plasticity. In fact, multiple studies have shown that stress can

affect synaptic plasticity in the BNST (Conrad *et al*, 2011; Dabrowska *et al*, 2013b; Francesconi *et al*, 2009; Glangetas *et al*, 2013; McElligott and Winder, 2007), however the results of these studies are seemingly inconsistent. In this section, we will re-examine these studies in light of how stress interacts with neuromodulators as discussed above and new research on the distinct roles of different BNST sub-nuclei in modulating anxiety-like behavior.

Stress can result in structural and morphological changes in the BNST that are associated with changes in synaptic strength. For example, chronic unpredictable stress causes an increase in BNST but not amygdala volume (Pêgo *et al*, 2008). Similarly, there is a significant increase in dendritic branching in the BNST but not the CeA after chronic immobilization stress (Vyas *et al*, 2003). These studies suggest that the BNST is uniquely sensitive to significant neuronal plasticity after stress. In addition to gross morphological changes, alterations in glutamatergic receptor content and localization can occur with synaptic plasticity. A recent study looked at the effect of chronic stress on AMPA receptor distribution in the BNST. After 4 days of USS, no significant change was found in the labeling of the AMPA receptor subunit, GluR1 in the dBNST. However there was a trend towards an increase in the ratio of GluR1-labeled spines to GluR1-labeled dendrites after stress (Hubert and Muly, 2014). This indicates that there may be more AMPA receptors in the spines than other parts of the dendrites after stress. The authors speculate that looking at a specific cell type in the BNST may reveal a significant change in AMPA receptor expression that is being washed out in the average of all cell types in the dBNST. In fact, there is evidence that the Type III neurons are more susceptible to stress-induced alterations in plasticity than Type I and Type II neurons as discussed shortly (Dabrowska *et al*, 2013b).

Understanding how stress differentially affects the unique components of the BNST circuit will be critical to determining how the BNST contributes to the long lasting increase in anxiety after chronic stress. It is also possible that stress does not affect AMPA receptor distribution, but rather changes NMDA receptor distribution (Hubert and Muly, 2014). Indeed, after 4 days of repeated restraint stress, there is a significant increase in protein expression of the NMDA subunit, GluN1 in the synaptic membrane fraction of the dBNST (Dabrowska *et al*, 2013b). These changes in receptor distribution and dendritic morphology reflect long lasting changes in the way the BNST responds to input after stress.

There are multiple studies that have begun to explore how acute or chronic stress modulates the response of the BNST to upstream inputs. Acute stress can cause a 10 Hz stimulation of the medial prefrontal cortex (mPFC) input into the BNST to switch from resulting in a long-term depression (LTD) to a long-term potentiation (LTP). The functional consequence of this switch from LTD to LTP is unknown; perhaps it acts to boost the signal of salient events after acute stress (Glangetas *et al*, 2013). The BNST serves as a relay between the mPFC and VTA DA neurons. This pathway is under the control of the CB1-R, which decreases mPFC glutamate inputs in the BNST (Massi *et al*, 2008). Interestingly, cannabinoid receptor 1 (CB1) knock-out mice did not exhibit stable LTD in baseline conditions or stable LTP after the acute stress. In fact, infusion of the CB1 antagonist into the BNST blocked the LTP elicited by stimulation of the mPFC in stressed wild-type mice (Glangetas *et al*, 2013). Besides the VTA, the BNST relays to multiple nuclei critically involved in the stress response, therefore, the plastic change of the mPFC to BNST glutamate transmission after acute stress will undoubtedly impact more than the VTA DA system.

Whereas acute stress can cause a switch from LTD to LTP, chronic stress has been shown to cause a LTD in the BNST. As mentioned previously, chronic restraint stress can cause a long-term depression of the evoked EPSC in the BNST that is dependent on $\alpha 1$ -ARs (McElligott *et al*, 2010). This LTD changes the set-point for the response to future incoming stimuli. Because this LTD is maintained by a post-synaptic loss of function of CP-AMPARs, it is possible that different neurons in the BNST could experience different relative levels of LTD. The neurons that are incorporated into the circuit to reduce anxiety could experience a more significant depression than those in the anxiogenic pathway, thereby shifting the balance of the opposing circuits. On the other hand, the LTD could reduce the input that activates the anxiogenic circuit. Additionally, it is possible some synapses will be depressed more than others in the same neuron, causing the cell to respond more or less to different inputs. Isolating the different inputs into the BNST and the different cell types within the BNST through optogenetic and other molecular techniques will help to decipher how chronic stress affects the multiple circuits within the nucleus.

A few studies have examined how LTP in the BNST changes in response to stress. In un-stressed animals, Type III cells in the dBNST achieve a significantly lower magnitude of LTP in response to high frequency stimulation than both Type I and Type II cells; however, after 4 days of repeated restraint stress, Type III cells achieve a significantly higher magnitude of LTP than Type III cells of non-stressed animals. In contrast, there is no significant change in the magnitude in Type I and Type II cells after stress. This cell-type specific change in LTP is at least partially due to STEP down-regulation after chronic stress (Dabrowska *et al*, 2013b). STEP is a known modulator of synaptic plasticity by dephosphorylating subunits of the NMDA receptor promoting their internalization

(Goebel-Goody *et al*, 2012). In fact, STEP has been reported to regulate LTP in the amygdala, and the down-regulation of STEP is thought to play a role in the etiology of stress-induced anxiety disorders (Paul *et al*, 2007; Yang *et al*, 2012). As mentioned previously, STEP is specifically expressed in CRF neurons in the dBNST. Importantly, rats that underwent the repeated restraint stress showed less STEP mRNA and protein expression than controls, and there was a reduction in the number of Type III cells that expressed the mRNA for STEP (Dabrowska *et al*, 2013b). Consequently, NMDA receptor dephosphorylation and internalization by STEP is attenuated. This evidence supports the idea that Type III cells are buffered against LTP by STEP in control conditions; however the loss of STEP after chronic stress makes them more susceptible to LTP induction. In support of this theory, intracellular administration of STEP abolished the stress-induced increase in LTP magnitude but had no effect in control animals (Dabrowska *et al*, 2013b). These data suggest that Type III CRF neurons of the oval BNST are protected against over-activation during an acute stressor. Interestingly, a systemic injection of interleukin-1 β , an immune challenge that activates the BNST, results in c-Fos activation of ENK but not CRF containing neurons (Day *et al*, 1999). This could be a result of the inhibitory influence of STEP buffering the CRF cells against activation due to a single stressor. Loss of this buffer would cause ectopic CRF cell activation resulting in over-activation of the anxiogenic pathway in the BNST.

Not all studies have shown an increase in LTP magnitude in the BNST after stress. In mice, both chronic treatment with cortisol and chronic social isolation caused an increase in anxiety-like behavior as measured in the elevated zero maze and open field test; however there was a corresponding blunting of LTP in both groups (Conrad *et al*, 2011).

Additionally, there was significant blunting of LTP in animals that underwent an acute social isolation stressor (24 hours instead of 6 to 8 weeks) although there was no effect of the acute social isolation on anxiety-like behavior. This suggests that the physiological changes due to stress precede the behavioral outcome. It is unknown why chronic stress in one case causes an increase in LTP magnitude in a population of cells in the dBNST while another shows that chronic stress results in a decrease in LTP magnitude in the dBNST (Conrad *et al*, 2011; Dabrowska *et al*, 2013b), but there are many differences in the experiments that could contribute to this discrepancy. For example, although both studies were performed *ex vivo*, Dabrowska *et al* used single cell patch-clamp recordings whereas Conrad *et al* used extracellular field potential recordings. Additionally, the nature of the stressor was different; in the experiment performed by Dabrowska *et al*, the rats underwent 1 hour of restraint stress for 4 consecutive days whereas the mice in this experiment were either given 10 days of cortisol treatment or 6 to 8 weeks of social isolation. Other studies have shown different effects on the BNST from different types of stressors; for example, dorsal and ventral CRF mRNA both increase after an intermittent foot-shock stressor but are differentially

affected by social defeat and yohimbine (Funk *et al*, 2006). Not all stressors have the same behavioral or physiological effect. Another potentially crucial difference between these experiments is the delay after the end of the stressor until the collection of the data. In the paper by Dabrowska *et al*, there were 6 days between the last day of restraint stress and recording, whereas in the paper by Conrad *et al*, there were only 24 hours between the end of the stressor and data collection. It is possible that the 6-day-delay allowed for a necessary incubation period during which there are long-term changes to the circuit. The

time course and mechanism of these different changes in synaptic plasticity after stress need to be studied more to better understand the effect stress has on the circuit.

Another study showed withdrawal from alcohol and other drugs of abuse caused a long lasting impairment in a different form of LTP in the juxtacapsular BNST, long-term potentiation of intrinsic excitability (LTP-IE) (Francesconi *et al*, 2009). Importantly, this study only included neurons in the juxtacapsular portion of the BNST (see **Figure 1.1B**). However, there is not a well-defined line between the juxtacapsular and oval portion of the BNST. Therefore, it is likely that the population sampled in the study performed by Francesconi *et al* was not entirely separate from the population sampled in Dabrowska *et al*, but rather, overlapped to some unknown degree. Like stress, withdrawal from drugs of abuse is characterized by an increase in anxiety-like behavior, and drug withdrawal is known to be a potent stressor. In this study, a high frequency stimulation of the stria (100 Hz for one second repeated five times with 10 second intervals) does not result in a long-lasting increase in the excitatory postsynaptic potential, but rather a long-lasting decrease in the threshold for action potential and corresponding increase in temporal fidelity of spiking. Protracted withdrawal from alcohol in alcohol dependent rats lead to a significant reduction in LTP-IE in the BNST (Francesconi *et al*, 2009). This was replicated in withdrawal from cocaine and heroin, as well as with repeated ICV administration of CRF. Additionally, treatment with the selective CRFR1 antagonist R121919 during withdrawal restored LTP-IE in alcohol dependent rats. The authors conclude with a model in which the BNST acts as a brake on the central amygdala (CeA). When the BLA is active during times of stress or drug craving, the BNST can undergo LTP-IE, and with that an increase in temporal fidelity of firing, thus providing a bigger inhibitory control on the CeA, the

output of the amygdala. But with drug dependence, or with chronic CRF and potentially chronic stress, there is a reduced capacity for LTP-IE, as well as reduced temporal fidelity in firing, making the BNST a less efficient brake on the CeA, resulting in increased emotional arousal (Francesconi *et al*, 2009). However, this conclusion needs to be re-examined in light of new evidence for opposing circuits of the BNST—one that promotes and another that inhibits anxiety (Kim *et al*, 2013, Jennings *et al*, 2013). Although there was no reported difference in the effect of protracted withdrawal on the different cell types, the loss of LTP-IE could have a relatively different effect on Type III, putative CRF cells than Type I and II cells. Type II cells in the oval nucleus of the BNST have a significantly lower threshold for action potential than Type III cells in the oval and no significant difference in threshold than the Type I cells (unpublished observation). Additionally Type III cells have a lower resting membrane potential than both Type I and Type II cells (Hammack *et al*, 2007). If all of the cells in the BNST have a similar decrease in threshold after LTP-IE, Type III cells will still be harder to activate than the Type I and II cells. In fact, the authors report that there was a significant reduction in threshold for all three cell types in the BNST [Type I, $5.63 \pm 1.4\text{mV}$ ($t = -4.04$, $p < 0.01$, $n=6$); Type II, $5.22 \pm 1.0\text{ mV}$ ($t = -5.49$, $p < 0.01$, $n= 6$), and Type III, $3.52 \pm 1.0\text{ mV}$ ($t = -3.44$, $p < 0.05$, $n= 4$)], but they do not directly compare the reduction in threshold between cell types. A one-way ANOVA using the average reduction in threshold, standard deviation, and sample size for the three cell types provided shows a significant difference between cell types ($p < 0.05$, $F=4.160$). Furthermore, Tukey's multiple comparison test shows Type III cells have a significantly lower reduction in threshold than Type I cells ($p < 0.05$). This might be consistent with a role for STEP in buffering Type III cells against both forms of potentiation, classic LTP

and LTP-IE, and move the threshold for Type III cells further away from that of Type I and Type II. Perhaps only the Type I and Type II cells are the “brake” on the CeA. A more detailed knowledge of the circuit between the BNST and CeA as defined by electrophysiological cell type would help clarify this possibility. If the Type I and Type II cells are the “brake” on the CeA and the Type III cells promote an anxiety response, the lower threshold for action potential in the Type I and Type II cells could increase their ability to inhibit anxiety. But after withdrawal, or potentially chronic stress, this reduction in threshold is impaired, but the relative action potential thresholds between the cell types remain intact. However, as Dabrowska *et al* suggests, the Type III neurons may have lost STEP, an inhibitor of LTP (Dabrowska *et al*, 2013b). In this scenario, Type I and Type II cells will not be able to act as the proper brake on the CeA, and the Type III CRF cells of the dBNST will have lost their intrinsic brake on plasticity, resulting in a shift in the balance of the opposing circuits in the BNST from anxiolytic to anxiogenic.

Clinical Implications

Research across species, from mice and rats to non-human primates and humans, is now highlighting the importance of the BNST in anxiety and addiction. For example, Pleil *et al* (2015) found an effect of chronic alcohol drinking on the BNST that was conserved between mice and monkeys. Importantly, recent neuroimaging studies have shown that the connectivity of the BNST in humans is in large part similar to that of rodents and non-human primates, with the addition of connections between the BNST and more rostral cortical areas such as the orbitofrontal cortex (Avery *et al*, 2014, Krüger *et al*, 2015). Functional imaging studies have shown that the BNST is hyperactive in patients with generalized anxiety disorder (Yassa *et al*, 2012) and in patients with specific-phobias

(Straube *et al.*, 2007), consistent with a role for the BNST in pathological anxiety in humans. As we increase our understanding of the computing power of the BNST based on knowledge about discrete microcircuits and distinct cell types and how they are affected by stress, we hope to identify novel targets to pharmacologically manipulate portions of the circuit for clinical intervention. For example, targeted manipulations aimed to enhance the activity of STEP may lead to a novel treatment strategy for anxiety disorders as it has been shown to play an important role in the modulation of CRF cell plasticity (Dabrowska *et al.*, 2013b). Additionally, learning more about the role of specific serotonin receptor subtypes and how they change after stress may help to find pharmacological agents that could act to enhance the anti-depressive and anxiolytic effects of SSRIs by blocking 5-HT receptors that may facilitate anxiogenic circuits. This review only begins to scratch the surface of the complex effects neuromodulators have on the BNST (for a brief summary see **Table 1.4**). Defining models of microcircuits within the BNST, like that depicted in **Figure 1.1D**, will allow clinical research to hone in on therapies that can act to maintain the critical balance between opposing pathways.

Beyond treatments for anxiety and depression, modulating the circuitry of the BNST has the potential to reveal possible treatments for drug addiction. With both aversive and rewarding pathways that are sensitive to stress modulation, the BNST is a prime target for intervention to prevent stress-induced drug relapse. Learning more about how dopamine and norepinephrine affect different portions of the BNST circuit during drug-use, withdrawal, and stress may help to find pharmacological agents that could buffer the detrimental effects of stress in recovering drug addicts thereby preventing relapse. As we learn more about these separate cell populations and their particular role in the circuitry of

the BNST, future clinical studies will be able to better select drugs that can target the appropriate circuit for modulation.

Future Research Directions

With more precise molecular tools now available to dissect circuits in the BNST on the cellular level, the field has begun to move beyond the notion that the BNST has a univalent effect on anxiety-like behavior. Consequently, we must now extend these observations to examine how stress and drugs of abuse may affect the opposing portions of the circuit to modulate behavior. The use of optogenetic strategies like those used in experiments by Kim *et al* (2013) and Jennings *et al* (2013) will be crucial in furthering our understanding of the role of specific inputs into the BNST as well as the local circuitry of the nucleus. These tools are made even more powerful by transgenic animals expressing Cre in specific cell populations allowing for targeted expression of viral vectors (for a review on the use of optogenetic strategies in the BNST see Sparta *et al*, 2013). The designer receptors exclusively activated by designer drugs (DREADDs) will also be useful in teasing apart the behavioral role of specific cell types within the BNST as done in Pleil *et al*, 2015. Moreover, our increasing knowledge of distinct cell types within the BNST and how they are affected by stress may be used to pharmacologically isolate portions of the circuit for clinical intervention.

Finally, future research will need to investigate how individual differences within the BNST circuit contribute to resiliency or sensitivity to chronic stressors. Clearly, not all people who experience chronic stress develop an anxiety disorder. Evidence suggests that the BNST mediates inter-individual variation in anxiety-like behavior and generalization of fear in rats (Duvarci *et al*, 2009) and primates (Fox *et al*, 2010; Kalin *et al*, 2005; Oler

et al, 2009), however little is known about how this variation is coded in the circuit. Future research should investigate individual variation in anxiety behavior, stress response, and drug addiction, and aim to define electrophysiological and molecular correlates of these characteristics in the BNST. This will help to further narrow down potential targets for pharmacological intervention in people suffering from affective and anxiety disorders.

Chapter 2: Comparison of neurons in the BNST_{ALG} in the mouse, rat, and rhesus macaque

Introduction

There is a growing literature that describes the importance of the anterior BNST in a variety of behaviors including anxiety behavior and drug addiction. Although most of this research has been done in rodents, there is now evidence from both human and non-human primate studies that supports the role of the BNST as a modulator of anxiety behavior, drug self-administration, binge alcohol drinking, threat monitoring, and anticipatory anxiety (Macey et al., 2003; Straube et al., 2007; Fox et al., 2010; Somerville et al., 2010; Alvarez et al., 2011; Pleil et al., 2015). These studies strongly indicate that the role of the BNST is conserved across species from the rodent to the primate, suggesting the structure of the BNST may be conserved as well.

The BNST is not a homogenous structure; the rat BNST can be divided into at least 16 unique subregions and contains numerous distinct cell populations (Ju et al., 1989; Dong et al., 2001b; Dong and Swanson, 2004; Larriva-Sahd, 2006; Bota et al., 2012). Most neurons in the anterolateral group of the BNST (BNST_{ALG}) of the rat can be classified into three distinct cell types based on their spiking and rectification properties and rebound depolarization in response to hyperpolarizing and depolarizing current injection: Type I (regular spiking), Type II (low-threshold bursting), and Type III (fast inward rectifiers) (Hammack et al., 2007; Rodriguez-Sierra et al., 2013). Importantly, these cell types differ in their expression profile of mRNA for ion channel subunits, serotonin receptor subtypes, and the neuropeptide, corticotropin releasing factor (CRF), in addition to their differences in electrophysiological phenotype (Guo et al., 2009; Hazra et al., 2011; Dabrowska et al., 2013b). Hence, the electrophysiological cell type of neurons in the BNST_{ALG} may be

indicative of the functional role the neurons play in the circuit. Indeed, the vast majority of Type III neurons in the rat BNST_{ALG} express the mRNA for CRF and are affected by stress in different ways than Type I and Type II cells (Dabrowska et al., 2013b), providing further evidence that cell types play different roles in the circuit.

Although Type I, Type II, and Type III cells were defined in the BNST_{ALG} of the rat, the classification system has been appropriated for describing neurons in the mouse BNST (Silberman et al., 2013). Because the role of the BNST in anxiety behavior is conserved across multiple species, it is assumed that the neurons in the mouse BNST are similar to that of the rat. However, no study has systematically examined the neurons of the mouse BNST_{ALG} to determine if the classification system defined in the rat is appropriate for describing neuron-heterogeneity in the mouse. Similarly, it is unknown if the electrophysiological cell types of the rat BNST_{ALG} are conserved in the BNST of the primate.

Here, we used whole-cell patch clamp electrophysiology to describe the electrophysiological properties of BNST_{ALG} neurons in the mouse, rat, and rhesus macaque using the classification system initially described in the rat (Hammack et al., 2007). We, then, compared and contrasted the physiological properties of neurons of the same cell type in the three species. Furthermore, we described the characteristics of neurons that do not fit the description of a Type I, Type II, or Type III cell. Finally, we filled neurons with biocytin for post hoc morphological reconstruction and analysis to compare the dendritic arbor of BNST_{ALG} neurons in the three species.

Methods

Animal Subjects

All procedures were approved by the Institutional Animal Care and Use Committee of Emory University and were in compliance with National Institute of Health guidelines. For rats, recordings were performed in male Sprague-Dawley rats aged 30 – 60 days old (n = 63; Charles River Laboratories, Wilmington, Massachusetts). For mice, recordings were performed in wild-type male mice (n = 13) from CRFp3.0Cre mice crossed with a green fluorescent protein (GFP) Cre-reporter strain (Martin et al., 2010). Animals were housed in same-sex groups, two to four rats per cage and two to six mice per cage. Rats and mice were maintained on a 12:12-hour light-dark cycle with *ad libitum* access to food and water.

The primate tissue for this study was obtained from juvenile (18– 36 months) *Macaca mulatta* monkeys of both genders. The primates were born into the breeding colony housed at the Yerkes National Primate Research Center Field Station and raised in normal social groups. They were provided with ad libitum access to food and water and monitored by the Yerkes Veterinary Staff. Animals used in this study were selected for sacrifice by the veterinary staff for failure to thrive and/or chronic diarrhea refractory to treatment as part of the animal care end-points approved for our monkey colony. Once identified, the animals were moved to the Yerkes Main Station and scheduled for sacrifice within the week.

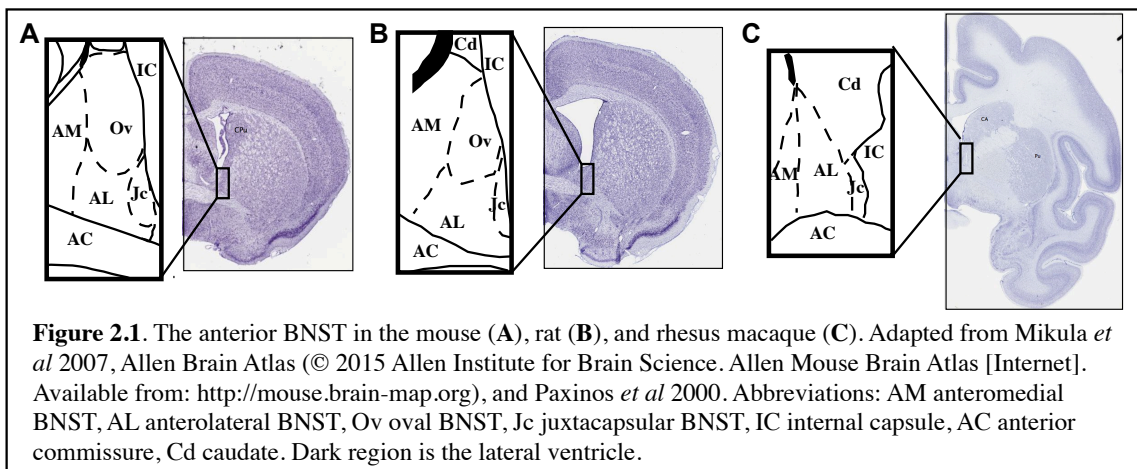
Preparation of BNST slices

Preparation of mouse and rat BNST slices

BNST slices were obtained as previously described for rats (Hammack et al., 2007). The same procedure was done for mice. Briefly, rats were decapitated under isoflurane anesthesia (Med-Vet International, IL), and the brains were rapidly removed and placed in ice-cold kynurenic acid-based “cutting solution” which contained (mM): NaCl (130), KCL (3.50), KH_2PO_4 (1.10), MgCl_2 (6.0), CaCl_2 (1.0), glucose (10), supplemented with kynurenic acid (2.0). Coronal sections containing BNST were cut 350- μm thick using a Leica VTS-100 vibratome (Leica Microsystems, Bannockburn, IL, USA). Slices were kept in oxygenated cutting solution at room temperature for 1 h before transferring to regular artificial cerebrospinal fluid (ACSF) containing (mM): NaCl (130), NaHCO_3 (30), KCl (3.50), KH_2PO_4 (1.10), MgCl_2 (1.30), CaCl_2 (2.50), and glucose (10). Slices were kept in oxygenated ACSF for at least 30 min before recording.

Preparation of rhesus macaque BNST slices

The primate BNST slices were obtained as previously described (Muly et al., 2009; Ryan et al., 2012). The animals were sacrificed with an overdose of pentobarbital (100 mg/kg) and hand-cut blocks of tissue were mounted in a vibratome and 400 μm coronal



slices were cut as previously described (Muly et al., 2009). Slices were then treated the same as the mouse and rat BNST slices: first kept in oxygenated cutting solution for 1 h before transferring to ACSF.

General patch clamp recording procedures

Individual slices were transferred to a recording chamber mounted on the fixed stage of a Leica DM6000 FS microscope (Leica Microsystems Inc., Bannockburn, IL) equipped with an IR sensitive CCD camera (Orca ER, Hamamatsu, Tokyo Japan), allowing for use of differential interference contrast (DIC) optics and infrared illumination to identify individual BNST neurons. The slices were maintained fully submerged and continuously perfused with oxygenated 32 °C ACSF with a speed of ~2 ml/min. All recordings were confined to the dorsal anterolateral cell group including the oval, juxtacapsular, and anterolateral nucleus of the BNST (BNST_{ALG}; **Figure 2.1**). The delineation of the anterolateral and anteromedial regions of the BNST in the rhesus macaque is not well defined, so recordings were limited to the anterolateral BNST as best as possible. Whole-cell recordings were obtained using recording pipettes pulled from borosilicate glass and having a resistance of 4-6 MΩ. Pipettes were filled with a potassium-based patch solution containing the following (mM): K-gluconate (130), KCl (2), HEPES (10), MgCl₂ (3), K-ATP (2), Na-GTP (0.2), and phosphocreatine (5), and was titred to pH 7.3 with KOH and 290 mOsm. Biocytin (0.35%) was added to the patch solution in some cases to allow for post hoc histochemical processing and neuronal reconstruction.

Analysis of electrophysiological properties

Basic electrophysiological properties were collected from each cell recorded. A DC holding current was injected to maintain the membrane potential at -60 mV in current

clamp. To characterize neurons, a series of 10 hyperpolarizing and depolarizing, 750 or 1000 ms long, square-wave current steps were injected and scaled so that the peak negative voltage deflection was to approximately -80 mV (Hammack et al., 2007; Hazra et al., 2011). Then, linear ramps of depolarizing current were injected, lasting 250 ms, and scaled to depolarize the neuron to elicit a single action potential. Data were analyzed by importing the raw voltage and current traces into Matlab (The MathWorks, Natick, MA, USA) using scripts provided with sigTOOL (<http://sigtool.sourceforge.net/>, developed at King's College London) and processed with customized scripts (available upon request).

Analysis of electrophysiological properties was completed as described elsewhere (Ehrlich et al., 2012). Briefly, input resistance (R_{in}) was calculated using the deflection in response to the smallest hyperpolarizing current step (approx. 5 mV) and calculated as the ratio of peak voltage deflection to the current injected. The I_h score was calculated as the ratio of the magnitude of I_h (measured as peak deflection at the beginning of the trace minus steady state at the end) to the membrane potential at the point of peak deflection in the trace with the peak deflection closest to -80 mV (smaller positive values indicate less voltage deflection due to I_h). The I_{AR} score was calculated as the ratio of the peak magnitude of the smallest hyperpolarizing trace to the difference between the peak-magnitude of the two most hyperpolarizing traces (larger values indicate more inward rectification). R_{in} , and the I_h and I_{AR} score all require a relatively stable membrane potential at a particular portion of the voltage trace (*ie* at the beginning of the smallest hyperpolarizing step for accurate calculation of R_{in}). Cells with unstable membrane potentials at the necessary time points were removed for these analyses. This resulted in removal of one rat Type III cell for calculation of R_{in} ; one mouse Type I cell, one mouse Type III cell, and two rat Type III

cells for calculation of the I_h score; and two rat Type III cells and one primate Type III cell for calculation of the I_{AR} score. The latency to the first action potential was calculated as the duration of time after the initiation of the depolarizing current step and before the first action potential. If the latency to the first action potential was > 750 msec it was not used in the analysis as most cells only had current steps 750 msec long. This resulted in removal of two mouse Type I cells and one primate Type I cell from the analysis for latency to first action potential.

Neuronal morphology

Histochemical processing

Some of the patched neurons were labeled with biocytin (Sigma Aldrich, St Lois, MO, USA) included in the patch pipette recording solution and used for neuronal reconstruction as previously described (Ryan et al., 2014). After neurons were recorded for at least 10 min, slices were fixed in 10 % buffered formalin (Fisher Scientific, Hanoverpark, IL, USA) for 12-72 h, and then transferred to cryoprotectant for storage at -20 C. After three consecutive 10 min washes in 0.05 M phosphate buffered saline (PBS), slices were permabilized for 30 min in PBS and 0.5 % Triton-X 100 (Sigma-Aldrich, St Louis, MO, USA). Slices were then treated with Alexa Fluor 488 or 568- conjugated Streptavidin (Invitrogen, Grand Island, New York, USA) diluted to 1: 1,000 in PBS with Triton-X for 36 – 48 h at 4 C. Slices were then washed 2 times for 1 h each in 0.05 M PBS and washed for 10 min in 0.05 M phosphate buffer. The slices were then mounted on glass slides, air dried for 3 – 12 h, and cover-slipped with mowiol mounting medium (Sigma-Aldrich, St Louis, MO, USA).

Neuronal reconstruction and analysis

Z-stack images of the filled neurons were taken at either 10 or 20x magnification with a 0.4 or 0.3 μm step size respectively using a Leica DM5500B spinning disk confocal microscope (Leica Microsystems Inc.m Bannockburn, IL, USA) and SimplePCI data acquisition software (Compix, Sewickley, PA). For morphological analysis, the dendritic arbor and cell body of each neuron was reconstructed by hand using NeuroLucida neuron tracing software (MicroBrightField, Colchester, VT). Quantitative analysis of reconstructions was performed using NeuroLucida Explorer (MicroBrightField).

Statistical Analysis

Statistical analyses were carried out using Prism 6 (GraphPad Software Inc., San Diego, CA). Distribution of cell types was compared using a χ^2 -test when samples being compared had > 10 cells per cell type. Due to the small sample size of some data sets, normality was estimated by visual discrimination. For data sets with a normal distribution, an ordinary one-way ANOVA (when not dividing by cell type) or two-way ANOVA (with cell type and species as the two factors) with Tukey's multiple comparisons test was used. For data sets with a non-normal distribution, such as input resistance, a Kruska-Wallis test with Dunn's multiple comparisons test was used. An alpha level of 0.05 was used for all statistical tests, and data are presented as mean \pm SEM.

Results

Comparison of this rat sample with previous published samples

For this study, neurons in the BNST_{ALG} were divided into three groups based on a visual discrimination of current clamp traces showing the voltage response to hyperpolarizing and depolarizing square-wave current injections as previously described (Hammack et al., 2007). Type I neurons are characterized by a depolarizing sag in response to hyperpolarizing current injection indicative of an I_h current and a steady firing rate, but do not exhibit low-threshold depolarizing waves or burst-firing activity. In contrast, Type II neurons exhibit rebound spiking after the hyperpolarizing current steps, burst firing activity, and/or a prevalent low-threshold depolarizing wave indicative of a prominent I_T current. Finally Type III cells are classified based on the presence of a pronounced fast inward rectification in response to hyperpolarizing current injection indicative of an inwardly rectifying potassium current (I_{AR}) and do not exhibit any signs of an I_T current and little-to-no I_h current.

Here, we used two separate samples of recordings from cells in the rat BNST_{ALG} as a basis from which to compare the cells from the mouse and primate. Sample 1 was obtained for the purposes of learning the relative distribution of Type I, II, and III cells in the BNST_{ALG} (107 cells from 39 rats; includes cells described in Chapter 2). For this sample, patch-clamp recording was attempted for cells regardless of their physical appearance in order to achieve an accurate representation of their distribution. In contrast, Sample 2 was obtained from the control rats in a chronic shock stress study (127 cells from 24 rats; described in Chapter 4). The goal of this study was to examine changes in physiological parameters of the cell types after stress; therefore patch-clamp recording was

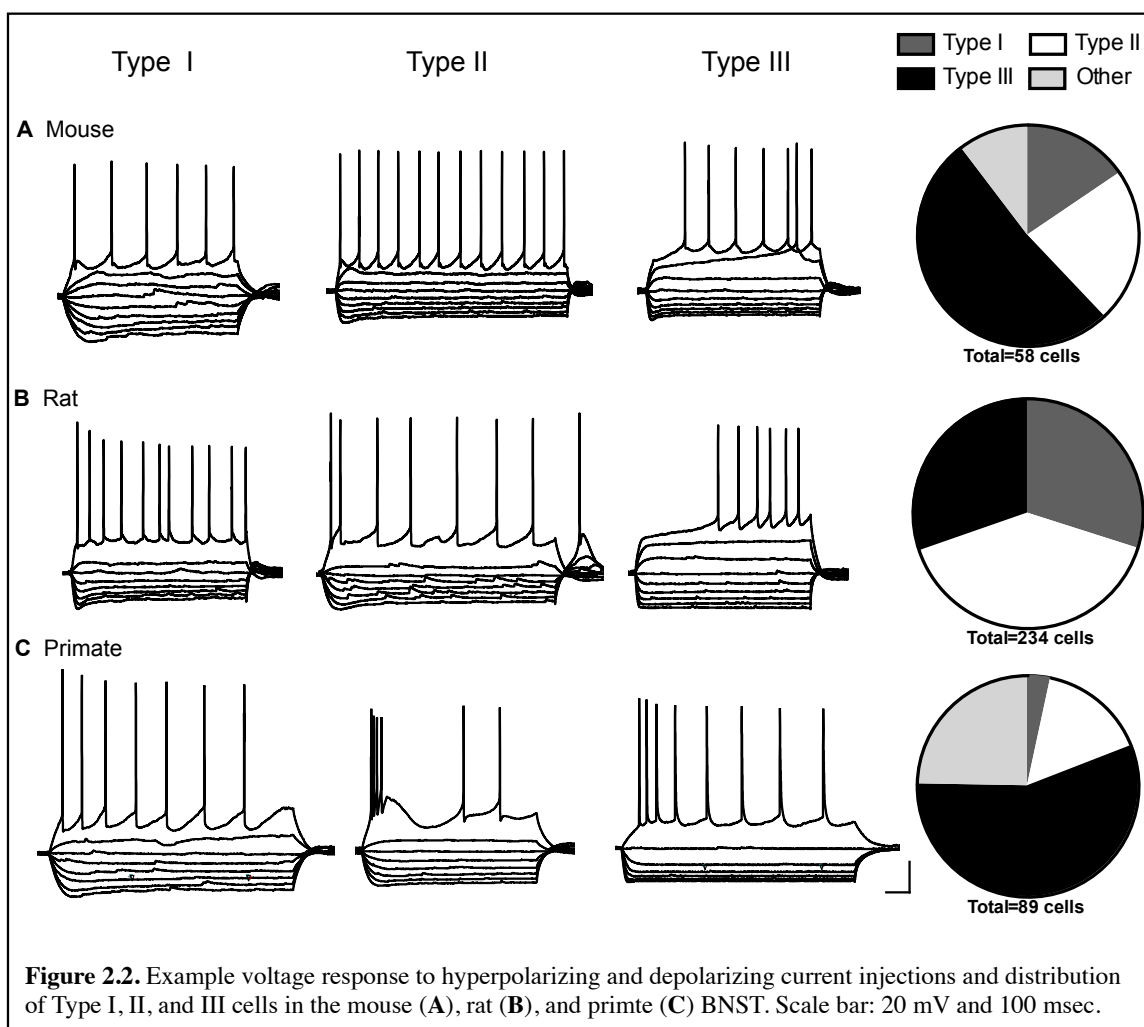
only attempted for cells with a healthy (round, smooth membrane) appearance, potentially skewing the distribution of cell types. However, the distribution of cell types for these two samples was not significantly different from one another (**Table 2.1**; $\chi^2 = 4.345, P > 0.05$). For this reason, we combined Sample 1 and Sample 2 to create a large sample population to compare with the mouse and primate cells.

	Type I (RS)	Type II (LTB)	Type III (fIR)	LF (also Type III)
Hammack <i>et al</i> 2007	29%	55%	16%	
Hazra <i>et al</i> 2011	11%	66%	21%	
Rodriguez-Sierra <i>et al</i> 2013**	24.9%	54.5%	16.5%	1.7%*
Sample 1	34.6%	38.3%	27.1%	
Sample 2	26%	41%	33%	
<p>Table 2.1. Distribution of cell types seen in the anterolateral BNST of the rat from previously published papers and two recent samples. The following are acronyms given by Rodriguez-Sierra <i>et al</i> (2013): RS, regular spiking; LTB, low-threshold bursting; fIR, fast inward rectification; LF late firing. *These cells are most likely a part of the classification of Type III in our classification scheme. **From the anterior BNST, including the medial BNST and ventral BNST.</p>				

The distribution of cell types that we observed in this large sample is different from what has been reported in previous publications (**Table 2.1**; Hammack *et al.*, 2007; Hazra *et al.*, 2011; Rodriguez-Sierra *et al.*, 2013). The current sample has a significantly different distribution of cell types from that seen in the original study describing the three cell types ($\chi^2 = 28.09, P < 0.0001$). However, the distribution of observed cell types differs between other publications as well (**Table 2.1**; Hazra *et al.*, 2011; Rodriguez-Sierra *et al.*, 2013). Importantly, there is a common trend in all populations observed; Type II cells are the most

common cell type, ranging from 38 - 66% of BNST_{ALG} neurons. The relative percentage of Type I and Type III cells varies between studies with Type I cells reported as 11 - 34.6% of the population and Type III cells as 16 - 33% of the population.

The classification of cells types in the BNST has been independently verified by a group separate from Rainnie and colleagues (Rodriguez-Sierra et al., 2013). Here, Pare and colleagues looked at the distribution of cell types in the anterior BNST across the anterolateral, anteromedial, and anteroventral regions. They reported low-threshold bursting (LTB; matching the description of Type II cells) and regular spiking (RS; matching the description of Type I cells) were the two most common cell types found in

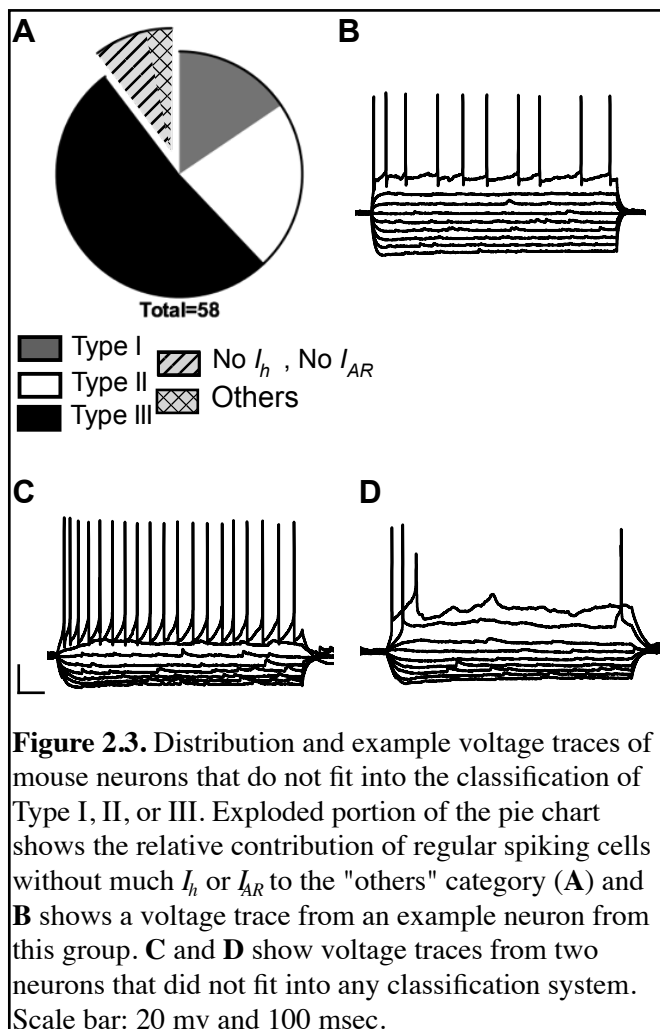


all three regions of the anterior BNST. A cell type matching the Rainnie classification of Type III cells was defined as fast-inward rectifiers (fIR) and found primarily in the anterolateral portion of the BNST. Additionally, a separate population of cells was termed late-firing (LF), due to a prolonged latency to the first action potential in response to a depolarizing current trace, and was only found in the region of the oval nucleus. From our experience recording in the BNST_{ALG}, these late firing neurons also exhibit a strong fast inwardly rectifying current in response to hyperpolarizing current injections, suggesting they are part of the Type III classification. Additionally, there does not seem to be a separate population of Type III neurons from our sample that have a particularly long duration to the first spike (data not shown). For this reason, we believe that the LF neurons defined by Pare and colleagues can be reasonably termed Type III cells.

Distribution of cell types in the mouse

In 58 cells from 13 mice, neurons with similar electrophysiological phenotypes as rat Type I, Type II, and Type III cells were observed. However, there was a different distribution of these cells types than what was observed in the rat, both from previously published data (Hammack et al., 2007; Hazra et al., 2011) and from this sample (**Figure 2.2 A-B**). Unlike the rat where Type II cells were the most prominent phenotype, Type III cells were the most common cell type in the mouse BNST_{ALG} with 51% of neurons exhibiting strong fast-inward rectification (**Figure 2.2B**).

Additionally, 6 out of the 58 cells recorded did not adequately meet the criteria for Type I, Type II, or Type III cells, and were therefore labeled as “other”. Of those 6, 4 cells (about 7% of total population) were regular spiking neurons similar to Type I and Type III cells, however, unlike Type I cells, they did not exhibit a depolarizing-sag, and unlike Type III cells, they did not exhibit fast-inward rectification with hyperpolarizing current



injection (**Figure 2.3B**). The final 2 mouse cells were different from each other but did not conform to any of the previously defined cell types. Both cells had strong fast-inward rectification with hyperpolarizing current injections and a small, slow depolarizing sag with hyperpolarizing current injection (**Figure 2.3C-D**). Although the fast-inward rectification would point toward Type III cells, Type III cells of the rat and those Type III cells defined in the mouse have either no depolarizing-sag or a small but fast depolarizing sag. Additionally, the spiking pattern was different than the typical Type III cell. The first cell (**Figure 2.3C**) showed a regular spiking neuron with a small amount of spike frequency

adaptation, however, the action potential waveform was unique with a large fast after hyperpolarization (fAHP). This unique spike characteristic and slow depolarizing-sag made this cell stand apart from Type III neurons while the fast-inward rectification prevented it from being classified as a Type I neuron. The second cell (**Figure 2.3D**) exhibited spike accommodation. In the rat, 5 out of 70 Type I cells and 1 out of 71 Type III cells showed spike accommodation, however, in these cases the fast-inward rectification and depolarizing-sag corresponded more closely to that of a particular cell type. For this reason, this cell is not included in the cell classification.

Distribution of cell types in the rhesus macaque

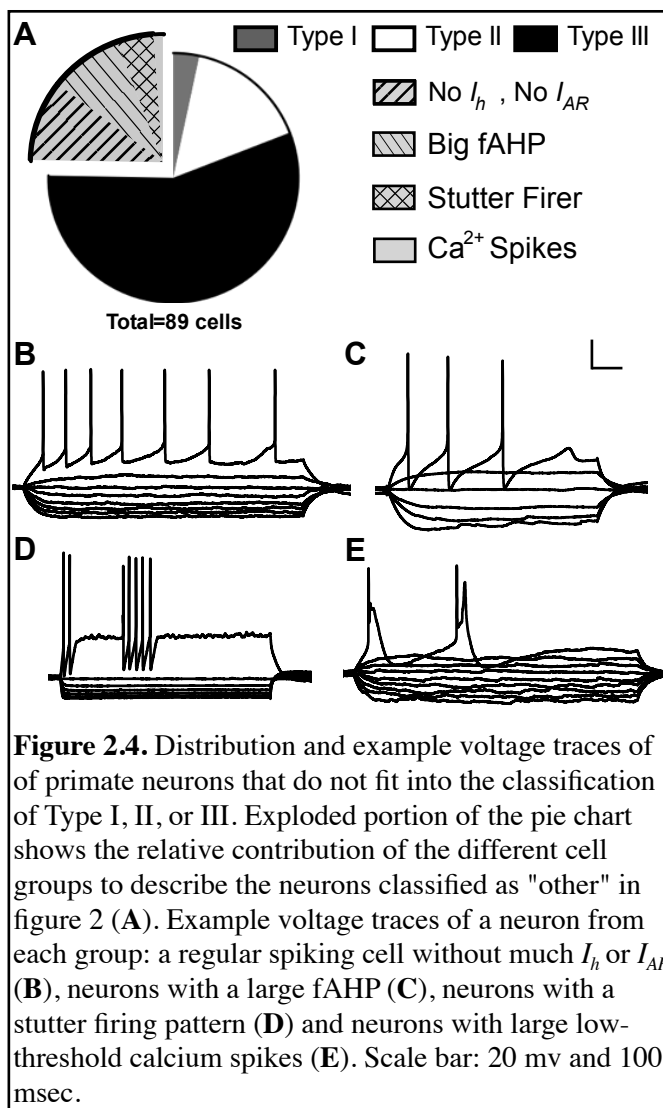
Neurons with similar electrophysiological phenotypes as rat Type I, Type II, and Type III cells were observed in the BNST_{ALG} of the rhesus macaque, however only 75% of the cells recorded could be classified in those terms (**Figure 2.2C**). Here we recorded 89 neurons in the region of the BNST_{ALG} from 9 rhesus macaques. Like the mouse, the majority of primate neurons (56%) recorded fit the description for Type III cells.

Only 3 out of 89 cells in the primate had the characteristics of Type I cells including a regular firing rate, depolarizing-sag in response to hyperpolarizing current, and little-to-no fast inward rectification. There were 9 other cells (about 10% of the total population) that showed a regular firing rate similar to that of Type I cells, however these cells did not exhibit the depolarizing-sag indicative of an I_h current or strong fast-inward rectification (**Figure 2.4B**). For this reason, these cells did not fit into any of the previously defined cell types.

Whereas Type II cells are the most common cell type in the rat, only about 16% of the cells in the primate could be classified as Type II. Type II cells are characterized by the presence of an observable I_T current, either in the form of rebound firing after the hyperpolarizing step, or calcium waves visible at the beginning of the depolarizing step, with or without additional spikes. Type II cells of the rat also have a depolarizing-sag with hyperpolarizing current injections, indicative of an I_h current. Here, only 6 cells (6.8 %)

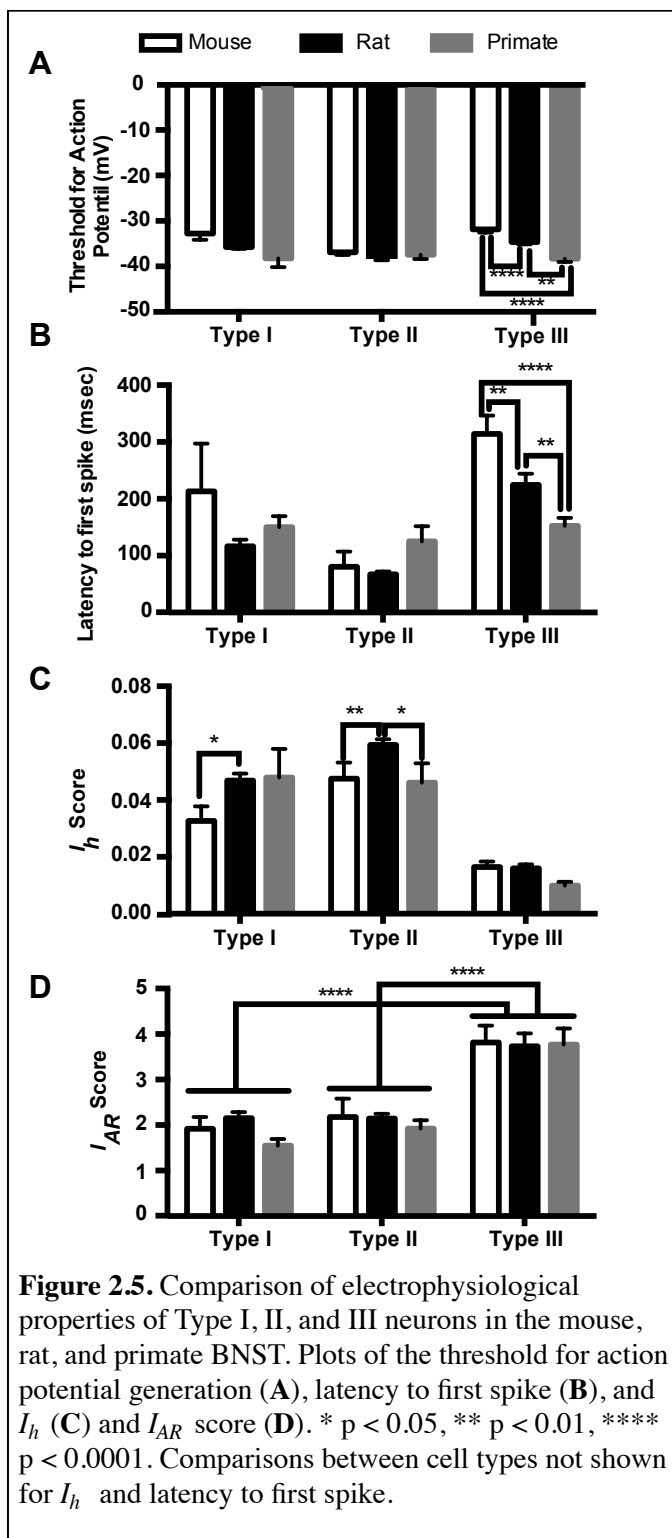
had an observable I_T current and depolarizing-sag. However, because the defining characteristic of a Type II cell is the presence of an I_T current, we included cells that showed an I_T current but little-to-no depolarizing-sag. Using these criteria, 14 (15.9 %) of the primate neurons were classified as Type II.

The 25% of cells from the primate that did not fit into the Type I, Type II, or Type III classification can be grouped into 4 categories: regular spiking without indications of I_h or I_{AR} (as described above, about 10% of total population), cells with a large fAHP and



mAHP (about 9% of total population), cells with a stuttering firing pattern (about 4.5% of total population), and cells with low-threshold calcium spikes (about 1% of the population; **Figure 2.4**). Unlike the cell with the large fAHP seen in the mouse, the cells with the large fAHP in the primate had a relatively slow firing rate, with an average of 5.8 spikes / sec compared to 20 spikes / sec in the mouse cell with the large fAHP (**Figure 2.4C**). Additionally, these cells had a prominent mAHP that comes in before the offset of the fAHP. Besides the slow firing rate and large fAHP, these cells differed from one another in other characteristics; 4 out of the 8 large fAHP primate cells exhibited the depolarizing sag indicative of an I_h current, and 1 cell exhibited fast inward rectification in response to the hyperpolarizing current. However, the consistent action potential waveform set these cells apart from the other cell types. Another group of primate cells that did not fit into a particular cell type exhibited repeated low-threshold calcium spikes in response to one depolarizing current pulse (**Figure 2.4E**). One of the 2 cells that exhibited this phenotype also had spontaneous low-threshold calcium spikes when held at -60 mV (not shown). The relative low frequency of this cell type calls into question its prevalence in the primate BNST_{ALG}; more recordings would need to be done to confirm if there is indeed a consistent presence of these cells.

The final group of primate cells seen displayed a unique stutter-firing pattern (**Figure 2.4D**). These cells looked similar to Type III cells in that they have little-to-no depolarizing sag in the hyperpolarizing traces and have strong inward rectification, however, they do not exhibit a regular firing pattern. At the more depolarizing current steps, these cells will fire 2 to 7 action potentials at a rate ranging from 37 to 75 spikes / sec followed by an abrupt break in firing before another period of rapid spikes. These spikes



did not occur on calcium waves but rather were initiated from a steady membrane potential. Additionally, each spike was followed by a large fAHP and mAHP, giving them a unique spike waveform. Of the outlying cell types, this was the most unique phenotype that has never been reported in the mouse or rat BNST.

Type I cells

Type I cells were defined in the rat as cells that exhibit an I_h current resulting in a depolarizing sag in response to hyperpolarizing current injections and do not exhibit burst firing activity (Hammack et al., 2007). Although cells that meet this description were found in both the mouse and primate BNST_{ALG}, the proportion of cells classified as

Type I was significantly reduced from that seen in the rat (Figure 2.2). However, the Type I cells that were seen did not differ much between species. Although there was a significant

effect of species for threshold for action potential and latency to first spike (threshold: $p < 0.001$, $F_{(2,334)} = 7.733$; latency to first spike: $p < 0.05$, $F_{(2,340)} = 3.646$), multiple comparisons test did not show a difference between species in the Type I cells (**Figure 2.5A-B**). Additionally, there was only a significant effect of cell type for the I_{AR} score, with Type I and Type II cells having a significantly lower I_{AR} score than Type III cells in all species (Type I: 2.11 ± 0.12 , Type II: 2.12 ± 0.10 , Type III: 3.76 ± 0.19 ; $p < 0.0001$, $F_{(2,229)} = 13.66$; **Figure 2.5D**). The depolarizing sag in the mouse Type I cells was generally smaller than that seen in the rat. This is reflected in the I_h score: here, although there was not an overall effect of species ($p = 0.067$, $F_{(2,344)} = 2.726$), a multiple comparisons test showed mouse Type I cells had a significantly smaller I_h score than rat Type I cells (mouse Type I: 0.033 ± 0.006 , rat Type I: 0.047 ± 0.002 , $p < 0.05$; **Figure 2.5C**). Although there was no significant difference in I_h score between mouse and primate, this result is inconclusive due to the small sample size of Type I cells in the primate.

Type II cells

Type II cells are distinguished by the presence of a voltage-dependent calcium current (I_T) that causes re-bond firing after hyperpolarizing current injections and / or a low-threshold calcium wave at the beginning of depolarizing current injections. Type II cells are the most common cell type in the rat but only represented about 22 and 16 % of the cells in the mouse and primate BNST_{ALG}, respectively. This included any cell that had any indication of a prominent I_T , including cells that did not show an I_h . As mentioned previously, only half of the primate Type II cells exhibited any signs of an I_h current. Unsurprisingly then, the I_h score was significantly smaller in primate Type II cells than the I_h score in Type II rat cells (primate Type II: 0.046 ± 0.010 , rat Type II: 0.059 ± 0.002 ; $p <$

0.05 **Figure 2.5C**). Unlike the primate Type II cells, 13 of the 14 Type II cells in the mouse BNST_{ALG} had a depolarizing sag in response to hyperpolarizing current. However, the I_h score in the mouse Type II cells was also significantly smaller than that in the rat (mouse Type II: 0.033 ± 0.006 , $p < 0.05$).

In addition to the variable size of the I_h current, the I_T current also varied between species. Often the I_T in the mouse Type II cells was only seen as a small depolarizing current at the beginning of the depolarizing step without initiating action potentials (**Figure 2.2A**). In contrast, primate Type II cells often had many spikes on top of the low-threshold calcium wave (**Figure 2.2C**). Rebound firing after a hyperpolarizing current injection was most common in rat Type II cells with 8 out of 33 (about 24%) exhibiting rebound firing, followed by primate Type II cells with 2 out of 14 cells (about 14%) and mouse Type II cells with 1 out of 13 cells (about 8%). This is another indication that the I_T current was potentially weaker in mouse Type II cells than that in rat and primate Type II cells.

There was no significant difference in the threshold for action potential generation, latency to first spike, or I_{AR} score between Type IIs of different species. However, there was an interesting difference in how the threshold for action potential generation in Type II cells relates to other cell types within the same species. In addition to the significant effect of species on threshold, there was a significant effect of cell type ($p < 0.001$, $F_{(2, 334)} = 7.33$) and the interaction of the two ($p < 0.01$, $F_{(4, 334)} = 3.738$). In both the mouse and rat, Type II cells had a lower threshold for action potential generation than Type III cells (mouse Type II: 36.9 ± 0.6 mV, mouse Type III: -31.9 ± 0.7 mV, $p < 0.001$; rat Type II: -38.2 ± 0.4 mV, rat Type III: $-34.6 \pm .5$ mV, $p < 0.0001$) and in this sample of rat neurons, Type II cells also had a lower threshold for action potential than the Type I cells (rat Type

I: -35.8 ± 0.6 mV, $p < 0.001$). In contrast, there was no significant difference in threshold for action potential between Type I, Type II, and Type III cells in the primate (Type I: -39.0 ± 2.0 , Type II: -37.4 ± 1.0 , Type III: -38.5 ± 0.7 ; **Figure 2.5A**).

Type III cells

The physiological profile of Type III cells seems to be the most conserved across the three species. Type III cells were seen in all three species and were the most common cell type in both the mouse and primate (**Figure 2.2**). In all species, there was a significant population of cells in the BNST that displayed a strong fast inward rectification in response to hyperpolarizing current injection without low-threshold spiking or burst firing activity. This was reflected in the significantly higher I_{AR} score seen in Type III cells compared to Type I and Type II cells as reported above (**Figure 2.5D**). Additionally, these neurons tended to only exhibit a small, fast depolarizing sag indicative of either little-to-no I_h current or an I_h current with faster kinetics than that found in Type I and Type II neurons. This is reflected in the smaller I_h score seen in all Type III cells regardless of species (**Figure 2.5C**). There was also a significant effect of cell type in the I_h score ($p < 0.0001$, $F_{(2, 344)} = 52.3$) and multiple comparisons showed that Type III cells had a significantly smaller I_h score than both Type I (Type III: 0.014 ± 0.001 , Type I: 0.046 ± 0.002 ; $p < 0.0001$) and Type II cells (Type II: 0.057 ± 0.002 ; $p < 0.0001$). Type II cells also had a significantly bigger I_h score than Type I cells ($p < 0.0001$).

Although the electrophysiological phenotype of Type III neurons from the three species looked very similar, there were some notable differences. First, the latency to the first spike with a depolarizing current injection was significantly different across the three species, with the latency shortening from mouse (314 ± 32.3 msec) to rat (224.5 ± 19.7

msec) to primate (152.4 ± 14.0 msec; mouse vs rat $p < 0.01$; mouse vs primate $p < 0.0001$; rat vs primate $p < 0.01$, **Figure 2.5B**). A long latency to the first spike is indicative of a voltage-dependent potassium current such as I_A or I_D (Molineux et al., 2005; Francesconi et al., 2009). It is possible that the amount of I_A or I_D current varies significantly between species. However, the threshold for action potential generation also varied significantly across the three species, decreasing from mouse (-31.9 ± 0.7 mV) to rat (-34.6 ± 0.5) to primate (-38.5 ± 0.7 mV; mouse vs rat $p < 0.01$, mouse vs primate $p < 0.0001$, rat vs primate $p < 0.0001$; **Figure 2.5A**). The shorter latency to the first action potential in primate Type III cells may be due to a lower threshold for action potential generation.

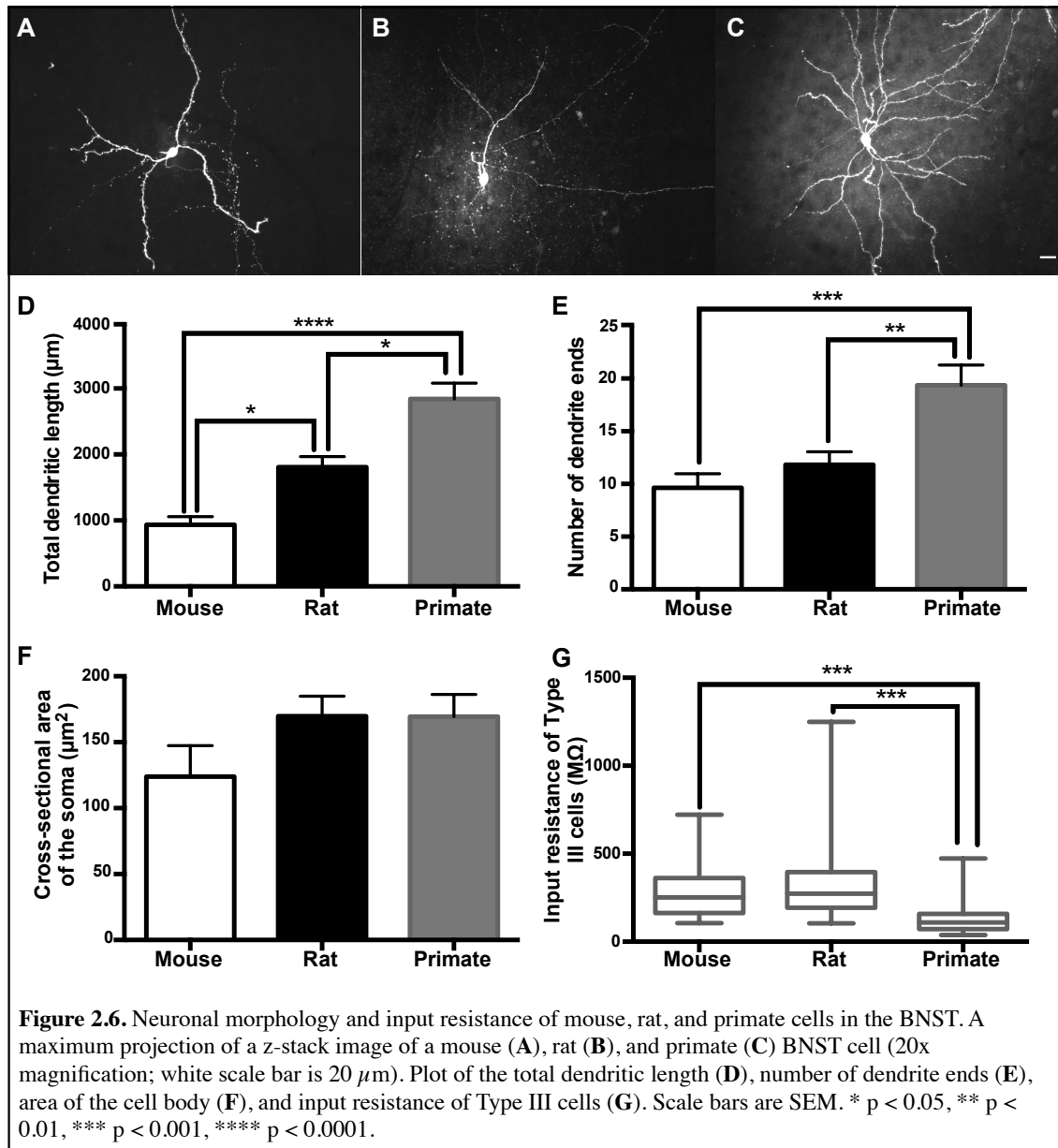
Morphology and Input Resistance

In previous studies our lab has not seen any correlation between morphology of rat BNST_{ALG} neurons and their electrophysiological phenotype, and another independent study confirmed this observation (Rodriguez-Sierra et al., 2013). For this reason, we presented data on the neuronal morphology with all cell types combined. Here, 12 mouse, 11 rat, and 14 primate biocytin-filled neurons were traced using NeuroLucida (MicroBrightField, Colchester, VT) to provide us with a measure for total dendritic length, number of dendrites, number of dendritic branches, and cross-sectional area of the soma. There was a significant difference between the dendritic length in all species ($p < 0.0001$, $F_{(2,33)} = 24.86$) with primate neurons having significantly longer total dendritic length (2842 ± 241.3 μm) than the neurons from the rat (1810 ± 159.5 μm ; $p < 0.01$) and mouse (935.9 ± 122.4 μm ; $p < 0.0001$) and the rat having significantly longer total dendritic length than the neurons from the mouse ($p < 0.05$; **Figure 2.6D**). As seen in **figure 2.6A-C**, the dendritic arbor of the representative primate neuron was more complex than that of the neurons from the

mouse and rat BNST_{ALG}. Although there was no difference in the number of dendrites between species ($p = 0.13$, $F_{(2,33)} = 2.195$), there was a significant difference in the number of dendritic ends ($p < 0.001$, $F_{(2,33)} = 10.57$) with primate neurons having significantly more (19.36 ± 1.93 ends) than both mouse (9.64 ± 1.32 ends, $p < 0.001$) and rat (11.82 ± 1.23 ends, $p < 0.01$), indicating there was more dendritic branching in the primate BNST_{ALG} neurons (**Figure 2.6E**). On the other hand, there was no difference in the cross-sectional area of the soma between cell types ($p = 0.16$, $F_{(2,33)} = 1.915$; **Figure 2.6F**).

Because a change in morphology is tightly associated with a change in input resistance, we looked to see if the input resistance of the membrane in primate cells decreased as would be predicted by the increase in the size of the dendritic arbor (Barrett and Crill, 1974). Interestingly, there was a significant difference in input resistance between species ($p < 0.01$, Kruskal-Wallis statistic = 15.82), however, a multiple comparisons test showed that only the input resistance from the rat BNST_{ALG} neurons was significantly higher than the input resistance from the primate cells (rat: 349.8 ± 12.9 M Ω , primate: 340.4 ± 37.8 M Ω ; $p < 0.01$). However, input resistance is highly variable, especially between multiple cell types, so we analyzed the input resistance of the Type III cells alone. Here, there was a significant difference in input resistance of type III cells ($p < 0.0001$, Kruskal-Wallis statistic = 49.52), and both the mouse (277.1 ± 27.0 M Ω) and rat Type III cells (336.1 ± 28.1 M Ω) had a significantly higher input resistance than the Type III cells from the primate (141.1 ± 15.0 M Ω , $p < 0.0001$ for both comparisons; **Figure**

2.6G).



Discussion

Here we showed that neurons matching the electrophysiological phenotype of the cell types defined in the rat BNST_{ALG} were also found in the BNST_{ALG} of the mouse and rhesus macaque, however, these cell types were found in different proportions than has previously been reported in the rat BNST_{ALG} and did not adequately describe the entire

population. In the rat, Type II cells were the most common cell type ranging from 38 – 66% of all BNST_{ALG} neurons. In contrast, they only represented 22% of mouse neurons and 16% of primate BNST_{ALG} neurons. In both the mouse and primate, Type III cells, with strong fast inward rectification were the most common cell type observed describing 51% of cells in the mouse and 56% in the primate compared to only 27% of cells in the rat BNST_{ALG}. Moreover, although there were similarities in the physiological properties of BNST neurons across species, this study indicated that the overall landscape of the BNST_{ALG} in the primate and even mouse may significantly differ from that of the rat.

Despite both being in the Murinae subfamily, there were significant differences in the neuronal properties and cell type distribution between the BNST_{ALG} of the mouse and the rat. Overall, the mouse BNST cells were harder to differentiate from one another to be classified into cell types. Although there were some Type II cells in the mouse defined by the low-threshold calcium wave at the beginning of a depolarizing current injection, the calcium waves were not as pronounced as what is often seen in the rat. This makes Type II cells harder to differentiate from Type I cells. Similarly, the smaller I_h in mouse Type I cells made Type I cells hard to differentiate from Type III cells. It is possible that cells in the mouse BNST are not actually distinct populations based on their electrophysiological phenotypes, but rather exist on a continuum. The classification system for the rat BNST_{ALG} was originally based on the electrophysiological phenotype alone (Hammack et al., 2007), however, it has gained credence since it was shown that BNST_{ALG} neurons segregate into three distinct groups based on their mRNA expression profile for ion channel subunits using an unbiased cluster analysis and discrimination function (Hazra et al., 2011). Using single cell RT-PCR, and eventually using single cell micro arrays, we could better

determine if distinct cell types in the mouse can be identified based on electrophysiological characteristics.

Similarly, although there was only a small percentage of Type I cells seen in the primate and mouse relative to what is seen in the rat, it is possible that the other regular firing neurons that lack significant I_h and I_{AR} actually segregate into Type I cells when looking at mRNA expression profile and electrophysiological characteristics together. Appreciating how the genetic expression profile of BNST_{ALG} neurons relates to the electrophysiological phenotype will be a crucial step in understanding the heterogeneity of the nucleus. We have begun to make important strides in this area in the rat. For example, serotonin receptor subtypes have been shown to be differentially expressed depending on cell type in the rat (Hazra et al., 2012). Additionally, only 15-47% of Type I and 35-53% of Type II cells express CRF mRNA whereas 81-95% of Type III neurons express the mRNA for CRF (Dabrowska et al., 2011; 2013a) and are differentially effected by chronic stress (Dabrowska et al., 2013b). These data suggest that Type III cells in the rat BNST_{ALG} play a different role in the circuit than Type I and Type II cells. However, it seems unlikely that cells from the mouse and primate BNST_{ALG} that fit into the classification of Type III cells are also primarily CRF neurons. In characterizing the CRF-*tomato* transgenic mouse, CRF neurons in the BNST were described as fitting into the description of Type I, Type II, and Type III cells with majority of CRF neurons not fitting into any of these categories (Silberman et al., 2013). Also, Type III cells were much more common in the primate than in the rat, however, there is no evidence that the primate BNST contains more CRF neurons than the rat. This suggests that Type III neurons may not play the same role in the circuit

in mouse, rat, and primates. Using single cell PCR or microarray in the mouse and primate BNST would help us to understand how these cell types compare across species.

Importantly, cells with similar mRNA expression profiles across species will not necessarily display the same electrophysiological profile. Even with similar distributions of ion channels, differences in the morphology of the neurons can have significant effects on electrophysiological properties. For example, neurons with a larger dendritic surface area tend to have a smaller input resistance (Barrett and Crill, 1974). Here, we saw that there was a significant increase in total dendritic length of BNST_{ALG} neurons from mouse, to rat, to primate (**Figure 3.6D**). Interestingly, despite the drastic difference in dendritic length between mouse and primate, only rat BNST_{ALG} neurons had significantly higher input resistance than the primate. When only looking at the input resistance of Type III cells, we saw that the primate Type III neurons had a significantly lower input resistance than the mouse and rat (**Figure 3.6G**). With a more complex and extensive dendritic arbor, primate BNST neurons have a wider receptive field than BNST neurons from the mouse and rat, but a lower input resistance would suggest it would take more input to affect the cell.

In addition to affecting the input resistance, the change in dendritic arbor across species could have a drastic effect on the firing pattern of the cells. A change in dendritic surface area compared to soma/axon surface area, can significantly change the action potential waveform and firing properties of neurons, even without a change in types and densities of ion channels (Mainen and Sejnowski, 1996). With all else remaining equal, an increase in the ratio of dendritic membrane area to axo-somatic area results in a slowing of the firing rate and eventually leads to a burst-firing pattern. This could potentially

contribute to the different firing patterns seen in Type II cells between mouse, rat, and primate. In the mouse, even with a prominent low-threshold calcium spike at the beginning of the depolarizing current injection, the cells tended to have a regular firing pattern. In contrast, the rat and primate Type II cells displayed more burst firing, with primate Type II cells showing the most burst firing (**Figure 3.2**). This could be due to a change in voltage-gated calcium channels. However, the difference in dendritic arbor suggests that the differences seen in the electrophysiological phenotypes across species could at least in part be attributed to the increase in the dendritic arbor, without significant changes in ion channel distribution.

The increase in dendritic arborization between mouse, rat, and rhesus macaque BNST_{ALG} neurons suggests an increase in receptive field for these cells. Importantly, there is evidence that the connectivity of the BNST with the rest of the brain has been largely conserved from rodents to non-human and human primates alike with the major fiber tracks consisting of 1) the posterior bundle (stria terminalis), connecting the BNST to the thalamus and lateral amygdala, 2) the ventral bundle (ansa peduncularis), connecting the BNST to the basal forebrain and medial amygdala (Dong et al., 2001a; 2001b; Dong and Swanson, 2004; Avery et al., 2014; Krüger et al., 2015), and 3) the anterior bundle which connects the BNST to the nucleus accumbens and prefrontal cortex, but in primates, this fiber track extends to include the orbitofrontal cortex (OFC), a region important in decision making (Krüger et al., 2015). The vmPFC, which includes the OFC, has recently been shown to modulate the BNST in humans (Motzkin et al., 2015) providing further support for a structural and functional connection between the OFC and BNST in humans. Lesions of the OFC in monkeys alter anxiety behavior and BNST metabolism, suggesting that this

connection between the BNST and OFC exists in non-human primates as well (Fox et al., 2010). The BNST's connection with the OFC is unique to primates because the OFC does not exist in rodent brains (Preuss, 1995). Additionally, the stria terminalis, or posterior bundle, extends beyond the amygdala and into the temporal pole in humans (Avery et al., 2014; Krüger et al., 2015). These new connections of the primate BNST to other areas of the brain not observed in rodents suggests an evolutionary pressure for the primate BNST to adapt to an increase in diversity of inputs and projections as the cortex expands and diversifies. It is possible this pressure resulted in an increase in the complexity of the dendritic arbor and the heterogeneity of cell types. Interestingly, the electrophysiological phenotype in the BNST_{ALG} in the primate is potentially less diverse than that seen in the rat, as the majority of cells look like Type III neurons. However, there are also potential new cell types from those seen in the rat, such as the stutter firers and neurons with large fAHPs (**Figure 3.4**). Most likely, single cell microarray analysis in the primate would reveal an increase in heterogeneity in cell type compared to the rat.

Importantly, our sample of BNST neurons from the mouse and rat only came from male animals whereas both male and female rhesus macaques were used for the primate sample. No study has systematically examined the difference in the physiology of the female BNST, however there is evidence for sex-differences in the BNST in humans (Allen and Gorski, 1990), and the BNST of the rodent has been implicated in sex-differences in mood and anxiety disorders (Bangasser, 2013). Interestingly, a recent study on the structural and functional connectivity of the human BNST showed a significantly greater overall structural connectivity of the BNST in females compared to males (Avery et al., 2014). If this holds true in primates and rodents, it would be interesting to compare the

neuronal morphology of BNST cells from males and females to determine if there is a corresponding increase in dendritic arborization in the BNST of females.

In conclusion, we have described the electrophysiological phenotype of neurons in the BNST_{ALG} of the mouse and rhesus macaque using the classification system set forth for neurons in the rat BNST_{ALG}. Both the mouse and primate BNST_{ALG} contained cells that closely fit the description of Type I, Type II, and Type III cells in the rat, however they were observed in significantly different proportions. Additionally, we showed that the dendritic arbor becomes significantly more complex from the mouse to the rat to the primate. These data suggest electrophysiological cell types should be used with caution when looking at different species. In the rat, these electrophysiological phenotypes seem to reflect functional differences in the role the cells play in the circuit. However, there are multiple factors that go into the electrophysiological phenotype of a neuron, including morphology and ion channel expression and distribution. Although the electrophysiological phenotypes of the cells differ across species, there could still be analogous cell types in the different species, potentially better classified based on their mRNA expression profile. Future studies should examine cell types in the BNST_{ALG} of the mouse, rat, and primate using a combination of electrophysiology and single cell PCR or microarray to better understand differences in the circuitry across species.

Chapter 3: Comparison of cell types in the oval and anterodorsal BNST

Introduction

The BNST is composed of multiple nuclei, defined by differential inputs and projections (Dong et al., 2001b; Dong and Swanson, 2004). The small size of the nuclei and the lack of clear boundaries between regions has made studying the roles of these nuclei difficult. Recently however, progress has been made in gaining insight into the differential roles of the oval nucleus of the BNST (ovBNST) and the surrounding undifferentiated area, the anterodorsal BNST (adBNST) (Kim et al., 2013). Here, Deisseroth and colleagues targeted the ovBNST using a cre-dependent eNpHR3.0 virus in the BNST of dopamine receptor 1a (Drd1a::Cre) mice. This allowed for optogenetic control of neurons restricted to the ovBNST. In contrast, the adBNST was targeted by an injection of a eNpHR3.0 virus into the anterior basolateral amygdala (BLA), which resulted in the optogenetic control of glutamatergic fibers in the adBNST. Using these paradigms, Deisseroth and colleagues showed that inhibition of these two subnuclei had opposing effects on anxiety-like behavior; the ovBNST acts to promote anxiety-like behavior whereas the adBNST attenuates it. The differential roles of these two adjacent regions of the BNST suggest that the neurons that compose these nuclei may also be distinct from one another.

Previous work from our lab has defined three cell types in the BNST_{ALG} based on their electrophysiological phenotype, Type I-III (Hammack et al., 2007; Hazra et al., 2011). These cell types have been shown to be differentially distributed throughout the lateral, medial, and ventral portions of the anterior BNST (Rodriguez-Sierra et al., 2013), however, no one has directly compared the distribution of cell types in the ovBNST with the

adBNST. In this study, we compared the electrophysiological properties of neurons found in these two regions to further understand the organization of the BNST as a whole.

As shown by the use of the *Drd1a::Cre* mouse line, transgenic mice can be a useful tool for studying the composition of neurons in different regions of the BNST (Kim et al., 2013). Here, we used a *Thy1-YFP* transgenic mouse line to characterize a small population of neurons in the BNST restricted to the region of the adBNST. Interestingly, the majority of neurons labeled by this transgenic line have been shown to be glutamatergic projection neurons (Feng et al., 2000; Sugino et al., 2005). The majority of neurons in the BNST_{ALG} are GABAergic (Day et al., 1999; Kudo et al., 2012), however, the presence of these YFP-labeled neurons in the *Thy1-YFP* mouse suggests the possibility of a population of glutamatergic neurons in the adBNST that are not found in the ovBNST. Here, we used *in vitro* whole-cell patch clamp recording to characterize the electrophysiological properties of the *Thy1-YFP* neurons in the adBNST and single cell RT-PCR to determine if these neurons are indeed glutamatergic. By comparing the distribution of cell types in these two regions and using the *Thy1-YFP* to characterize a population of cells restricted to the adBNST, this study aimed to determine ways in which the composition of the ovBNST and adBNST differ.

Methods

Animal Subjects

All procedures were approved by the Institutional Animal Care and Use Committee of Emory University and were in compliance with National Institute of Health guidelines. For rats, recordings were performed in male Sprague-Dawley rats aged 30 – 60 days old (Charles River Laboratories, Wilmington, Massachusetts). For mice, recordings were

performed in male *Thy1*-YFP-expressing mice (B6.Cg-Tg HJrs/J-Thy1-YFP, Jackson Labs, Bar Harbor, Maine) aged 60 – 80 days old. Animals were housed in same-sex groups, two to four rats per cage and two to five mice per cage. Rats and mice were maintained on a 12:12-hour light-dark cycle with *ad libitum* access to food and water. Surgeries were performed on male *Thy1*-cre-expressing mice (FVB/N-Tg(Thy1-cre)1Vln/J-006143, Jackson Labs, Bar Harbor, Maine) aged 64 days old.

Preparation of BNST slices

BNST slices were obtained as previously described for rats (Hammack et al., 2007). The same procedure was done for mice. Briefly, animals were decapitated under isoflurane anesthesia (Med-Vet International, Mettawa, IL, USA), and the brains were rapidly removed and placed in ice-cold kynurenic acid-based “cutting solution” which contained (mM): NaCl (130), KCl (3.50), KH_2PO_4 (1.10), MgCl_2 (6.0), CaCl_2 (1.0), glucose (10), supplemented with kynurenic acid (2.0). Coronal sections containing BNST were cut 350- μm thick using a Leica VTS-100 vibratome (Leica Microsystems, Bannockburn, IL, USA). Slices were kept in oxygenated cutting solution at room temperature for 1 h before transferring to regular artificial cerebrospinal fluid (ACSF) containing (mM): NaCl (130), NaHCO_3 (30), KCl (3.50), KH_2PO_4 (1.10), MgCl_2 (1.30), CaCl_2 (2.50), and glucose (10). Slices were kept in oxygenated ACSF for at least 30 min before recording.

General patch clamp recording procedures

Individual slices were transferred to a recording chamber mounted on the fixed stage of a Leica DM6000 FS microscope (Leica Microsystems Inc., Bannockburn, IL) equipped with an IR sensitive CCD camera (Orca ER, Hamamatsu, Tokyo Japan), allowing for use of differential interference contrast (DIC) optics and infrared illumination to

identify individual BNST neurons. *Thy1*-YFP cells were visualized with 488 nm fluorescence illumination and targeted for whole cell recording. The slices were maintained fully submerged and continuously perfused with oxygenated 32 °C ACSF with a speed of ~2 ml/min. All recordings were confined to the dorsal anterolateral cell group including the oval, juxtacapsular, and anterolateral nucleus of the BNST (BNST_{ALG}). Location of recording was approximated by the cell's relative proximity to the internal capsule and anterior commissure visualized at low magnification (3.5x). Cells were determined to either be in the region of the ovBNST or adBNST (**Figure 3.1**). In the *Thy1*-YFP mouse, recordings were confined to region of the anterior BNST with *Thy1*-YFP cells. This was consistently in the adBNST very near where the anterior commissure and internal capsule meet. Whole-cell recordings were obtained using recording pipettes pulled from borosilicate glass and having a resistance of 4-6 MΩ. Pipettes were filled with a potassium-based patch solution containing the following (mM): K-gluconate (130), KCl (2), HEPES (10), MgCl₂ (3), K-ATP (2), Na-GTP (0.2), and phosphocreatine (5), and was titred to pH 7.3 with KOH and 290 mOsm. Biocytin (0.35%) was added to the patch solution in some cases to allow for histochemical processing and neuronal reconstruction.

Analysis of electrophysiological properties

Basic electrophysiological properties were collected from each cell recorded. A DC holding current was injected to maintain the membrane potential at -60 mV in current clamp. To characterize neurons, a series of 10 hyperpolarizing and depolarizing, 750 or 1000 ms long, square-wave current steps were injected and scaled so that the peak negative voltage deflection was to approximately -80 mV (Hammack et al., 2007; Hazra et al., 2011). Then, linear ramps of depolarizing current were injected, lasting 250 ms, and scaled

to depolarize the neuron to elicit a single action potential. Data were analyzed by importing the raw voltage and current traces into Matlab (The MathWorks, Natick, MA, USA) using scripts provided with sigTOOL (<http://sigtool.sourceforge.net/>, developed at King's College London) and processed with customized scripts (available upon request).

Analysis of electrophysiological properties was completed as described elsewhere (Ehrlich et al., 2012). Briefly, input resistance (R_{in}) was calculated using the deflection in response to the smallest hyperpolarizing current step (approx. 5 mV) and calculated as the ratio of peak voltage deflection to the current injected. The I_h score was calculated as the ratio of the magnitude of I_h (measured as peak deflection at the beginning of the trace minus steady state at the end) to the membrane potential at the point of peak deflection in the trace with the peak deflection closest to -80 mV (smaller positive values indicate less voltage deflection due to I_h). The I_{AR} score was calculated as the ratio of the peak magnitude of the smallest hyperpolarizing trace to the difference between the peak-magnitude of the two most hyperpolarizing traces (larger values indicate more inward rectification). Action potential rise time and decay time were measured as time from 10% to 90% of maximum amplitude with linear interpolation between samples to increase resolution. Action potential half-width was measured as the width of action potential at half-maximal amplitude with linear interpolation to increase resolution. The amplitude of the action potential was measured as the difference between the peak voltage of the spike and the threshold for action potential, and the fast after-hyperpolarization (fAHP) was measured as the difference between the minimum voltage immediately following the spike and the threshold for action potential.

Neuronal morphology

Histochemical processing

Some of the patched neurons were labeled with biocytin (Sigma Aldrich, St Lois, MO, USA) included in the patch pipette recording solution and used for neuronal reconstruction as previously described (Ryan et al., 2014). After neurons were recorded for at least 10 min, slices were fixed in 10 % buffered formalin (Fisher Scientific, Hanoverpark, IL, USA) for 12-72 h, and then transferred to cryoprotectant for storage at -20 C. After three consecutive 10 min washes in 0.05 M phosphate buffered saline (PBS), slices were permabilized for 30 min in PBS and 0.5 % Triton-X 100 (Sigma-Aldrich, St Louis, MO, USA). Slices were then treated with Alexa Fluor 488 or 568- conjugated Streptavidin (Invitrogen, Grand Island, New York, USA) diluted to 1:1,000 in PBS with Triton-X for 36 – 48 h at 4 C. Slices were then washed 2 times for 1 h each in 0.05 M PBS and washed for 10 min in 0.05 M phosphate buffer. The slices were then mounted on glass slides, air dried for 3 – 12 h, and cover-slipped with mowiol mounting medium (Sigma-Aldrich, St Louis, MO, USA).

Neuronal reconstruction

Z-stack images of the filled neurons were taken at 20x magnification with a 0.3 μm step size using a Leica DM5500B spinning disk confocal microscope (Leica Microsystems Inc.m Bannockburn, IL, USA) and SimplePCI data acquisition software (Compix, Sewickley, PA). For neuronal reconstruction, the dendritic arbor, cell body, and, if seen, the axon of each neuron was reconstructed by hand using Neurolucida neuron tracing software (MicroBrightField, Colchester, VT).

Single cell RT-PCR

For single cell RT-PCR, at the end of a recording session, the cell cytoplasm was aspirated into the patch recording pipette containing $\sim 5 \mu\text{l}$ of RNase-free patch solution under visual control, by applying gentle negative pressure. The contents of the patch pipette were then expelled into a microcentrifuge tube containing $5 \mu\text{l}$ of the reverse transcription cocktail (Applied Biosystems, Foster City, CA, USA). The RT product was amplified in triplicate and screened for 18S rRNA. Only those cell samples that were positive for 18S rRNA were subjected to amplification with primers. The procedure used to determine mRNA transcript expression in single cells has been described (Hazra et al., 2011; 2012). The sequence for the oligonucleotide primers of the 5-HT receptor subtypes, VGLUT, and GAD used in this study have been described elsewhere (Guo et al., 2009; Dabrowska et al., 2013a). Polymerase chain reaction (PCR) products were visualized by staining with ethidium bromide and separated by electrophoresis in a 1% agarose gel.

Controls for the RT-PCR

PCR conditions were optimized using total RNA isolated from rat BNST_{ALG} so that a PCR product could be detected from (250 pg– 1 ng) of total RNA without contamination caused by non-specific amplification. For each PCR amplification, sterile water was used instead of cDNA as a control for contaminating artifacts. A second control with no RT present was also used in each amplification step. Both the controls gave negative results throughout the study. All primers were intron-spanning to exclude amplification of genomic DNA.

Test of Thy1-Cre mouse line

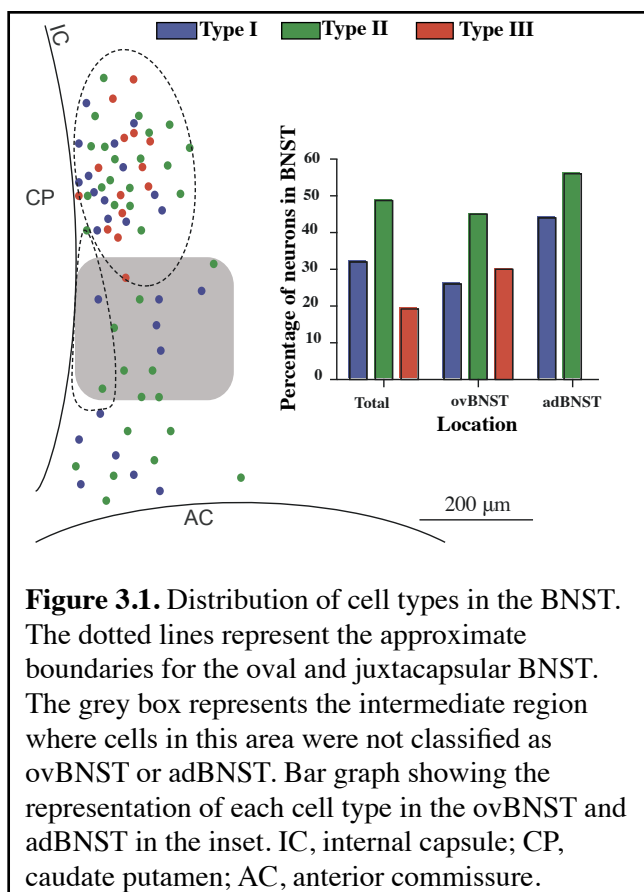
To address the question if the *Thy1*-cre mouse line labels the same neuronal population as the *Thy1*-YFP line, we bilaterally injected a cre-dependent virus (AAV5-hsyn-DIO-eGFP) into the BNST_{ALG} of two male (64 days old) *Thy1*-cre transgenic mice in order to label the cre-expressing neurons with enhanced green fluorescent protein (eGFP). Mice were anesthetized with an IP injection of Dexdomitor (Orion Pharma, Espoo, Finland) and Ketamine hydrochloride (Bioniche Pharma, Bogart, GA, USA) mixture and infused with AAV (500 nl) during stereotaxic surgery according to the following coordinates from Bregma: AP =0.5, ML \pm 2.1, DV -4.2 with the 15 ° coronal angle to avoid the lateral ventricle. Four weeks after the AAV injection, mice were anesthetized with an overdose of sodium pentobarbital (Butler- Schein Animal Health, Dublin, OH, USA), and then transcardially perfused with ice-cold 0.05 M PBS (pH 7.4) followed by 4% paraformaldehyde in PBS. Brains were removed and post-fixed in 4% paraformaldehyde in PBS overnight and then cryo-protected in 30% sucrose in PBS overnight at 4 °C. Coronal brain sections (50 μ m) were cut on a Leica CM 3050S cryostat and stored at 20 °C in a cryoprotective medium consisting of 25% glycerol and 30% ethylene glycol in 0.05 M phosphate buffer until needed. After three consecutive 10 min washes in 0.05 M PBS and a final 10 min wash in 0.05 M PB, slices containing the BNST were mounted on glass slides, air dried for 3 – 12 h, and cover-slipped with mowiol mounting medium (Sigma-Aldrich, St Louis, MO, USA). The virus injection site was visualized using a Leica DM5500B spinning disk confocal microscope (Leica Microsystems Inc.m Bannockburn, IL, USA) and SimplePCI data acquisition software (Compix, Sewickley, PA). The eGFP expression profile was compared to the expression of YFP in the BNST of *Thy1*-YFP mice.

Statistical analysis

Statistical analyses were carried out using Prism 6 (GraphPad Software Inc., San Diego, CA). The electrophysiological properties of the cell types within the ovBNST were compared using a one-way analysis of variance (ANOVA) with Tukey's multiple comparison tests. The electrophysiological properties of Type I and Type II cells in the ovBNST and adBNST were compared using a two-way ANOVA with Sidak multiple comparison tests with cell type and location as the two factors. Populations with unequal variance were transformed (\log_{10}) and then analyzed. A t-test was used to compare the electrophysiological properties of the *Thy1*-YFP and non-YFP cells with Welch's correction when the populations had significantly different variance. An alpha level of 0.05 was used for all tests, and variance is reported as the standard error of the mean (SEM) unless otherwise noted.

Results

Comparison of cell types in the oval and anterodorsal BNST in the rat



Distribution of cell types

We recorded the electrophysiological properties of neurons in the BNST_{ALG} using *in vitro* whole-cell patch clamp electrophysiology. The location of the neurons recorded was approximated relative to the anterior commissure and internal capsule using a low magnification (3.5x) in order to visualize the dorsal BNST in the tissue slice in its entirety (**Figure 3.1**). Neurons were classified into

Type I, Type II, or Type III cells based on visual discrimination of current clamp traces showing the voltage response to hyperpolarizing and depolarizing square-wave current injections as previously described (Hammack et al., 2007). We obtained stable recordings from 69 neurons: 43 of those were in the region of the ovBNST and 21 were in the region of the adBNST. Because there are no anatomical markers defining the borders of the ovBNST and adBNST, we created a transition zone for which any cell in this area was not classified as in either location. There were 5 cells that fell in this region.

Overall, 33.3 % of the neurons recorded were classified as Type I, 46.4 % classified as Type II, and 20.3 % were classified as Type III, however, this distribution differed when looking at the ovBNST and adBNST separately (**Figure 3.1**). The clearest difference is that 13 of the 14 Type III cells identified were in the region of the ovBNST, describing 30.2 % of cells in the ovBNST. The remaining Type III cell was in the transition area between the ovBNST and adBNST and there were no Type III cells found in the region of the adBNST (**Figure 3.1**). In the ovBNST, 27.9 % of the cells were Type I and 41.9 % of the cells were Type II. In contrast in the adBNST, 47.6 % of the cells were Type I and 52.4 % were Type II.

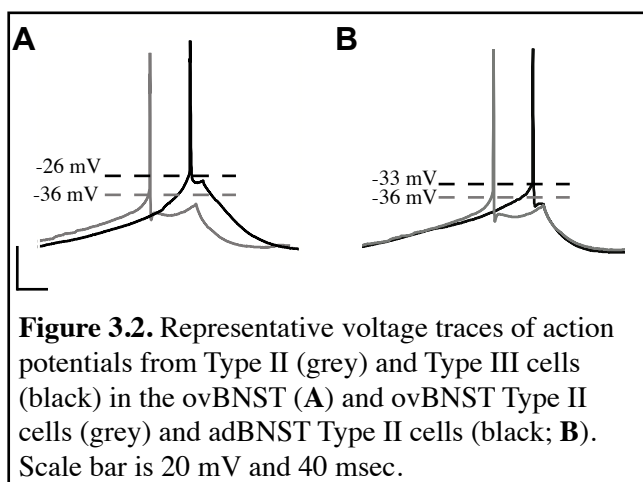


Figure 3.2. Representative voltage traces of action potentials from Type II (grey) and Type III cells (black) in the ovBNST (A) and ovBNST Type II cells (grey) and adBNST Type II cells (black; B). Scale bar is 20 mV and 40 msec.

Comparison of Type I, II, and III cells in the oval BNST

Here, we compared the electrophysiological properties of Type I, II, and III cells in the region of the ovBNST (summarized in **Table 3.1**). First, the resting membrane potential (RMP) was significantly

different between cell types in the ovBNST ($p < 0.0001$, $F_{(2,35)} = 15.03$) with Type III cells having a lower RMP than both Type I ($p < 0.001$) and Type II cells ($p < 0.0001$). As expected, there was a significant difference in the amplitude of the I_h current between cell types represented by the I_h score ($p < 0.0001$, $F_{(2,39)} = 25.77$). Type III cells had a significantly lower I_h score than both Type I and Type II cells in the ovBNST ($p < 0.0001$ for both comparisons). There was also a significant difference in the amount of fast inward

rectification observed between cell types in the ovBNST represented by the I_{AR} score ($p < 0.01$, $F_{(2,40)} = 7.081$). Here,

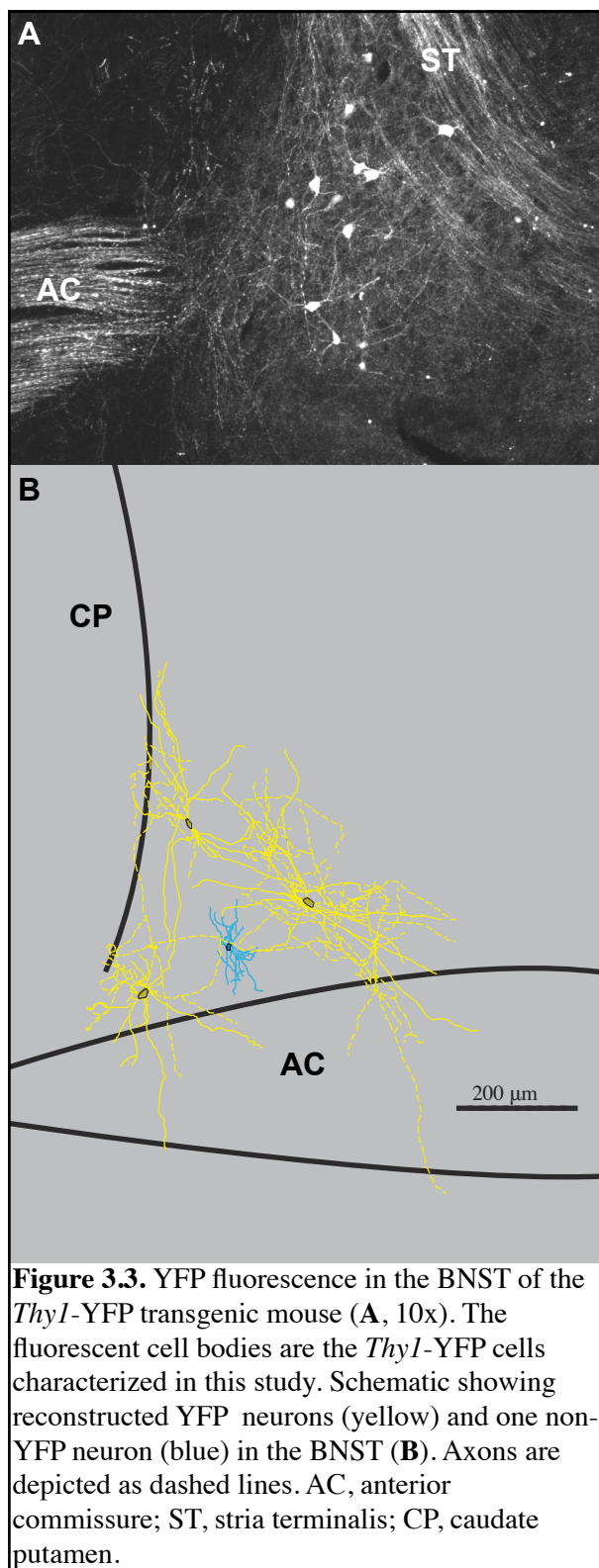
Type III cells had a significantly larger I_{AR} score than Type II cells in the ovBNST ($p < 0.01$). Finally, there was a significant difference in the threshold for action potential between cell types in the ovBNST ($p < 0.05$, $F_{(2,36)} = 5.049$). The threshold for action potential generation was significantly higher in Type III cells compared to Type II cells in the ovBNST (**Figure 3.2A**, $p < 0.01$).

	ovBNST			adBNST	
	Type I (n = 12)	Type II (n = 18)	Type III (n = 13)	Type I (n = 10)	Type II (n = 11)
RMP (mV)	-58.6 ± 1.8^3	-57.4 ± 1.2^3	$-67.3 \pm 1.2^{1,2}$	-52.3 ± 4.1	-56.0 ± 1.1
R_{in} (M Ω)	271.3 ± 36.0^A	284.4 ± 35.9	242.7 ± 30.9	466.0 ± 82.3^O	270.0 ± 31.1
I_h score	$0.051 \pm 0.006^{3,A}$	0.051 ± 0.004^3	$0.012 \pm 0.003^{1,2}$	0.033 ± 0.006^O	0.055 ± 0.003
I_{AR} score	2.46 ± 0.38	1.82 ± 0.13^3	4.00 ± 0.76^2	2.22 ± 0.53	1.34 ± 0.12
Spike					
Threshold (mV)	-35.8 ± 0.96	$-37.2 \pm 3.5^{3,A}$	-33.1 ± 1.1^2	-33.7 ± 1.4	-33.5 ± 1.2^O
Amplitude (mV)	66.2 ± 3.0	63.4 ± 2.4^A	64.6 ± 3.1	61.3 ± 3.1	53.2 ± 3.7^O
Half- width (ms)	0.789 ± 0.041	0.785 ± 0.040^A	0.898 ± 0.054	0.916 ± 0.052	0.942 ± 0.059^O
Rise time (ms)	0.327 ± 0.014	0.357 ± 0.073	0.348 ± 0.023	0.376 ± 0.019	0.381 ± 0.020
Decay time (ms)	0.784 ± 0.059	0.773 ± 0.070	0.919 ± 0.068	0.923 ± 0.108	0.898 ± 0.081
fAHP Diff (mV)	-4.49 ± 1.38	-8.20 ± 1.31	-3.97 ± 1.28	-7.67 ± 1.78	-3.81 ± 1.59

Table 3.1. Electrophysiological properties of Type I, Type II, and Type III cells in the ovBNST and adBNST. Values are expressed as mean \pm SEM. Superscripts following the SEM indicates cell type and location differences based on analysis of variance (ANOVA, $p < 0.05$) 1 = Type I in ovBNST, 2 = Type II in ovBNST, 3 = Type III in ovBNST, A = same cell type in adBNST, O = same cell type in ovBNST.

Comparison of Type I and Type II cells of the oval and anterodorsal BNST

Although both Type I and Type II cells were found in the ovBNST and adBNST, we wanted to determine if there were any differences in the electrophysiological properties of these neurons based on location. For a summary of the electrophysiological properties see **Table 3.1**. There was a trend toward a significant effect of location ($p = 0.08$, $F_{(1,47)} = 3.167$) and an interaction of cell type and location ($p = 0.07$, $F_{(1,47)} = 3.415$) on input resistance. Here, Type I cells in the adBNST had a significantly higher input resistance than Type I cells in the ovBNST ($p < 0.05$). Additionally, there was a significant effect of cell type ($p < 0.05$, $F_{(1,46)} = 5.177$) and an interaction of cell type and location ($p < 0.05$, $F_{(1,46)} = 4.594$) on the I_h score, with Type I



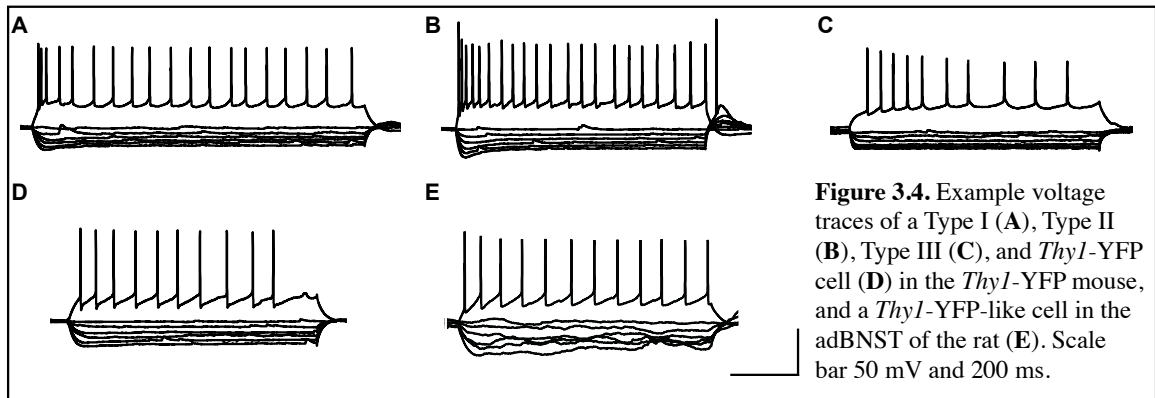
cells in the adBNST having a significantly lower I_h score than Type I cells in the ovBNST. In this sample, Type I and Type II cells in the ovBNST do not differ significantly in their I_h score, however, Type I cells in the adBNST have a significantly lower I_h score than Type II cells in the adBNST ($p < 0.05$).

These BNST cells also differed based on location in their action potential threshold and waveform. There was a significant effect of location on the threshold for action potential generation ($p < 0.05$, $F_{(1,44)} = 6.845$). Here, Type II cells in the adBNST had a significantly higher threshold for action potential generation than the Type II cells in the ovBNST ($p < 0.01$). Similarly, there was a significant effect of location on the action potential half-width ($p < 0.01$, $F_{(1,44)} = 8.304$) and amplitude ($p < 0.05$, $F_{(1,44)} = 6.088$). Again it was the Type II cells that differed by location: Type II cells in the adBNST had a significantly wider ($p < 0.05$) and shorter ($p < 0.05$) action potential than Type II cells in the ovBNST (**Figure 3.2B**).

Characterization of a novel subpopulation of neurons in *Thy1-YFP* transgenic mice

*Electrophysiological phenotype of *Thy1-YFP* cells*

The *Thy1-YFP* transgenic mouse has a small population of YFP cells confined to the adBNST, very close to the corner created by the anterior commissure and internal capsule and at the base of the stria terminalis (**Figure 3.3**). Here, we used fluorescent-guided whole-cell *in vitro* patch clamp electrophysiology to record the electrophysiological phenotype of 33 YFP cells. We also recorded from 16 non-YFP cells in the immediate vicinity of the YFP cells for comparison.



If appropriate, cells were classified into Type I, Type II or Type III as described previously (Hammack et al., 2010), however many of the cells did not fit into those classification schemes. In fact, the YFP cells did not fully resemble any of the three cell types (**Figure 3.4**). The YFP cells had a small slow depolarizing sag in response to hyperpolarizing current indicative of an I_h current. Additionally, there was a moderate amount of fast inward rectification in the YFP cells that is not as strong as the inward rectification commonly seen in Type III cells. Finally, these neurons do not show any indications of burst or rebound firing common to Type II cells. The YFP cells could potentially be classified as Type I neurons, however, there was a unique action potential waveform common to all YFP cells created by the presence of a large fast after-hyperpolarization (fAHP) followed by a medium after-hyperpolarization (mAHP) after each action potential (**Figure 3.4**). Of the 16 non-YFP cells recorded, 3 could be classified as Type I, 6 as Type II, and 1 as Type III. The remaining 6 non-YFP cells had a similar electrophysiological phenotype as the YFP cells.

Comparison of Thy1-YFP cells and non-YFP cells

	<i>Thy1</i> -YFP cells (n = 33)	Non-YFP cells (n = 16)
R_{in} (M Ω)	267.8 \pm 16.8 ^{###}	353.1 \pm 49.0
I_h score	0.032 \pm 0.003 [#]	0.043 \pm 0.007
I_{AR} score	1.60 \pm 0.08 [#]	2.03 \pm 0.21
Spike		
Threshold (mV)	-33.7 \pm 0.7*	-36.6 \pm 0.9
Amplitude (mV)	69.4 \pm 1.9	70.7 \pm 3.8
Half-width (ms)	0.759 \pm 0.031	0.814 \pm 0.066
Rise time (ms)	0.327 \pm 0.010 [#]	0.398 \pm 0.037
Decay time (ms)	0.639 \pm 0.029 [#]	0.797 \pm 0.083
fAHP Diff (mV)	-15.48 \pm 0.61 ^{**##}	-9.59 \pm 1.61

Table 3.2. Electrophysiological properties of *Thy1*-YFP and non-YFP cells. Values are expressed as mean \pm SEM. Superscripts following the SEM in the *Thy1*-YFP column indicates differences in means (*) and variance (#) from the non-YFP cells. * $p < 0.05$, ** $p < 0.01$, *** $p < 0.001$. Same pattern for #.

Here we compared basic electrophysiological properties of the *Thy1*-YFP cells with the non-YFP cells in the same area (**Table 3.2**). Overall, the *Thy1*-YFP cells had a more consistent electrophysiological phenotype than the non-YFP cells. For example, although there was no significant difference in the average input resistance between the two groups ($p = 0.12$), the input resistance of the YFP cells was significantly less variable than the input resistance of the non-YFP cells (F test, $p < 0.001$). Similarly, the YFP cells had a less variable I_h and I_{AR} score than the non-YFP cells (F test, $p < 0.05$ for both comparisons).

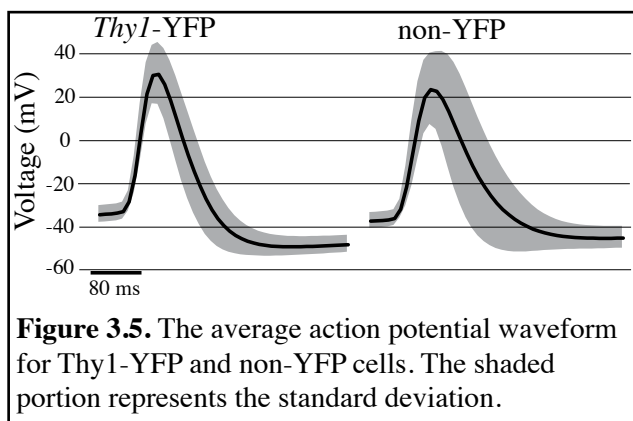


Figure 3.5. The average action potential waveform for *Thy1*-YFP and non-YFP cells. The shaded portion represents the standard deviation.

This reduction in variability for these properties supports the idea that the *Thy1*-YFP mouse labels a group of cells with a consistent electrophysiological phenotype.

The action potential waveform was the most obvious difference between the

Thy1-YFP and non-YFP cells. Here, we compared the action potential amplitude, half-width, rise time, decay time and threshold for action potential generation

Gene	<i>Thy1</i> -YFP (%) n = 12	non-YFP (%) n = 9
VGLUT1	75	0
VGLUT2	67	0
VGLUT3	0	0
VGLUT	83	0
GAD67	0	100
GAD65	0	0
GAD	0	100
5-HT _{1A}	0	67
5-HT _{1B}	0	0
5-HT ₅	0	22
5-HT G_{v6}	0	67
5-HT _{2A}	0	56
5-HT _{2C}	0	0
5-HT G₄	0	56
5-HT ₄	33	0
5-HT ₆	50	0
5-HT ₇	0	0
5-HT G_s	67	0

Table 3.3. The percentage of YFP and non-YFP cells that express the mRNA for the gene indicated.

between the *Thy1*-YFP and non-YFP cells (Figure 3.5 and Table 3.2). There was no significant difference in the average rise time or decay time of the action potential, however, there was a significant difference in the variance of these factors ($p < 0.001$ and $p < 0.01$ respectively) with the *Thy1*-YFP cells having a more consistent action potential waveform (Figure 3.5). The *Thy1*-YFP cells also had a significantly higher threshold for action potential than the non-YFP cells ($p < 0.05$). Finally, the amplitude of the fAHP in *Thy1*-YFP cells

was significantly larger ($p < 0.01$) and less variable ($p < 0.01$) than the fAHP in non-YFP cells.

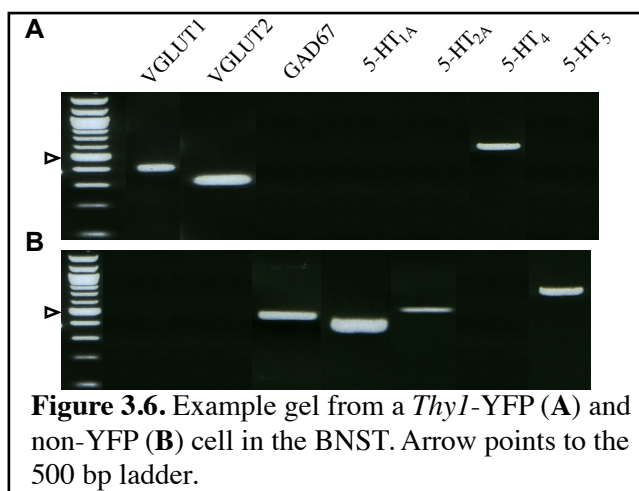
Potential Thy1-YFP-like cells in the adBNST of the rat

In order to determine if there are neurons in the rat that resemble the electrophysiological phenotype of *Thy1*-YFP cells, we looked for cells in the rat BNST that had the characteristic spike waveform of *Thy1*-YFP cells. There were 4 Type I cells from the rat that exhibited a similar spike waveform with an fAHP of -13.1 ± 1.4 mV on average (Figure 3.4E). Importantly, all four of these cells were found in the adBNST.

Single cell RT-PCR

Here, we wanted to determine if the YFP cells in the *Thy1*-YFP mouse were GABAergic or glutamatergic neurons. To do this, we used single cell RT-PCR to screen for the presence of vesicular glutamate transporter (VGLUT) 1, 2, and 3, which would indicate the neuron is glutamatergic, and glutamate decarboxylase (GAD) 65 and 67, which would indicate the neuron is GABAergic. Of the 9 non-YFP neurons screened with single cell RT-PCR, all 9 expressed the mRNA for GAD67 and no cells expressed the mRNA for GAD 65 or any of the VGLUT transcripts, indicating all of the non-YFP neurons in this area are GABAergic (**Table 3.3** and **Figure 3.6**). In contrast, of the 12 *Thy1*-YFP neurons screened with single cell RT-PCR, 10 YFP neurons expressed the mRNA for VGLUT1 and/or VGLUT2, and no cells expressed the mRNA for VGLUT3 or either of the GADs. This provides evidence that the *Thy1*-YFP mouse line labels a small population of glutamatergic neurons in the adBNST of the mouse.

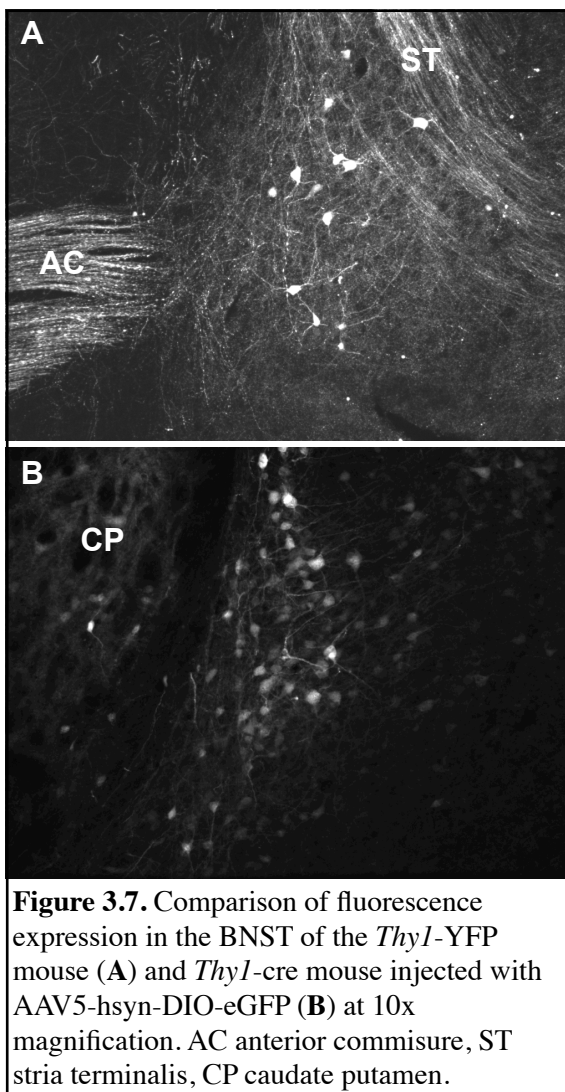
In addition to differences in neurotransmitter systems, we wanted to determine if the *Thy1*-YFP and non-YFP cells expressed different serotonin receptor subtypes. Interestingly, there was no overlap in the serotonin receptor subtype expressed in the *Thy1*-YFP cells with those expressed in the non-YFP cells (**Table 3.3** and **Figure 3.6**). Of the *Thy1*-YFP cells, 4 expressed the mRNA for 5-HT₄ and 6 expressed the mRNA for 5-HT₆. Importantly, both 5-HT₄ and 5-HT₆ are generally



coupled to the G_s signaling cascade. Alternatively, of the non-YFP cells, 6 expressed the mRNA for 5-HT1A and 2 expressed the mRNA for 5-HT1B, both of which are coupled to the $G_{i/o}$ signaling cascade. Additionally, 5 of the non-YFP cells expressed the mRNA for 5-HT2A, a G_q -coupled receptor subtype.

Attempt at targeting Thy1-YFP with the Thy1-cre mouse and a cre-dependent virus

In order to target the *Thy1*-YFP cells in the BNST alone, we used a cre-dependent adeno-associated virus that expressed eGFP injected into the BNST of *Thy1*-cre transgenic mice. Although both the cre and YFP are under the *Thy1* promoter in these mouse lines, the transgene was randomly inserted into the genome, and the location of the insertion site determines the expression profile (Feng et al., 2000). We compared the fluorescent expression pattern of the *Thy1*-cre mice with the injected virus to the expression pattern of the YFP in the *Thy1*-YFP mouse to determine if both mouse lines have the transgene expressed in the same cell population in the BNST. The *Thy1*-cre mouse had a much more diffuse labeling of cell bodies in the BNST than the *Thy1*-YFP mouse line,



suggesting these two transgenic mice target significantly different cell populations (**Figure 3.7**).

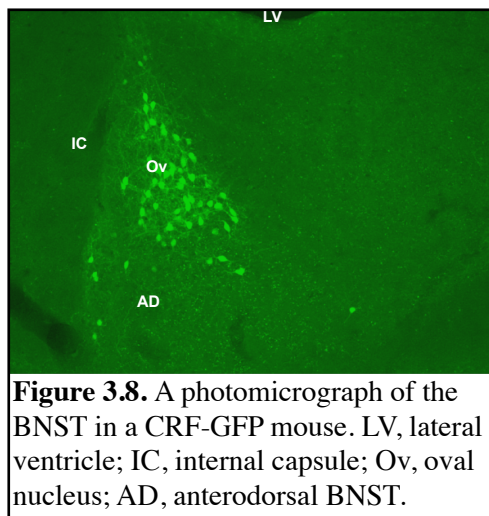
Discussion

The current study provides evidence that the ovBNST and adBNST contain electrophysiologically distinct populations of neurons. The different roles for these two regions of the BNST are only recently coming to light; a recent study suggested that the ovBNST facilitates anxiogenic responses whereas the adBNST facilitates anxiolytic responses (Kim et al., 2013). Although the neurons throughout the anterior BNST have similar electrophysiological phenotypes, some differences have been reported in the distribution of cell types in the anterolateral, anteromedial, and ventral BNST (Rodriguez-Sierra et al., 2013). Here we extended those observations to specifically compare the distribution of cell types found in the region of the ovBNST and adBNST as well as compare the electrophysiological properties of cells of the same cell type in the two regions. Additionally, we showed evidence of a new subpopulation of glutamatergic Type I-like cells in the adBNST using a *Thy1*-YFP transgenic mouse line.

As reported previously, Type II cells were the most common cell type found in the BNST_{ALG} and Type III cells were the least common (Hammack et al., 2007; Rodriguez-Sierra et al., 2013). Interestingly, Type III cells were only found in the region of the ovBNST, and only Type I and Type II cells were found in the adBNST (**Figure 3.1**). This is similar to the results reported by Pare and colleagues (Rodriguez-Sierra et al., 2013). They report a cluster of fast inward-rectifiers (fIR, Type III) in the region of the ovBNST and one cell in the region of the adBNST, however they do not separate out these regions in their analysis. fIR cells were also reported to be found in the medial and ventral BNST

although less frequently. In both this and the current study, fIR (or Type III cells) were shown to be concentrated in the region of the ovBNST. Pare and colleagues also reported another population of cells, termed late firing (LF), was found in the anterolateral BNST, with the distribution of these LF cells seemingly restricted to the ovBNST. We have also seen late firing neurons in our population, however, in all other aspects, these late firing cells are identical to other Type III neurons. In fact, on average the latency to the first action potential in Type III cells is significantly longer than in Type I and Type II cells (**Figure 2.5**). Therefore, we considered the LF neurons to be a subpopulation of Type III neurons. This is supported by their restriction to the region of the ovBNST with the other Type III neurons in the BNST_{ALG}.

The vast majority of Type III neurons in the rat have been reported to express mRNA for CRF (Dabrowska et al., 2011; 2013a). This, combined with our current observation that Type III neurons in the BNST_{ALG} are restricted to the ovBNST, suggests that there is a cluster of CRF neurons located in the oval nucleus. Importantly, there have been multiple reports of a population of CRF-immunoreactive neurons restricted to the oval nucleus (Cummings et al., 1983; Ju et al., 1989). More recently, we have replicated these studies showing a concentration of CRF-immunoreactive cell bodies in the ovBNST of colchicine-treated rats (Dabrowska et al., 2013a). The restriction of the CRF expression to the ovBNST, together with the observation that the Type III neurons are confined to the ovBNST provides further evidence that the Type III neurons represent a population of CRF neurons.



Although Type III neurons almost certainly represent a population of CRF neurons, they do not represent all CRF neurons in the BNST. Different transgenic CRF-reporter mice seem to represent slightly different populations of CRF-mRNA expressing cells (Martin et al., 2010; Silberman et al., 2013). One mouse line seems to show CRF neurons more widely distributed

through the BNST, and the labeled cells are not consistently Type III neurons (Silberman et al., 2013). In contrast, the CRF-reporter mouse created by Owens and colleagues shows a group of CRF neurons restricted to the ovBNST with the majority of these labeled cells exhibiting Type III-like characteristics (Martin et al., 2010; **Figure 3.8**). However, the presence of CRF mRNA does not always accurately predict the presence of the full protein. Indeed, CRF mRNA is also found in a smaller, but significant, portion of Type I and Type II cells in the BNST_{ALG} (Dabrowska et al., 2011; 2013a). Importantly, cell types in the mouse and rat differ significantly, with the mouse BNST containing a much higher percentage of Type III-like cells than the rat. It is possible that the more restricted expression of CRF-labeled cells in the mouse created by Owens and colleagues under-represents CRF neurons in the BNST, and/or the expression pattern seen in the other CRF-reporter mouse used by Silberman *et al* over-represents the expression of CRF neurons. It is important to remember, however, that the distribution of neuropeptides may not be the same in both the mouse and rat.

In the rat, in addition to the population of CRF-immunoreactive neurons seen in the ovBNST, another population exists in the ventral BNST in a region corresponding with the fusiform nucleus (fuBNST) (Cummings et al., 1983; Ju et al., 1989). The current study was restricted to recordings dorsal to the anterior commissure, however Pare and colleagues did report the presence of fIR neurons in the ventral BNST (Rodriguez-Sierra et al., 2013). However, it is reasonable to believe that the CRF neurons in the fuBNST are a separate and distinct population of CRF neurons and, therefore, may not be the same electrophysiological cell type. For example, we have shown that CRF neurons in the ovBNST and paraventricular nucleus of the hypothalamus (PVN) exhibit distinct electrophysiological properties. Furthermore, CRF neurons of the ovBNST and PVN are fundamentally different from one another in that CRF neurons in the ovBNST are GABAergic and those in the PVN are glutamatergic (Dabrowska et al., 2013a). Although we have yet to compare the electrophysiological properties of CRF neurons in the ovBNST and fuBNST directly, we know that these populations of CRF neurons have distinct response profiles to varying stressors (for review see **Table 1.1**). Interestingly, a recent study confirms that CRF neurons in the dorsolateral BNST are GABAergic and suggests that a significant population of the CRF neurons in the ventral BNST are glutamatergic (Nguyen et al., 2015). This supports the hypothesis that Type III neurons in the ovBNST are a distinct population of GABAergic CRF neurons.

Here we showed that Type III neurons in the ovBNST had a significantly lower resting membrane potential than Type I and Type II cells found in the ovBNST as well as a higher threshold for action potential generation than Type II cells in the ovBNST. This is similar to what has been reported previously when comparing the electrophysiological

properties of neurons throughout the BNST_{ALG} (Hazra et al., 2011). The lower resting membrane potential and higher threshold for action potential of Type III cells suggests this population of CRF neurons in the ovBNST requires more excitatory drive than the Type I and Type II cells to become activated. In fact, there is evidence that CRF neurons in the ovBNST are resilient to activation. For example, an intraperitoneal injection of interleukin 1 beta (IL-1 β) results in the expression of the immediate early gene, c-fos specifically in the ovBNST, however, very few of these cells expressed the mRNA for CRF (Day et al., 1999). Instead, the majority of the c-fos labeled cells expressed the mRNA for enkephalin. Although this experiment does not prove that CRF cells are not activated in response to IL-1 β , it does suggest that enkephalin and CRF neurons in the ovBNST are activated at different times. Interestingly, we have shown that 50% of Type II neurons in the BNST_{ALG} express the mRNA for enkephalin (Dabrowska et al., 2013a). Perhaps the Type II enkephalin neurons are easily activated in times of stress due to their higher resting membrane potential, lower threshold for action potential generation, and low-threshold bursting properties, potentially providing a negative feedback to the stress response (Bali et al., 2015). In contrast, Type III CRF cells may require more input to become activated, perhaps only in times of prolonged stress or fear states.

Although Type III cells were only found in the ovBNST, Type I and Type II cells were found in both the ovBNST and adBNST. The ovBNST and adBNST are functionally and anatomically distinct regions, therefore, we wanted to compare the electrophysiological properties of the Type I and Type II cells of the different locations. Indeed, there were differences between cells of the same cell type in the two areas; Type I cells in the adBNST had a higher input resistance and lower I_h score than Type I cells in

the ovBNST, and Type II cells in the adBNST had a higher threshold for action potential generation and a shorter and wider action potential waveform than the Type II cells in the ovBNST (**Table 3.1**). These differences may have arisen due to the different environments of the two regions. For example, the ovBNST and adBNST have different amygdalar inputs; the ovBNST receives input from the lateral and medial central nucleus of the amygdala and the amygdalo-piriform transition area whereas the adBNST receives input from the basolateral amygdala and posterior basomedial amygdala to name a few (McDonald, 1991; Dong et al., 2001a; Kim et al., 2013). Electrophysiological properties are not fixed by cell type, but rather, fluctuate with changes in input and extracellular environment. It is widely understood that differences in the amount of input into a neuron can have a measurable effect on the activity and electrophysiological properties of that neuron. For example, a period of GABA_A-blockade in the CA1 region of the hippocampus results in a reduction in the apparent input resistance and an increase in I_h conductance (Gasselín et al., 2015). Additionally, in the CA3 region of the hippocampus, there is an activity-dependent shift in the basis of action potential repolarization from Kv3 to Kv2 potassium channel dominance, thereby altering action potential waveform in response to changes in input (Steinert et al., 2011). The Type I and Type II cells of the ovBNST and adBNST receive different amounts of input at different times, potentially resulting in the shifts in electrophysiological properties that we observed here.

The neurons in the ovBNST and adBNST seem to play different roles in the anxiety circuit. Inhibition of neurons in the ovBNST, using a cre-dependent eNpHR3.0 virus in the BNST of dopamine receptor 1a (Drd1a::Cre) mice, resulted in a reduction of anxiety-like behavior and respiratory rate whereas inhibiting the BLA input into the adBNST, using a

eNpHR3.0 virus injected into the BLA, resulted in an increase in anxiety-like behavior and respiratory rate (Kim et al., 2013). This suggests the ovBNST promotes anxiety-like behavior whereas the adBNST attenuates it. However it is important to note that the *Drd1a::Cre* mouse is only targeting a subset of neurons in the ovBNST, particularly those that express the D1 receptor. Indeed, there is evidence that CRF neurons in the BNST are depolarized by dopamine, suggesting these are at least some of the neurons targeted in the *Drd1a::Cre* mouse (Silberman et al., 2013). Although Type I and Type II cells are found in the ovBNST and adBNST, and the functional output of these two regions seems to be in opposition to one another, this does not prove that the Type I and Type II neurons in ovBNST act to promote anxiety. It is possible that there is a population of cells in the ovBNST, such as neurons that express enkephalin, that oppose the anxiogenic actions of the ovBNST (**Figure 1.1D**). However, even if Type I and Type II cells in the ovBNST and adBNST both act to oppose anxiety, the neurons in the different regions may still play distinct roles in the circuit.

The ovBNST and adBNST project to different locations, suggestive of the different roles they play in the circuit. The ovBNST primarily projects within the BNST, sending projections to the adBNST, fusiform nucleus, rhombic nucleus, and subcommisural zone, and projects out of the BNST to the substantia innominata, central amygdala, retrorubral field, and parabrachial nucleus (Dong et al., 2001b). In contrast, the adBNST primarily projects outside of the BNST to areas such as the nucleus accumbens, ventral tegmental area, ventrolateral periaqueductal grey, and thalamocortical feedback loops, as well as the same regions the ovBNST projects to outside of the BNST listed above (Dong and Swanson, 2004). These projection patterns suggest the neurons of the oval nucleus

primarily act to control the output of the BNST. In fact, the ovBNST provides GABAergic control over the adBNST (Kim et al., 2013). Although the ovBNST primarily projects within the BNST, the CRF neurons in the ovBNST project out of the nucleus to the paraventricular nucleus of the hypothalamus (Dabrowska et al., 2011). Additionally, we have recent data showing multiple regions in the brain contained projections originating from cells in the ovBNST that were also labeled by the CRF antibody including the nucleus accumbens, hypothalamus, VTA, substantia nigra pars compacta, and the dorsal division of the dorsal raphe, (manuscript submitted; Dabrowska *et al*). However, it is important to remember that the CRF neurons are primarily inhibitory neurons, potentially having dual actions on target regions depending on the inclusion or absence of CRF in the vesicles being released.

Importantly, the vast majority of neurons in the BNST_{ALG} are GABAergic, with the exception of some glutamatergic neurons in the ventral BNST (Georges and Aston-Jones, 2002; Jalabert et al., 2009; Poulin et al., 2009). However, here we show evidence for a potential population of glutamatergic neurons in the adBNST. Over the past fifteen years, Sanes and colleagues have developed transgenic mouse lines that label individual neurons with a fluorescent protein. Many of these lines use the promoter for *Thy1*, a member of the immunoglobulin superfamily that is highly expressed in the nervous system (Feng et al., 2000). Interestingly, each of the 25 independently generated lines expressing a fluorescent protein under the *Thy1* promoter (*Thy1*-XFP) expressed the fluorescent protein in a unique pattern (Feng et al., 2000). The expression pattern is consistent among the offspring of each founder mouse, suggesting the variability in expression is due to differences in the location and / or copy number of the inserted transgene. The *Thy1*-YFP cells from the YFP-H line

used here have been shown to label glutamatergic cells in the amygdala, hippocampus, cingulate cortex, and somatosensory cortex (Sugino et al., 2005), suggesting YFP-labeled cells throughout the brain in this mouse line are glutamatergic. Although the expression profile varies in the different transgenic lines, it is not just a random population of cells being labeled in a single mouse line. Instead, the *Thy1*-YFP line used here labels a particular class of neurons, all of which, presumably are glutamatergic. It was surprising then, to see a small population of *Thy1*-YFP neurons in the adBNST, a region thought to be almost entirely GABAergic (Day et al., 1999; Kudo et al., 2012). Here, we recorded from the *Thy1*-YFP neurons in the adBNST to characterize their electrophysiological properties as well as use single cell RT-PCR to determine if they express mRNA indicative of being glutamatergic neurons.

All of the *Thy1*-YFP cells recorded showed a consistent electrophysiological phenotype. These neurons were regular spiking, similar to Type I cells, but had a large fAHP that made them stand out as a unique population. The *Thy1*-YFP neurons had a less variable input resistance, action potential waveform, and I_h and I_{AR} score than the non-YFP cells. The non-YFP cells in the surrounding area were of varying phenotypes, including cells that resembled the rat Type I, Type II, and Type III cells. Importantly, only one neuron in the adBNST was classified as a Type III cell. This is in stark contrast to the mouse BNST_{ALG} as a whole that contained more than 50% Type III cells (**Chapter 2**). Although we have not specifically examined the distribution of cell types in the mouse BNST_{ALG}, this suggests the Type III cells in the mouse are similarly underrepresented in the adBNST. A few of the non-YFP cells recorded from in this area resembled the *Thy1*-YFP cells, indicating the *Thy1*-YFP cells have a consistent, but not entirely unique

electrophysiological phenotype (**Figure 3.4**). Interestingly, we found 4 Type I cells in the adBNST of the rat that also exhibited the large fAHP characteristic of the *Thy1*-YFP cells in the mouse. This may suggest the presence of this putative glutamatergic cell population in the adBNST of the rat as well as the mouse, however this would need to be confirmed with single cell RT-PCR.

The restriction of the expression of YFP to glutamatergic neurons elsewhere in the brain strongly suggested the YFP neurons seen in the adBNST would also be glutamatergic (Sugino et al., 2005), and here, we used single cell RT-PCR to verify this. As expected, none of the *Thy1*-YFP neurons screened expressed the mRNA for any of the GAD variants (GAD65 or GAD67), and all of the non-YFP cells expressed the mRNA for GAD67 (**Table 3.3**). This suggests the majority (if not all) of the non-YFP neurons in the adBNST are GABAergic and not glutamatergic. Additionally, 10 of the 12 *Thy1*-YFP neurons expressed the mRNA for either VGLUT1 or VGLUT2, suggesting these neurons are indeed glutamatergic. We did not detect the mRNA for any of the VGLUTs or GADs in 2 of the 12 *Thy1*-YFP cells screened. Importantly, since performing these screens, we have changed and optimized our technique for detecting mRNA in neurons (see methods for chapter 4). These results will need to be validated with the new technique before making any firm conclusions, however, from the evidence we have, it seems very likely that the *Thy1*-YFP cells in the adBNST are glutamatergic. Interestingly, we do not know if these glutamatergic neurons are a part of the projections originating from the adBNST. As the rest of the adBNST seems to be GABAergic, these glutamatergic neurons, although perhaps small in number, have the potential to have strong effects at their target sites.

Previously, our lab has shown that serotonin receptor subtype expression varies by cell type in the BNST_{ALG}, resulting in serotonin's ability to differentially modulate Type I-III neurons (Guo et al., 2009). Many cells in the BNST_{ALG} respond to serotonin with a mixed response comprised of a hyperpolarization followed by a depolarizing response (5-HT_{Hyp-Dep}). The hyperpolarizing response is mediated by the 5-HT_{1A} receptor whereas the depolarizing response can be mediated by the 5-HT_{2A}, 5-HT_{2C}, and/or 5-HT₇ receptors. Interestingly, none of the *Thy1*-YFP cells expressed any of these common 5-HT receptor subtypes. Instead, 4 of the 12 expressed the mRNA for 5-HT₄ and 6 of the 12 expressed the mRNA for 5-HT₆. Both of these receptor subtypes are G_s-coupled receptors, suggesting serotonin may have an excitatory effect on the *Thy1*-YFP cells. However, there is no study, to my knowledge, on the role of 5-HT₄ and 5-HT₆ receptors in the BNST. In fact, there is very little data on the role these receptors play in the brain in general. None of the non-YFP cells expressed the mRNA for these serotonin receptors. Instead, the majority of the non-YFP cells expressed the mRNA for the 5-HT_{1A} receptor, suggesting serotonin would inhibit these neurons. A smaller percentage of non-YFP cells expressed the mRNA for 5-HT₅ and 5-HT_{2A}. The difference in 5-HT receptor mRNA expression in the *Thy1*-YFP population suggests these neurons could respond to drugs targeting the serotonin system in unique ways.

Although the adBNST is thought to act to attenuate anxiety-like behavior, it is unknown how the *Thy1*-YFP cells contribute to the circuit. It is possible these neurons are one of the main effectors of the anxiolytic role of the BNST, however, we need to be able to directly manipulate the activity of these neurons in order to discover their role in the circuit. For this reason, we wanted to see if one of the *Thy1*-cre transgenic mouse lines

would accurately label this restricted population of neurons in the adBNST. To do this, we injected a cre-dependent fluorescent virus into the BNST_{ALG} of *Thy1*-cre mice (FVB/N-Tg(*Thy1*-cre)1Vln/J-006143) and compared the expression profile with that seen in the *Thy1*-YFP mouse line (**Figure 3.7**). It became apparent that the *Thy1*-cre mouse line did not label the same population of neurons as seen in the *Thy1*-YFP mouse line. This is not surprising, as both of these lines were independently created, and as mentioned above, the *Thy1* transgenic mouse lines have distinct expression patterns (Feng et al., 2000). It is possible that the difference in expression patterns between the two lines is due to overly-sensitive production of the fluorescent protein in neurons that only express a small amount of cre. In this scenario, the *Thy1*-YFP line could contain low YFP expression in other neurons that is not visible due to the strong expression in a small number of neurons. The *Thy1*-cre line could then show more labeled neurons due to a more even expression of fluorescence. However this is unlikely as homozygotes of the the *Thy1*-XFP lines had stronger fluorescence expression but the pattern of expression was unaffected by gene dosage, suggesting the labeling of subsets of neurons is not an artificial consequence of dim labeling (Feng et al., 2000).

There are other *Thy1*-cre lines that could be tested, however, with the variability in the expression profile of all of the different *Thy1* founder lines (Feng et al., 2000; Campsall et al., 2002; Sugino et al., 2005), it is unlikely that another *Thy1*-cre line would result in the specific labeling of the *Thy1*-YFP cells labeled in this *Thy1*-YFP mouse line. To get an expression pattern true to the original line, the *Thy1*- cre line would need to be created from a knock-in of the cre transgene in place of the YFP transgene. Alternatively, the mRNA from YFP cells in the BNST could be isolated and analyzed using a microarray or RNA

sequencing to find a gene that is specifically expressed in this neuronal subtype and not in other cells in the surrounding area. This information could then be used to find a virus that could specifically target these neurons in order to determine their role in the circuit.

In conclusion, the data presented here provide evidence for different cell types in the ovBNST and adBNST, however, more research needs to be done in order to more accurately define the roles of the cell types and nuclei. The dissection of these circuits based on location has deepened our knowledge of the role the BNST plays in modulating anxiety. The next step will be to dissect these circuits by determining the roles individual cell types play in coordinating the behavioral and physiological output of the nucleus.

**Chapter 4: Chronic stress differentially affects Type III neurons in the bed nucleus
of the stria terminalis**

Introduction

The BNST acts to both promote and oppose anxiety behavior through the activity of functionally distinct subregions and cell types (Jennings et al., 2013; Kim et al., 2013). For example, neurons in the anterodorsal BNST (adBNST) oppose anxiety-like behavior, whereas a subset of neurons in the oval BNST (ovBNST) inhibits the adBNST, thereby promoting anxiety-like behavior (Kim et al., 2013). Importantly, both of these regions are primarily composed of GABAergic neurons suggesting local neurons within a subregion of the BNST could inhibit one another and play opposing roles in the behavioral output of the nucleus as a whole (Day et al., 1999; Kudo et al., 2012). Indeed, there are a significant number of intrinsic GABAergic connections within the anterolateral BNST (Turesson et al., 2013). Although neurons within one region of the BNST are likely to be playing opposing roles in the circuit, they are often investigated without an attempt to distinguish separate cell types.

The effects of stress on BNST neurons are generally examined by equating all neurons within a particular region (Vyas et al., 2003; Pêgo et al., 2008; McElligott et al., 2010; Conrad and Winder, 2011; Glangetas et al., 2013). For example, chronic stress was shown to cause a long term depression (LTD) through a reduction in calcium-permeable AMPA receptors (CP-AMPA) in the anterolateral BNST of mice, concluding that an increase in anxiety-like behavior after stress was due to the loss of the ability of the BNST to act as a “braking mechanism” on the paraventricular nucleus of the hypothalamus (PVN) (McElligott et al., 2010). This suggests all neurons in the anterolateral BNST act to inhibit anxiety-like behavior; however we now know that this is not the case (Kim et al., 2013). In contrast, previous work from our lab has shown an effect of chronic stress particular to

one cell type within the anterolateral group of the BNST (BNST_{ALG}; includes the ovBNST and adBNST). Three distinct neuronal subtypes exist in the BNST_{ALG}, Type I through Type III (Hammack et al., 2007; Hazra et al., 2011). After chronic restraint stress in rats, only the Type III neurons exhibited an enhancement of the magnitude of long term potentiation (LTP) corresponding with a decrease in expression of striatal-enriched protein tyrosine phosphatase (STEP; also known as protein tyrosine phosphatase nonreceptor 5; Dabrowska et al., 2013b). STEP acts as a molecular brake on synaptic plasticity in neurons (Paul et al., 2007), and the loss of this brake after stress causes Type III neurons to be more susceptible to LTP. Importantly, Type III neurons are thought to express corticotropin releasing factor (CRF) (Dabrowska et al., 2011; 2013a). As CRF generally acts to promote the anxiety response, these Type III neurons are thought to be a part of the anxiogenic pathway in the BNST. However, it is unknown if these cells also undergo the loss of CP-AMPA receptors after stress (McElligott et al., 2010).

The opposing circuits within the BNST suggest that stress may have differential effects on the individual neurons that comprise these circuits in order to shift the balance from an anxiolytic to an anxiogenic state. In the current study, we used a combination of patch-clamp electrophysiology and single cell quantitative reverse transcriptase polymerase chain reaction (scRT-PCR) to determine how chronic shock stress (CSS) affects the electrophysiological and genetic expression profile of Type I-III neurons in the BNST_{ALG}. In addition to examining general electrophysiological properties, we examined the effect of CSS on the relative contribution of AMPA, CP-AMPA, and NMDA receptors to the evoked excitatory post synaptic currents (EPSC) in Type III and non-Type III neurons, as well as the expression of mRNAs coding for AMPA and NMDA receptor

subunits in the different cell types. Finally, we used scRT-PCR to study the differential effect of CSS on the expression of mRNA coding for CRF, STEP, and other related proteins in Type I, Type II, and Type III cells. By examining the effect of CSS on the different cell types in the BNST_{ALG}, we attempt to shed light on ways in which stress can differentially affect opposing circuits within a subregion of the nucleus.

Methods

Animal Subjects

All experiments were performed in male Sprague-Dawley rats aged 40-60 days old (n = 63; Charles River Laboratories, Wilmington, Massachusetts), and procedures were approved by the Institutional Animal Care and Use Committee of Emory University and were in compliance with National Institute of Health guidelines. Animals were housed in same-sex groups, four animals per cage for one week after arrival. Once animals were designated to the chronic shock stress (CSS) or no stress (NS) group, they were separated into pairs, housed with another rat from the original cage and in the same stress condition. Rats were maintained on a 12:12-hour light-dark cycle with *ad libitum* access to food and water. The rat's body weight was measured periodically throughout the experiment. Experiments were performed in six cohorts of seven or eight rats (NS = 4; CSS = 4 or 3 per cohort) and one cohort of sixteen rats (NS = 8; CSS = 8).

Chronic stress and behavioral testing

Acoustic Startle Response

Before administering the CSS, rats, 40 days of age, were first matched for their basal anxiety level using a standard acoustic startle paradigm. Here, rats were placed in an

acoustic startle chamber for 5 min prior to presentation of acoustic stimuli to acclimatize the animals to the chambers. Four rats were tested simultaneously in identical 8 x 15 x 15 cm Plexiglas and wire mesh cages, each suspended between compression springs within a steel frame located within a custom-designed sound-attenuating chamber. Details of the recording apparatus have been described previously (Walker and Davis, 1997; Sink et al., 2011). After acclimation, the acoustic startle response (ASR) was measured following each of 30 acoustic stimuli. Startle responses were evoked by 50-ms 95, 100, and 110 dB white-noise bursts generated in a pseudorandom order by a Macintosh G3 computer sound file, amplified by a Radio Shack amplifier (100 W, Model MPA-200; Tandy, Fort Worth, TX, USA), and delivered through speakers located 5 cm in front of each cage. The presentation and sequencing of all stimuli was under the control of a Macintosh G3 computer using custom-designed software (The Experimenter; Glassbeads Inc., Newton, CT, USA). Startle amplitude was defined as the maximum peak-to-peak voltage during the first 200 ms after each noise burst. Similar measurements were taken ten times during pseudorandom intervals over the course of the 5 min acclimation period as a baseline measurement of cage-displacement. The ASR was measured once a day for two days prior to the start of the CSS. For each rat, the startle amplitudes for the 10 stimuli at a particular decibel were averaged and divided by the average measurements for baseline cage-displacement for that rat in order to normalize for the rat's weight. Then the normalized startle amplitude was averaged across the three decibels. This resulted in a single normalized startle amplitude for each rat. Rats in each cohort were matched according to their normalized startle response from the second presentation of the acoustic startle test and then divided into two groups, 32 NS rats and 31 CSS rats, so as to ensure the groups did not differ in their basal

anxiety. 47 rats (NS=24; CSS=23; from the first 6 cohorts of 7 or 8 rats) were tested for fear of the shock context one day after the final day of shock stress and underwent an acoustic startle post-test six days after the final day of shock stress. A normalized startle amplitude was calculated for the post test, and then the percent change in ASR from the pre-test to the post-test was calculated. These rats were also used for *in vitro* electrophysiology experiments completed 6 to 9 days after the final day of shock stress. Of those 47 rats, 39 (NS = 20; CSS = 19) were used to collect samples for single-cell quantitative polymerase chain reaction (PCR) and 24 (NS = 12; CSS = 12) were tested in the open field and elevated O tests six and seven days after the last day of shock stress, respectively. To test if the CSS caused a long-lasting fear of the shock context, the remaining 16 rats (NS=8; CSS=8; the last cohort of animals) were tested for fear of the shock context after the post-test for the ASR six days after the last day of shock stress (NS=8; CSS=8).

Chronic Shock Stress

The CSS group underwent 7 consecutive days of footshock. The CSS paradigm used in these experiments was adopted from previous studies in rat (Hazra et al., 2012). The NS animals received exactly the same handling procedures as the CSS group and were placed in the shock chamber for the same duration each day without being shocked. Each rat was placed inside one compartment of a passive avoidance chamber (GEMINI, San Diego Instruments) with the door separating the two compartments closed at all times. There were two passive avoidance chambers with two compartments each, allowing for four rats to be run through the shock paradigm simultaneously, with pair-housed rats in separate compartments of the same chamber. The floor of the chamber is made of 0.4 cm

diameter stainless steel bars spaced at 1.1 cm that conduct the electric shock. On day 1, the CSS rats were placed in the shock chamber and allowed to habituate to their environment for 5 min. Rats then received two 8-min periods of eight randomly applied footshocks (0.5 s, 0.5 mA) separated by an 8-min period of no shock. The CSS paradigm was repeated on each of the following 6 days for a total of 7 consecutive days of shock stress. Each rat was shocked at approximately the same time every day (between 11 AM and 1 PM) to control for diurnal hormone variations. Each compartment contained a camera to allow for monitoring of the session in real time. NS rats were run prior to the CSS rats each day, and the compartments were thoroughly cleaned between sessions.

Context Test

On day 8, one day after the final shock stress, rats were returned to the shock chamber to measure fear of the shock context. Here, the front panel of the door to each compartment was removed, leaving a clear Plexiglas door. The room was left dark with only red light to illuminate the inside of the chambers. Cameras were placed outside of the chambers to record movement and behavior of the rats for 5 minutes in the shock context. Freezing behavior was analyzed by stop-watch by an experimenter blind to experimental condition after the completion of the test. Rats were then returned to their home cage for four days. For sixteen rats (NS=8; CSS=8; from the last cohort) the context test was performed on day 13 (6 days after completion of the shock stress) instead of on day 8.

Open Field and Elevated Zero Maze Tests

On day 13, four of the rats (NS=2, CSS=2) from each of the first six cohorts were tested in the open field test after the acoustic startle test. The home cages were placed in the testing room with low levels of red light for at least 4 hours prior to testing in order to

habituate the animals to the room. Rats were placed in the center of the open field apparatus, an open box made of Plexiglas (93 cm x 93 cm x 30 cm), for ten minutes. The percentage of time spent in the center of the field (middle 50%) was used as a measure of anxiety (i.e., animals spending more time in this area were assumed to be less anxious than those spending less time in this area). On day 14, the same rats tested in the open field test were tested in the elevated zero maze (EZM) test. The EZM, a variant of the elevated plus maze, consists of a circle platform (50 cm diameter with platform 5 cm wide) elevated 50 cm above the floor with two opposing open and enclosed quadrants (Stoetling, IL, USA). The closed quadrants have walls extending 30 cm high whereas the open quadrants do not have walls on the platform. Here, rats were placed in the center of one of the open regions of the EZM and allowed to explore for five minutes. The percentage of time spent in the open quadrants of the EZM was used as a measure of anxiety. All activity within the open field and EZM was recorded and analyzed off-line using TopScan (CleverSys, INC.).

Electrophysiology

Preparation of BNST slices

Electrophysiology experiments were completed on days 13-16, 6-9 days after the last day of shock stress. BNST slices were obtained as previously described (Hammack et al., 2007). Briefly, rats were decapitated under isoflurane anesthesia (Med-Vet International, Mettawa, IL, USA), and the brains were rapidly removed and placed in ice-cold kynurenic acid-based “cutting solution” which contained (mM): NaCl (130), KCL (3.50), KH_2PO_4 (1.10), MgCl_2 (6.0), CaCl_2 (1.0), glucose (10), supplemented with kynurenic acid (2.0). Coronal sections containing BNST were cut 350- μm thick using a Leica VTS-100 vibratome (Leica Microsystems, Bannockburn, IL, USA). Slices were kept

in oxygenated cutting solution at room temperature for 1 h before transferring to regular artificial cerebrospinal fluid (ACSF) containing (mM): NaCl (130), NaHCO₃ (30), KCl (3.50), KH₂PO₄ (1.10), MgCl₂ (1.30), CaCl₂ (2.50), and glucose (10). Slices were kept in oxygenated ACSF for at least 30 min before recording.

Patch clamp recording

Individual slices were transferred to a recording chamber mounted on the fixed stage of a Leica DM6000 FS microscope (Leica Microsystems Inc., Bannockburn, IL) equipped with an IR sensitive CCD camera (Orca ER, Hamamatsu, Tokyo Japan), allowing for use of differential interference contrast (DIC) optics and infrared illumination to identify individual BNST neurons. The slices were maintained fully submerged and continuously perfused with oxygenated 32 °C ACSF with a speed of ~2 ml/min. All recordings were confined to the dorsal anterolateral cell group including the oval and anterolateral nucleus of the BNST. Whole-cell recordings were obtained using recording pipettes pulled from borosilicate glass and having a resistance of 4-6 MΩ. Neurons were patched using one of three different recording patch solutions depending on the experiment being done. For determining the AMPA-to-NMDA ratio and AMPA rectification plot, a cesium-based patch solution was used in order to block potassium currents to allow the neurons to be held at positive potentials and contained (mM): Cs-gluconate (131), HEPES (10), glucose (10), CaCl (2), EGTA (10), Mg-ATP (5), Na₃-GTP (0.4). Spermine (100 μM) was added to this patch solution in order to maintain the polyamine block of CP-AMPA receptors at positive potentials (Bellone and Lüscher, 2006; Soto et al., 2007). Other experiments used potassium-based patch solution containing the following (mM): K-gluconate (130), KCl (2), HEPES (10), MgCl₂ (3), K-ATP (2), Na-GTP (0.2), and

phosphocreatine (5), and was titred to pH 7.3 with KOH and 290 mOsm. For scRT-PCR, the potassium-based patch solution was supplemented with RNAase inhibitor (1 μg / ml; Qiagen). Data acquisition and analysis were performed using a Multiclamp 700B amplifier in conjunction with pClamp 10.0 software and a Digidata 132A AD/DA interface (Molecular Devices, Sunnyvale, CA, USA). Cells were excluded if they did not meet the following criteria: a stable access resistance changing less than 15% and action potentials crossing 0 mV.

Analysis of electrophysiological properties

Basic electrophysiological properties were collected from each cell recorded in the CP-AMPA and scRT-PCR experiments from 47 rats (NS = 24, CSS = 23). A DC holding current was injected to maintain the membrane potential at -60 mV in current clamp. To characterize neurons, a series of 10 hyperpolarizing and depolarizing, 750 ms long, square-wave current steps were injected and scaled so that the peak negative voltage deflection was to approximately -80 mV (Hammack et al., 2007; Hazra et al., 2011). Then, linear ramps of depolarizing current were injected, lasting 250 ms, and scaled to depolarize the neuron to elicit a single action potential. Data were analyzed by importing the raw voltage and current traces into Matlab (The MathWorks, Natick, MA, USA) using scripts provided with sigTOOL (<http://sigtool.sourceforge.net/>, developed at King's College London) and processed with customized scripts (available upon request).

Analysis of electrophysiological properties was completed as described elsewhere (Ehrlich et al., 2012). Briefly, input resistance (R_{in}) and time constant (τ) were calculated using the deflection in response to the smallest hyperpolarizing current step (approx. 5 mV). R_{in} was calculated as the ratio of peak voltage deflection to the current injected; τ

was defined as the time necessary for the cell to reach 63.2% of its maximal deflection. The I_h score was calculated as the ratio of the magnitude of I_h (measured as peak deflection at the beginning of the trace minus steady state at the end) to the membrane potential at the point of peak deflection in the trace with the peak deflection closest to -80 mV (smaller positive values indicate less voltage deflection due to I_h). The I_{AR} score was calculated as the ratio of the peak magnitude of the smallest hyperpolarizing trace to the difference between the peak magnitude of the two most hyperpolarizing traces (larger values indicate more inward rectification). Action potential rise time and decay time were measured as time from 10% to 90% of maximum amplitude with linear interpolation between samples to increase resolution. Action potential half-width was measured as the width of action potential at half-maximal amplitude with linear interpolation to increase resolution.

The rate of action potential firing as a function of injected current and subthreshold membrane potential was also analyzed. First, the number of spikes fired on the depolarizing traces described above that contained at least one action potential was plotted against the current injection for each cell, and a linear regression was done on the data from each individual cell using R. Then the resulting calculated slopes and intercepts from NS and CSS rats were compared within cell type. Similarly, the number of spikes fired on the depolarizing traces was plotted against the subthreshold membrane potential of the corresponding trace. The subthreshold membrane potential was calculated by determining the initiation point for each spike and removing the portion of the spike waveforms above their respective thresholds, then calculating the average of the remaining subthreshold portion of the trace. Cells were excluded if they did not meet the following criteria: more

than one sweep contained an action potential, the action potentials maintained their shape and amplitude, and the slope for the linear regression was > 0 .

Recording AMPA-to-NMDA ratio and AMPA rectification

When measuring the ratio of AMPA to NMDA receptor-dependent currents (AMPA:NMDAR), we held the BNST neurons at +40 mV in voltage-clamp and recorded stimulus-evoked excitatory postsynaptic currents (EPSCs). To record EPSCs, a concentric bipolar stimulating electrode (FHC, Bowdoinham, ME) was placed in the dorsal stria terminalis, the major afferent input to the BNST. Evoked EPSCs were recorded in the presence of the GABA_A receptor antagonist SR 95531 (5 μ M) to block the GABA_A receptor-mediated inhibitory postsynaptic currents. EPSCs were stimulated and recorded for 5 min at 0.1 Hz. Next, the NMDA receptor specific antagonist (RS)-CPP (100 μ M; Tocris Bioscience, Bristol, United Kingdom) was added to the bath to isolate the AMPAR-mediated EPSC, and EPSCs were recorded for another 5 min (0.1 Hz). This procedure allowed us to calculate the AMPAR:NMDAR ratio: first, an average EPSC was calculated for each condition; then the average trace for the AMPAR-mediated EPSC was subtracted from the average trace for the combined EPSC, resulting in an approximation of the NMDAR-mediated EPSC. The AMPAR:NMDAR was calculated as the amplitude of the AMPAR-mediated EPSC divided by the amplitude of the NMDAR-mediated EPSC. After recording the AMPAR-mediated EPSC at +40 mV, AMPAR-mediated EPSCs were recorded at +20 mV, 0 mV, -20 mV, -40 mV, and -70 mV in order to measure the rectification of the AMPAR. Measurements at -40 mV were excluded in the analysis as many cells fired action potentials at this voltage. The rectification index (RI) was calculated

by dividing the amplitude of the current at -70 mV by that at +40 mV within each cell (Bellone and Lüscher, 2006).

Contribution of CP-AMPA receptors in cell types

Here, we used the selective CP-AMPA antagonist 1-naphthylacetyl spermine trihydrochloride (Naspm) to assess the relative contribution of CP-AMPA to the AMPAR current in the NS and CSS condition. BNST neurons were first defined as Type I, II, or III cells based on their response to a series of hyperpolarizing and depolarizing current pulses as previously described (Hammack et al., 2007; Hazra et al., 2011). Neurons were then held at -70 mV in voltage-clamp in the presence of SR 95531 (5 μ M) to ensure the evoked EPSCs did not contain NMDAR- or GABA_AR-mediated current. EPSCs were stimulated and recorded as described above. Once 5 min of stable baseline EPSCs were recorded, Naspm (100 μ M) was applied for 10 min followed by a 10 min wash; EPSCs were recorded throughout Naspm application and wash. All EPSCs evoked during and after treatments were normalized to the mean baseline amplitude, and the normalized amplitude of three consecutive EPSCs was averaged to create a representative normalized amplitude for every 30 seconds. Because stress is known to differentially effect long term potentiation (LTP) in Type III cells of the BNST (Dabrowska et al., 2013b), the effect of stress on CP-AMPA current in Type III cells was analyzed separately from the Type I and Type II cells.

Single-cell quantitative PCR

Retrotranscription of mRNA

RNA was collected at the end of the recording by applying light suction until the cell had visibly shrunken. In order to obtain high quality RNA and good yield of cDNA

Gene name (protein name)	TaqMan assay reference
<i>Crh</i> (CRF)	Rn01462137_m1
<i>Crfr1</i>	Rn00578611_m1
<i>Ptpn5</i> (STEP)	Rn01480059_m1
<i>Ppp1ca</i> (PP1A)	Rn00580546_m1
<i>Ppp1cb</i> (PP1B)	Rn00565033_m1
<i>Ppp1cc</i> (PP1C)	Rn04339209_m1
<i>Ppp3ca</i> (Calcineurin A)	Rn00690508_m1
<i>Ppp3cb</i> (Calcineurin B)	Rn00566864_m1
<i>Ppp3cc</i> (Calcineurin C)	Rn01465907_m1
<i>Ppp1r1b</i> (DARPP-32)	Rn01452984_m1
<i>Gria1</i> (GluR1)	Rn00709588_m1
<i>Gria2</i> (GluR2)	Rn00568514_m1
<i>Gria3</i> (GluR3)	Rn00583547_m1
<i>Gria4</i> (GluR4)	Rn00568544_m1
<i>Grin1</i> (GluN1)	Rn01436034_m1
<i>Grin2a</i> (GluN2A)	Rn00561341_m1
<i>Grin2b</i> (GluN2B)	Rn00680474_m1
<i>Grin2c</i> (GluN2C)	Rn00561359_m1
<i>Grin2d</i> (GluN2D)	Rn00575638_m1
<i>Grin3a</i> (GluN3A)	Rn01448553_m1

Table 4.1. List of gene names and TaqMan reference numbers.

the patch solution was RNase free and supplemented with RNase inhibitor (1U/ μ l) (Life Technologies, CA). The content of the pipette was expelled in an RNase free tube containing 4 μ l of lysis buffer and 1 μ l of DNase (Single cell to CT kit - Life Technologies, CA). The mix was incubated for 5 min at room temperature to degrade any genomic DNA possibly present then 1 μ l of Stop solution (Single cell to CT kit - Life Technologies, CA) was added to inactivate the DNase and avoid further degradation of cDNA. The tube content was then incubated 5 min at 65°C with 1 μ l of oligodT₂₀ (50mM) and 1 μ l of dNTP (10mM) (Life Technologies, CA).

The mix was allowed to cool down on ice 1 min and the retrotranscription mix was added (2 μ l of RT buffer, 2 μ l of MgCl₂ 50mM, 2 μ l of DTT 0.1M and 1 μ l of SuperScript III

enzyme) (Life Technologies, CA). The cDNA synthesis was carried at 50°C for 50 min, followed by 5 min at 85°C to inactivate the retrotranscriptase. The cDNA was then stored at -20°C until used.

To test the quality of the newly synthesized cDNA, control PCRs were performed. We chose to use *Gapdh* and *Gad67* as positive controls and *VgluT1* as negative control. The PCR mix consisted of PCR buffer 1X, 2mM MgCl₂, 200μM of each dNTP, 0.1μM of primer mix, 2 units of HotStart Taq polymerase (Qiagen), 1μl of cDNA and water to adjust the final volume to 20μl. The amplification was performed as recommended by manufacturer: an initial denaturation of 15 min at 95°C, then 30 cycles of 30 seconds of denaturation at 94°C, annealing for 30s at 60°C and extension for 1min at 72°C and a final extension of 10min at 72°C. The results were visualized on 2% agarose gel with Ethidium bromide. We began with the intracellular contents of 161 cells. The cells which did not show a positive amplification for *Gapdh* (24 cells; 15 %) as well as the cells showing positive signals for both *Gad67* and *VgluT1* (7 cells; < 1 %) were discarded for the rest of the analysis leaving a remainder of 130 cells that were further processed for qPCR.

Pre- amplification

To be able to test the expression of several genes despite the small amount of the cDNA samples, we introduced a pre-amplification step. This step consists of an enrichment of genes of interest using TaqMan assays, prior to the actual quantitative PCR. We used the preamplification master mix from Applied Biosystems (Thermofisher, CA) with the combination of all the Taqman probes corresponding to our genes of interest (listed in **Table 4.1.**)

Preamplification uniformity was assessed using the $\Delta\Delta\text{Ct}$ method and a qPCR with both the original cDNA and the preamplified cDNA as a starting template. A $\Delta\Delta\text{Ct}$ value close to zero indicates that there was preamplification linearity, with limits set at ± 1.5 . All target genes produced $\Delta\Delta\text{Ct}$ values within these limits indicating that there was no significant amplification bias.

Quantitative PCR and analysis

qPCR reactions (20 μl), composed of 2 μl cDNA template, Universal TaqMan MasterMix (2x concentrated, Life Technologies), TaqMan assay (20x concentrated, Life Technologies) and H₂O, were performed with the 7500 Fast Real-Time PCR System (Life Technologies). Reactions, ran in triplicate, were incubated at 50°C for 2 min and 95°C for 10 min, followed by 40 cycles of 95°C for 15 s and 60°C for 1 min. Non-template controls (NTCs) were used as negative controls in every experiment. GAPDH and B2M, selected using the geNorm application, were used as endogenous controls. The relative expression of mRNA was normalized to the geometric mean of the calibrators GAPDH and B2M, using the ΔCt method (Vandesompele J, 2002; Livak KJ, 2001). Due to the sensitivity of detection of the Fast Real-time PCR system and the preamplification step, all samples with a Ct value greater than to 34.6 were discarded as this Ct value represents an initial amount of template equal to half a molecule of DNA for this gene. For most genes tested, sample sizes ranged from 17 – 32 cells per cell type in each condition. Some genes, including *Gria3*, *Gria4*, *Grin2c*, and *Grin2d* were tested on a smaller sample size, ranging from 4 – 8 cells per cell type in each condition. At least 92 % of the cells in each cell type in each condition had Ct values below the cut-off for *Gria1-2*, *Grin1*, *Grin2A*, and *Grin2b*. No cells had Ct values for *Gria3* or *Gria4* that were below the cut-off. The percentage of

neurons with Ct values below the cut-off for *Grin2c*, *Grin2d*, and *Grin3a* ranged from 50 – 100 %. For the rest of the genes, at least 65% of the cells from each cell type in each condition expressed enough mRNA to meet the cut-off. For a summary, see supplementary table 4.1. The lognormal distribution of the expression of each gene was assessed. The comparative analysis was done using geometric mean rather than the arithmetic mean to be consistent with the lognormal distribution of the level of expression.

Statistical Analysis

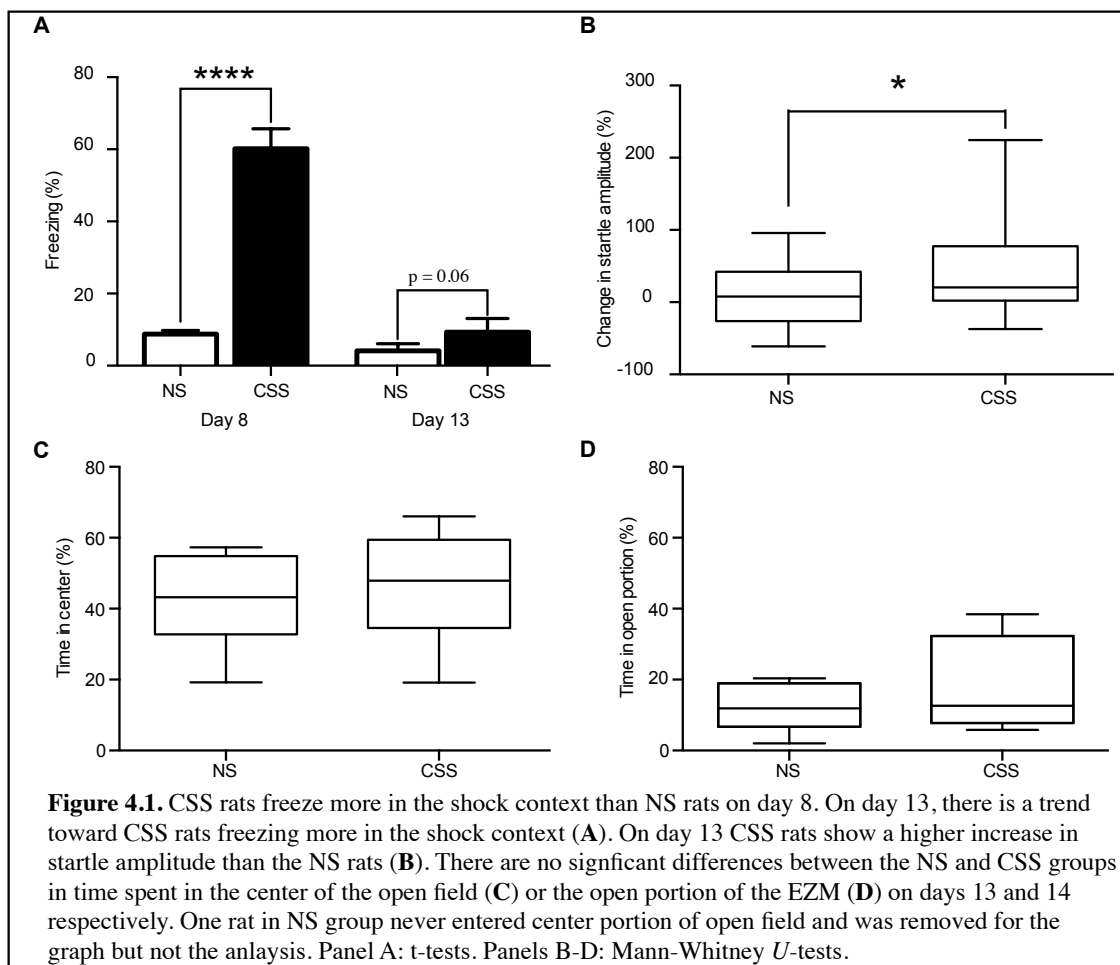
Behavioral and electrophysiological data sets were tested for normality using the Shapiro-Wilk test and for homoscedasticity using Levene's test, implemented in Matlab (The MathWorks, Natick, MA, USA). Statistical analyses were carried out using Prism 6 (GraphPad Software Inc., San Diego, CA), R (R version 3.2.3, RStudio v. 0.98.1103), or Matlab. For data sets with a normal distribution and equal variance, student's *t*-test or a two-way ANOVA was performed. For pairs of data sets that do not have equal variance, a Welch's unequal variance *t*-test was performed; for pairs of data sets that have equal variance but are not normally distributed, a Mann-Whitney *U*-test was performed. For data sets with unequal variance and normally distributed that include more than two groups, such as when comparing cell types and the effects of stress, single-parameter Box-Cox power transforms were used to transform the data until the groups met assumptions of normality and homoscedasticity. Then a two-way ANOVA was performed with Tukey's multiple comparisons test when appropriate. Normality and homoscedasticity were approximated in AMPA rectification and CP-AMPA experiments. An alpha level of 0.05 was used for all statistical tests for behavioral and electrophysiological data sets, and the standard error of the mean (SEM) is reported for the error.

The normalized quantities of mRNA from the scRT-PCR analysis were compared using the Mann-Whitney *U*-test for non-parametric samples and a *t*-test for parametric samples using Prism 6. Only non-zero values (cells that expressed enough mRNA to be below the Ct cut-off) were included in analyses and graphs. Due to the high number of genes and groups, the Bonferonni correction was used to correct for the multiple comparisons. A total of 54 comparisons was made for the scRT-PCR study. Therefore, the alpha level was corrected to 0.0009. However, this is a conservative correction, potentially resulting in false negative results. For this reason, any *p* values less than 0.05 are reported as a potential trend.

Results

Both NS and CSS animals gained an appropriate amount of weight over the course of the experiment and there was no difference between the two conditions (data not shown). A total of 63 rats were used for this study and each rat was used for multiple experiments. All 63 rats were tested in the acoustic startle test. 16 rats were tested in the context test on day 13. 47 rats were tested in the context test on day 8 and used for electrophysiological experiments. Of those, 24 rats were also tested in the open field and EZM tests. Electrophysiological properties were collected from all 47 rats (23 CSS and 24 NS). 30 rats (17 CSS and 13 NS) were used for the AMPAR:NMDAR and AMPA rectification experiments, 23 rats were used for the CP-AMPA experiment (9 CSS and 14 NS), and 39 rats were used for scRT-PCR experiments (19 CSS and 20 NS).

Context fear and anxiety-like behavior



After the 7 days of shock stress, rats were returned to the shock context to measure context fear. Fear behavior was measured as the percentage of time spent immobile (freezing) during the 5 min context test. CSS rats froze significantly more than NS rats ($60 \pm 6\%$ of time compared to $9 \pm 1\%$; $p \leq 0.0001$), indicating CSS rats learned to fear the shock context (Figure 4.1A). The fear of the shock context diminished after 8 days, however there was a trend toward the CSS animals freezing more than the NS animals on day 13 (Figure 4.1A; $p = 0.06$).

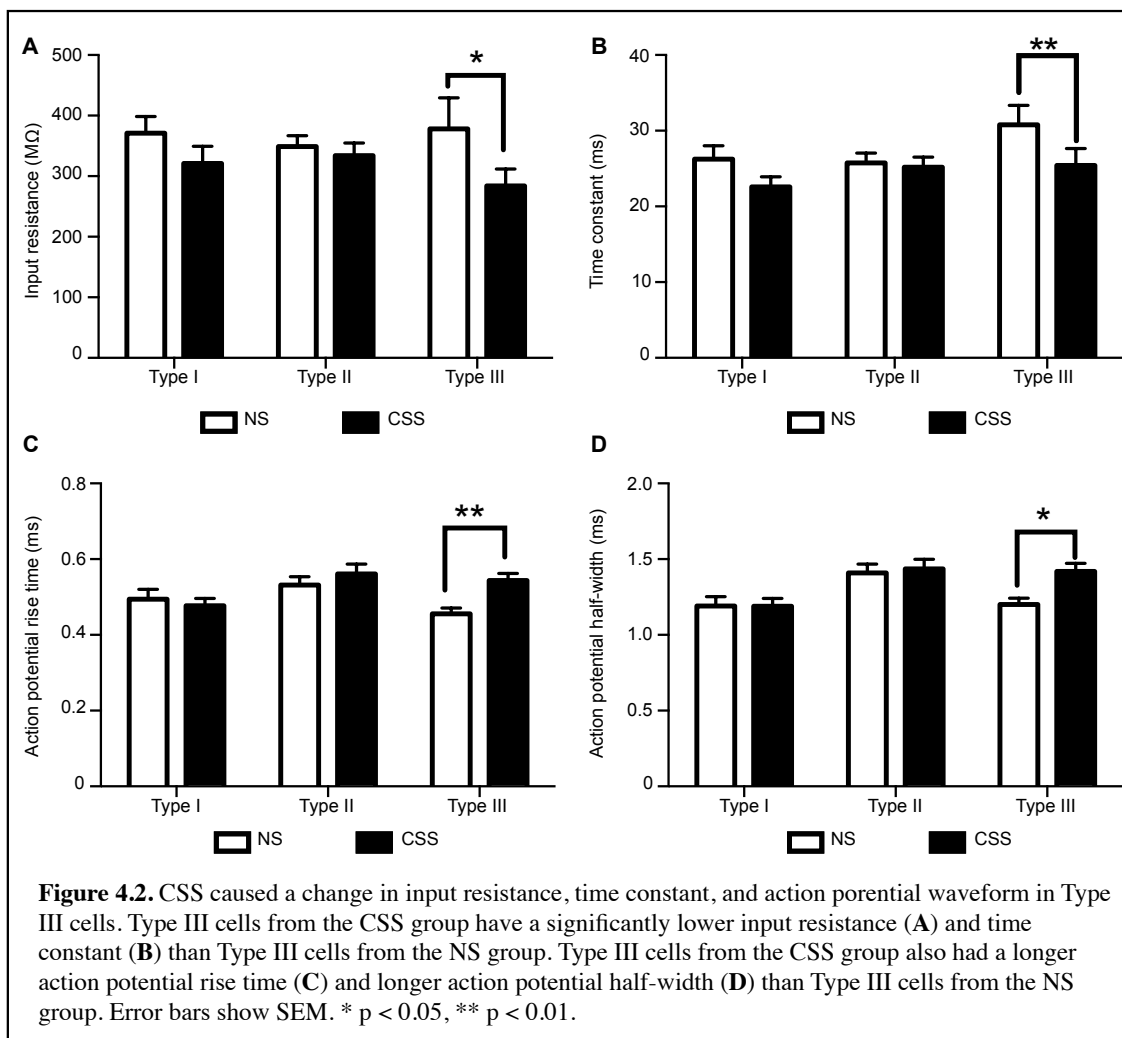
In addition to examining fear of the shock context, the acoustic startle test, open field test and EZM test were conducted to understand if the CSS resulted in an increase in

baseline anxiety-like behavior. The acoustic startle post-test was conducted on day 13, 6 days after the last shock presentation, and compared to the pre-test conducted the day before the CSS began. CSS rats had a significantly higher percent increase in the ASR than NS rats ($39 \pm 11\%$ compared to $8 \pm 7\%$ increase in ASR, $p \leq 0.05$), indicating CSS caused a long-lasting increase in anxiety-like behavior (**Figure 4.1B**). However, there was no difference in behavior of the CSS rats compared to the NS rats in the open field or EZM tested on days 13 and 14 respectively. CSS and NS rats spent similar amounts of time in the center of the open field maze (NS $40 \pm 5\%$, CSS $45 \pm 5\%$, $p = 0.51$) and in the open portion of the EZM (NS $12 \pm 2\%$, CSS $18 \pm 4\%$, $p = 0.31$; **Figure 4.1C-D**). There was also no significant difference in the distance travelled in either test (data not shown).

Effect of stress on other electrophysiological properties of BNST neurons

Basal electrophysiological properties of neurons in the BNST, including input resistance, tau, action potential threshold and waveform, I_h , and I_{AR} , were examined to determine if CSS affected these properties in different cell types (CSS: Type I $n = 31$, Type II $n = 49$, Type III $n = 52$; NS: Type I $n = 33$, Type II $n = 52$, Type III $n = 42$). There was a significant effect of cell type on the I_h score ($p \leq 0.0001$; $F_{2,253} = 298.8$), and a post-hoc multiple comparisons test revealed that Type I, II and III cells had significantly different I_h scores from each other ($p \leq 0.0001$ for all comparisons; Type I 0.0478 ± 0.0025 $n = 64$, Type II 0.0673 ± 0.0019 $n = 101$, Type III 0.0139 ± 0.0011 $n = 94$); however the I_h score was not affected by CSS. Similarly, there was a significant effect of cell type on the I_{AR} score ($p \leq 0.0001$; $F_{2,253} = 26.91$), and a post-hoc multiple comparisons test showed Type III cells had a larger I_{AR} score than Type I ($p \leq 0.0001$) and Type II ($p \leq 0.0001$) cells that was not affected by CSS (Type I 2.171 ± 0.1276 , Type II 2.481 ± 0.1165 , Type III $4.263 \pm$

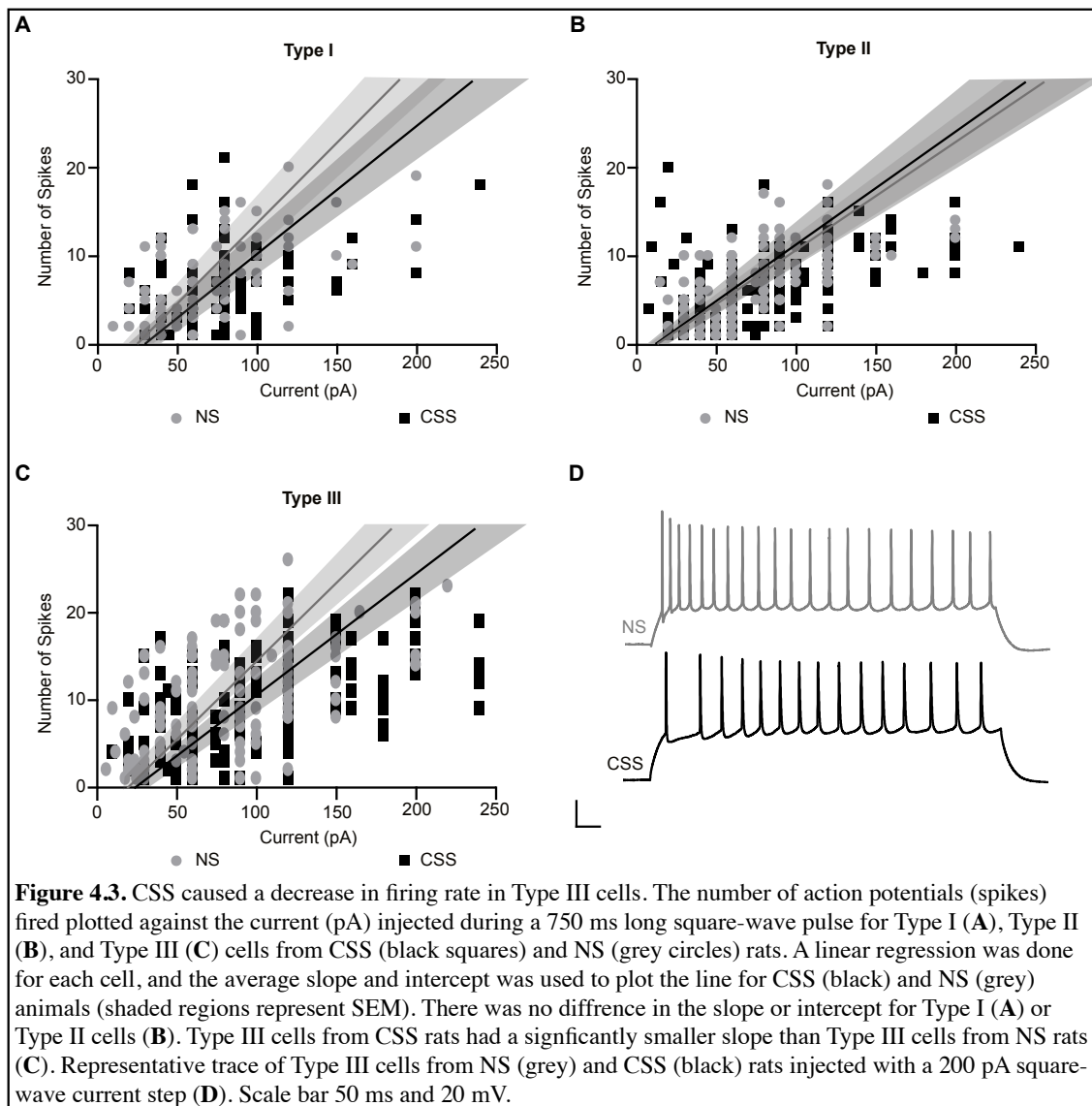
0.4833). Hence, these currents distinguish cell types from one another but are not differentially altered after CSS.



On the other hand, there was a significant effect of both cell type ($p \leq 0.01$; $F_{2,253} = 5.637$) and CSS ($p \leq 0.01$; $F_{1,253} = 8.137$) on input resistance (Figure 4.2A). A post-hoc multiple comparisons test showed that only Type III cells had an effect of CSS, with Type III cells from the CSS group having a significantly lower input resistance than that of the NS group ($283.8 \pm 28.1 \text{ M}\Omega$ compared to $378.3 \pm 28.1 \text{ M}\Omega$, $p \leq 0.05$). Similarly, there was a significant effect of CSS on the time constant of the cell membrane ($p \leq 0.01$; $F_{1,253} = 7.601$; Figure 4.2B), and the post-hoc multiple comparisons test revealed Type III cells

from the CSS group had a significantly faster time constant than those from the NS group (25.43 ± 2.235 ms compared to 30.77 ± 2.584 ms, $p \leq 0.01$). This change in time constant corresponded to the change in input resistance; there was no significant effect of stress on the capacitance of Type III neurons as calculated as the time constant divided by the input resistance for each cell (data not shown).

The action potential waveform of Type III cells was also affected by CSS. There was a significant effect of both cell type ($p \leq 0.05$; $F_{2,253} = 4.124$) and CSS ($p \leq 0.05$; $F_{1,253} = 4.097$) on the rise time of the action potential (**Figure 4.2C**), but only a significant effect of cell type ($p \leq 0.01$; $F_{2,253} = 9.416$) on the decay time of the action potential. A post-hoc multiple comparisons test showed that Type III cells from CSS rats had a significantly longer rise time than Type III cells from the NS group (0.544 ± 0.019 ms compared to 0.456 ± 0.015 ms, $p \leq 0.01$). Although the two-way ANOVA only showed a significant effect of cell type ($p \leq 0.001$; $F_{2,253} = 7.651$) and not CSS ($p = 0.08$; $F_{1,253} = 3.087$) on action potential half-width, a post-hoc multiple comparisons test showed that Type III cells from CSS rats had significantly wider action potentials than Type III cells from NS rats (1.42 ± 0.05 ms compared to 1.20 ± 0.04 ms, $p \leq 0.05$; **Figure 4.2D**). There was also a significant effect of cell type on action potential threshold ($p \leq 0.0001$; $F_{2,253} = 31.76$) but no effect of CSS ($p = 0.8$; $F_{1,253} = 0.07$). As reported previously a post-hoc comparisons test showed that Type I, Type II, and Type III cells have significantly different thresholds for action potential (Type I -36.5 ± 0.5 mV, Type II -39.4 ± 0.3 mV, Type III -34.8 ± 0.5 mV).



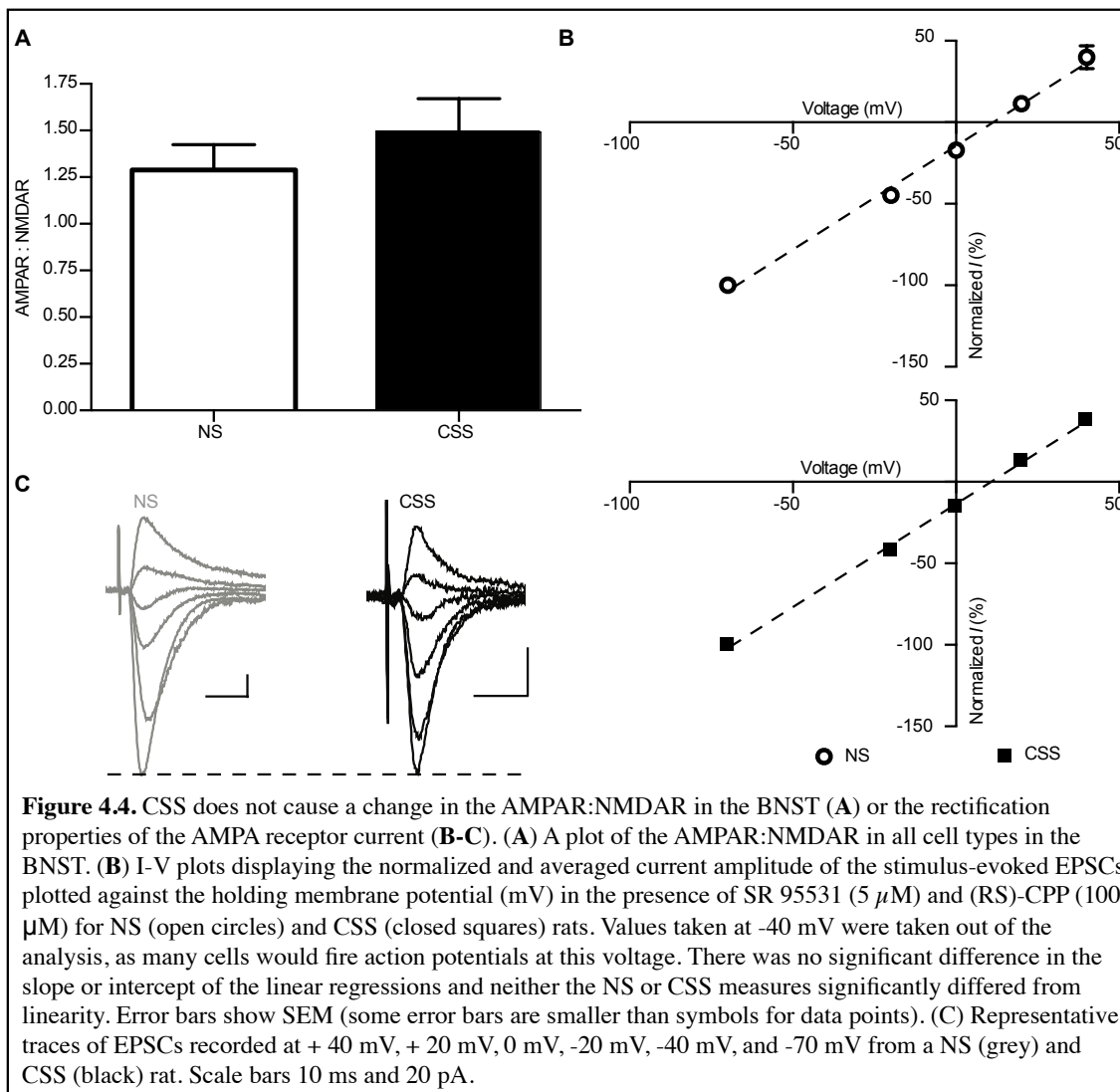
Finally, CSS had an effect on the firing rate of Type III cells in the BNST. When plotted against the current injection, there was no significant change in the slope of the linear regressions for Type I (NS 0.1811 ± 0.01963 spikes / pA $n = 28$, CSS 0.1449 ± 0.01647 spikes / pA $n = 28$) and Type II (NS 0.1230 ± 0.01003 spikes / pA $n = 47$, CSS 0.1297 ± 0.01930 spikes / pA $n = 47$) cells or intercept (Type I: NS -4.524 ± 0.9885 spikes, CSS -4.256 ± 0.8360 spikes; Type II: NS -1.816 ± 0.5706 spikes, CSS -1.890 ± 0.5361 spikes) caused by stress (Figure 4.3A-B). However, the slope in Type III cells from the

CSS group is significantly smaller than the slope from the NS group (0.1404 ± 0.01358 spikes / pA $n = 44$ compared to 0.1794 ± 0.01472 spikes / pA $n = 37$, $p \leq 0.05$; **Figure 4.3C-D**). To determine if this was just due to the decrease in input resistance in the Type III cells, the firing rate was plotted against the subthreshold membrane potential in Type III cells. Here, both the slope and intercept were significantly smaller in Type III cells from the CSS group ($p \leq 0.05$, data not shown), indicating CSS caused a reduction in the firing rate of Type III neurons independent of the change in the input resistance of the cells.

AMPA-to-NMDA ratio and AMPA rectification

We have previously shown that Type III neurons in the BNST are more susceptible to LTP after stress (Dabrowska et al., 2013b). Because LTP results in an alteration of synaptic strength, here, we wanted to determine if CSS itself caused a change in the strength of glutamatergic synapses in the BNST by measuring the AMPA-to-NMDA ratio. There was no significant difference in the AMPAR:NMDAR between the CSS and NS groups (1.49 ± 0.18 $n = 25$ compared to 1.29 ± 0.14 $n = 32$, $p = 0.34$; **Figure 4.4A**). Additionally, there was no difference in the AMPA rectification index (CSS: 3.016 ± 0.2128 $n = 23$; NS: 3.326 ± 0.3596 $n = 24$, $p = 0.77$) or the current-voltage relationship of the AMPA receptor between groups (**Figure 4.4B-C**). There was also no significant difference in the slopes ($p = 0.8493$, $F = 0.036$) or intercepts ($p = 0.67$, $F = 0.179$) of the linear regressions and neither the NS or CSS measures significantly differed from linearity

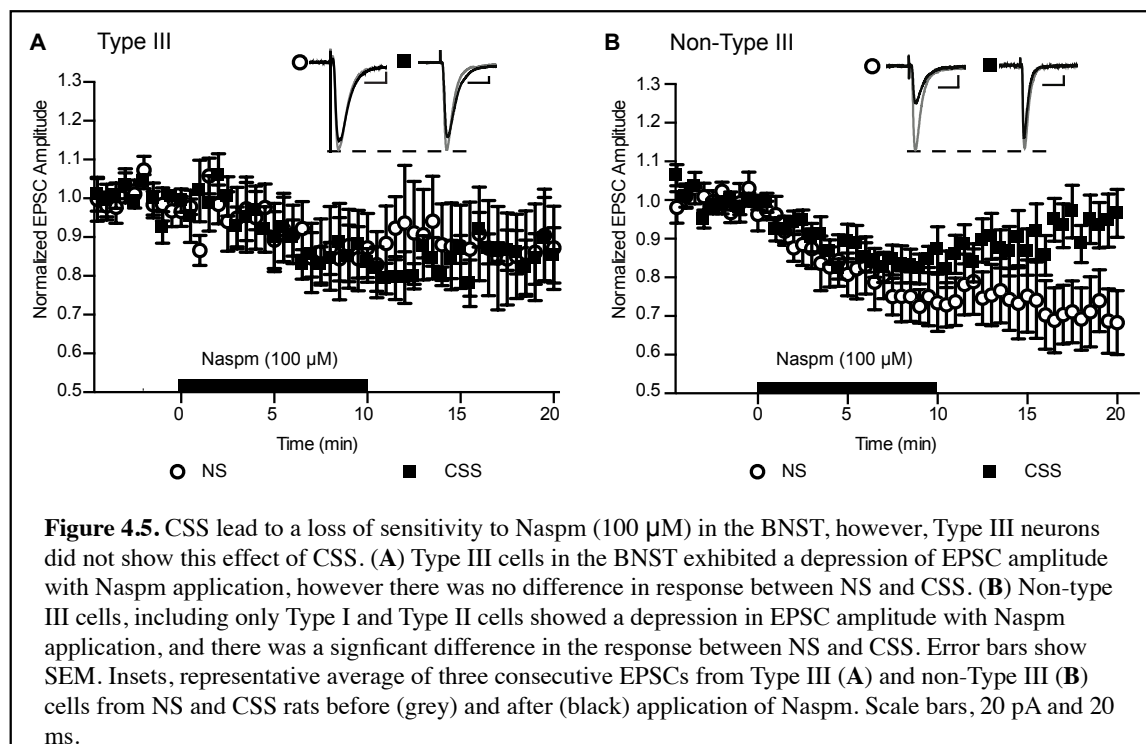
(NS $p = 0.5$ $n = 18$, CSS $p = 0.5$ $n = 17$; error bars are smaller than symbols for some data points).



Effect of stress on CP-AMPA receptors in Type III and non-Type III cells

Although there was no change in the AMPAR:NMDAR after CSS, a previous study reported a change in the contribution of CP-AMPA receptors to the AMPAR current after stress in the BNST of mice (McElligott et al., 2010). Here we wanted to determine if CSS caused a change in CP-AMPA current in the different cell types in the BNST of the rat. Across all cell types in the BNST, application of the CP-AMPA receptor antagonist Naspim (100

μM) resulted in a reduction in the amplitude of EPSCs (Time $F_{39,1560} = 4.281, p \leq 0.0001$). Furthermore, there was a significant interaction effect of time and CSS ($F_{39,1560} = 1.934, p \leq 0.001$; NS $n = 17$, CSS $n = 25$), signifying that the sensitivity to Nasp m is blunted after CSS. However, we have seen that Type III cells are uniquely sensitive to CSS due to their change in input resistance, time constant, action potential waveform, and firing rate (Figures 4.2-3). For this reason, we analyzed sensitivity to Nasp m separately in Type III and non-Type III cells. Here, we saw that there was a reduction in the amplitude of the EPSCs in Type III cells with Nasp m application (Time $F_{39,468} = 2.200, p \leq 0.0001$), however there was no difference in the response to Nasp m between the NS and CSS group (Interaction of time and stress $F_{39,4688} = 0.6802, p = 0.9305$; Stress $F_{1,12} = 0.04011, p = 0.8446$; NS $n = 8$, CSS $n = 6$; Figure 4.5A). In contrast, there was a significant interaction effect of time and CSS in the non-Type III cells (Interaction of time and stress $F_{39,1014} = 2.373, p < 0.0001$; Stress $F_{1,26} = 2.580, p = 0.1203$; NS $n = 9$, CSS $n = 19$; Figure 4.5B).



Effect of stress on gene expression

Effect of stress on mRNA for AMPA and NMDA receptor subunits in different cell types

In addition to examining the effects of CSS on CP-AMPA, AMPAR and NMDAR current, we compared the normalized quantities of mRNA for AMPA and NMDA receptor subunits in the three cell types from NS and CSS rats. First, there was no effect of stress on the expression of the AMPA receptor subunit, *Gria1* in any of the cell types (**Figure 4.6A**). However, both Type I ($p < 0.0001$) and Type II ($p < 0.0009$) cells had significant increases in mRNA levels for *Gria2* after CSS, whereas there was no significant change in the Type III cells after CSS (**Figure 4.6B**). Importantly, CP-AMPA receptors lack the GluA2 subunits, coded by *Gria2*. We also screened for the presence of the less common AMPA receptor subunits, *Gria3* and *Gria4*, however none of the cells in our sample expressed detectable levels of these transcripts.

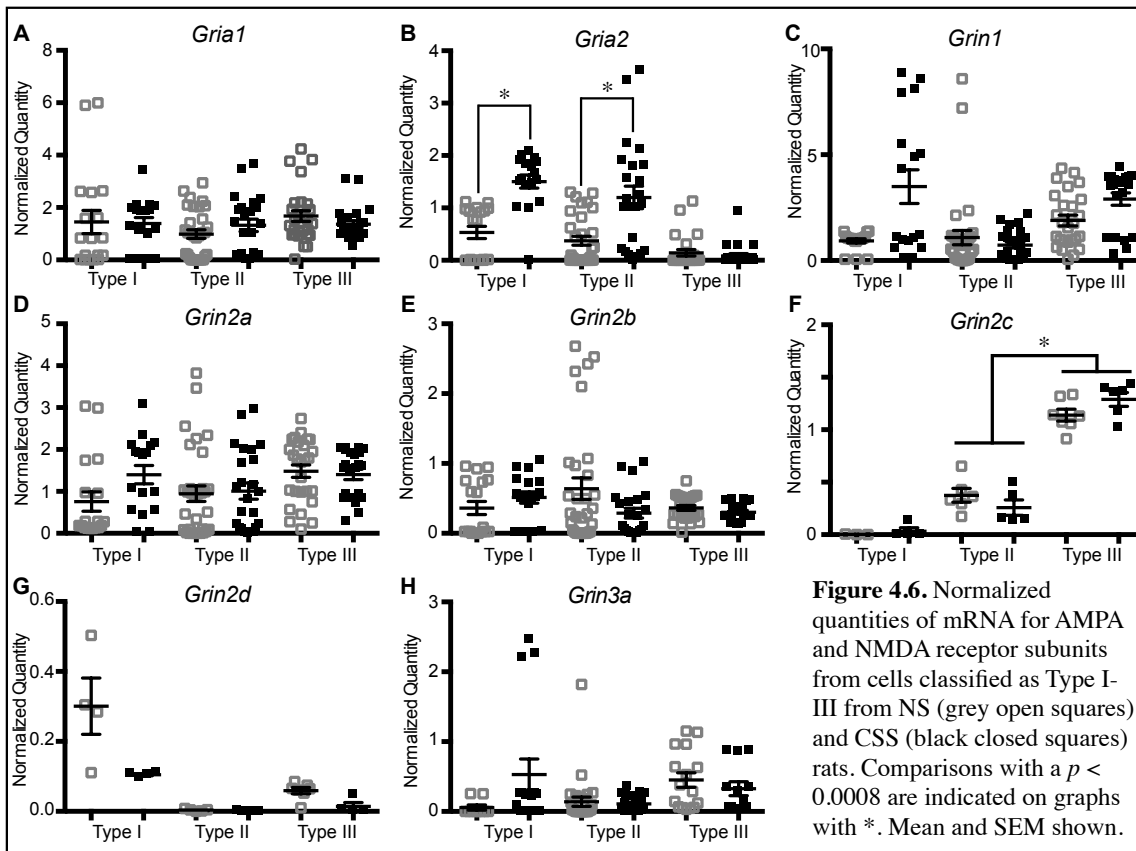
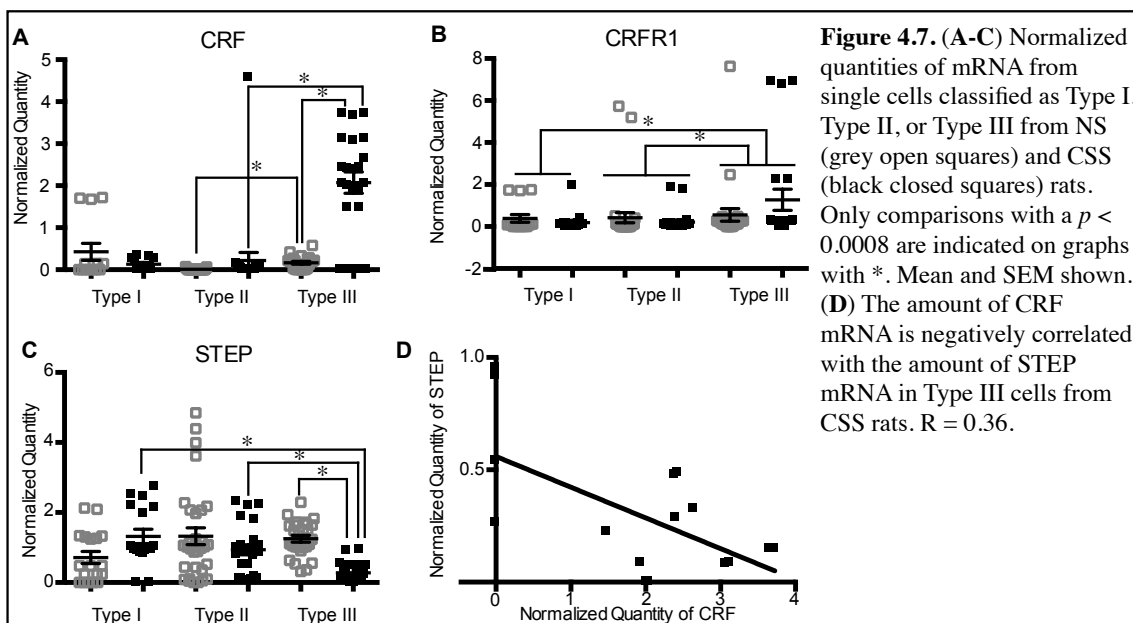


Figure 4.6. Normalized quantities of mRNA for AMPA and NMDA receptor subunits from cells classified as Type I-III from NS (grey open squares) and CSS (black closed squares) rats. Comparisons with a $p < 0.0008$ are indicated on graphs with * . Mean and SEM shown.

We also examined the normalized quantities of NMDA receptor subunits. There was no significant effect of CSS on the expression of *Grin1*, however there was a trend in the Type III cells, with Type III cells from the CSS group expressing more *Grin1* than cells from the NS group ($p = 0.01$; **Figure 4.6C**). We then looked at other NMDA subunits that could form the NMDA receptor with *Grin1*. The most common *Grin2* subunit was *Grin2a* (**Figure 4.6D**). Again, there was no significant effect of stress in any of the cell types, however there was a trend toward an increase in mRNA expression in the Type I CSS cells ($p = 0.02$). *Grin2b* was expressed in all cell types, but there was no effect of stress on its expression in any cell type (**Figure 4.6E**). *Grin2c* was expressed in all cell types, however, only at extremely low levels in the Type I cells. Here Type III cells had significantly more *Grin2c* expression than Type II cells ($p < 0.0001$; **Figure 4.6F**). In the Type II and Type III cells, there was no effect of stress on *Grin2c* levels. *Grin2d* was also expressed in all cell types, but at low levels, particularly in Type II cells (**Figure 4.6G**). In both Type I ($p = 0.03$) and Type III ($p = 0.01$) cells there was a trend toward a reduction in *Grin2d* levels with CSS. Finally, transcripts for *Grin3a* were also detected in all cell types, however, fewer than 60 % of Type III cells expressed the transcript at detectable amounts. There was a trend toward an increase in *Grin3a* mRNA in Type I cells after CSS ($p = 0.005$) as well as an increase in the percentage of cells expressing the transcript from 50 % of Type I cells in the NS condition to 89 % in the CSS condition (**Figure 4.6H**).

Cell-type specific expression of mRNA for CRF and related peptides



These results suggest that Type III neurons are uniquely sensitive to CSS, never showing the same effect of stress as Type I and Type II cells. Previously, we have shown that Type III neurons express the mRNA for CRF and STEP (Dabrowska et al., 2013a; 2013b). Here, we used scRT-PCR to examine the effect of stress on expression of mRNAs coding for CRF, STEP, and related proteins in the different cell types in the BNST to determine if expression of these mRNAs was also uniquely affected by stress in Type III neurons. The majority of cells in all cell types in both conditions had detectable amounts of mRNA for CRF and the CRF1 receptor (CRFR1), however, the amounts of transcript expression differed across cell type and stress condition. In the NS animals, Type III cells expressed significantly more CRF mRNA than Type II cells ($p < 0.0001$), and there was a slight trend toward Type I cells from NS animals also expressing more CRF mRNA than Type II cells from NS animals ($p = 0.04$). After stress, there was a significant increase in CRF mRNA in Type III cells ($p < 0.0001$). Interestingly, the CRF mRNA expression in Type III cells from CSS rats was bi-modally distributed, with 4 out of 22 neurons

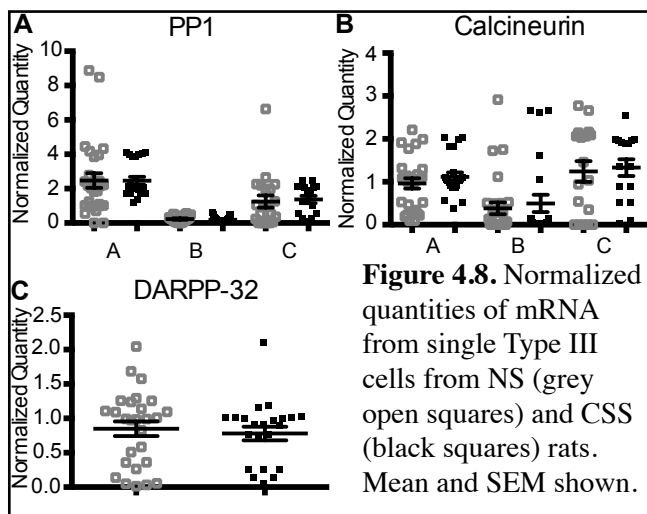
expressing CRF mRNA at normalized quantities less than 0.0001 and the rest expressing CRF mRNA at normalized quantities greater than 1 (**Figure 4.7A**). There was no effect of stress on CRF mRNA expression in the Type I or Type II cells. In the CSS rats, Type III cells expressed significantly more CRF mRNA than Type II cells ($p < 0.0009$), and there was a stronger trend toward the Type III cells also expressing more CRF mRNA than the Type I cells ($p = 0.002$).

There were also differences in the normalized quantities of mRNA for CRFR1 between cell types, however, there were no effects of stress in any cell type. Here, Type III cells in NS and CSS rats had more CRFR1 mRNA than Type I ($p < 0.0009$) and Type II cells ($p < 0.0001$; **Figure 4.7B**).

Effect of stress on expression of STEP mRNA and related signaling peptides in Type III cells

Like CRF, the majority of cells in each cell type and condition expressed some detectable amount of mRNA for STEP. In the NS animals, each cell type had similar levels of STEP mRNA, although there was a trend toward the Type III cells having more STEP mRNA than the Type I cells ($p = 0.007$). However, Type III cells in the CSS group had significantly lower levels of STEP than Type III cells from the NS group ($p < 0.0001$). Alternatively, there was no change in the normalized quantity of STEP mRNA in the Type II cells, and a slight trend toward an increase in STEP mRNA in the Type I cells after stress ($p = 0.048$). This resulted in Type III cells having significantly less STEP mRNA than Type I ($p < 0.0001$) and Type II cells ($p < 0.0009$) in CSS rats (**Figure 4.7C**). Importantly, there was a significant negative correlation between the amount of CRF mRNA and amount

of STEP mRNA expressed in Type III cells from CSS ($R^2 = 0.36, p < 0.01$), but not NS rats (Figure 4.7D).



Because Type III cells are the only cell type with STEP mRNA levels significantly affected by stress, we screened the Type III cells for mRNA coding for other proteins involved in the STEP signaling cascade: protein phosphatase 1 (PP1) A, PP1B, PP1C, Calcineurin A,

Calcineurin B, Calcineurin C, and DARPP-32. The majority of Type III cells expressed detectable levels of all of these transcripts, however, there were only low levels of PP1B (Figure 4.8A-C). There was no effect of stress on the expression of any of these genes in the Type III cells.

Discussion

In this study, we showed multiple ways in which stress uniquely affected Type III neurons in the BNST_{ALG}. Here we used a CSS paradigm that resulted in a strong context-conditioned fear and an increase in anxiety-like behavior as measured by the ASR but had no effect on exploratory behavior in the open field and EZM tests (Figure 4.1). Regardless, the CSS caused numerous long-lasting physiological and genetic changes in the BNST_{ALG}. Importantly, these changes were cell-type specific as no effect of stress was seen equally in all cell types. First, we reported that Type III cells exhibited a significant reduction in input resistance and time constant after CSS. Additionally, the action potential waveform

of Type III cells from the CSS group was wider with a slower rise-time and longer action potential half-width than Type III cells from the NS group (**Figure 4.2**). Type III cells from the CSS group also fired fewer action potentials at similar current injections and membrane potentials than Type III cells from the NS group (**Figure 4.3**). Finally, only Type III cells showed an increase in CRF and a decrease in STEP mRNA with CSS (**Figure 4.7A, C**). None of these changes are observed in Type I or Type II cells. In contrast, only non-Type III cells from the CSS group exhibited a loss of sensitivity to the CP-AMPA antagonist, Nasp_m, indicating a reduction in CP-AMPA-dependent current after stress. However, there was no change in Nasp_m sensitivity in Type III cells with CSS (**Figure 4.5**). Accordingly, only Type I and Type II cells showed an increase in mRNA expression for the AMPA subunit *Gria2* (**Figure 4.6B**). We also demonstrated for the first time that chronic stress had no effect on the AMPA-to-NMDA ratio in the BNST_{ALG} (**Figure 4.4**). Together, these experiments showed numerous examples of how chronic stress can uniquely affect individual cell types in the BNST_{ALG}.

Effect of CSS on context fear and anxiety-like behavior

Consistent with previous observations, the 7-day CSS paradigm caused a long-lasting increase in anxiety-like behavior as measured by an elevated ASR 6 days after the last day of shock stress. Previously our lab has shown a similar elevation in startle response after 4 days of repeated shock stress (Hammack et al., 2009; Hazra et al., 2012; Dabrowska et al., 2013b). We extended the duration of the shock stress in the hopes of causing a more prominent increase in anxiety-like behavior that could be measured in the acoustic startle test as well as the open field and EZM tests. Interestingly, only a moderate increase in the acoustic startle response was seen with CSS, and there was no significant difference in

behavior in the open field and EZM tests (**Figure 4.1**). In fact, there were some CSS rats that seemed to exhibit lower anxiety-like behavior in the EZM than NS rats (**Figure 4.1E**). We hypothesize that the CSS rats were over-trained to associate the foot-shock with the particular environment of the shock context. When placed in a different context for the open field and EZM tests, the rats had at least 4 hours to habituate to the room, giving the CSS rats time to learn this context did not predict foot-shock. The EZM test was always performed in the same room the day after the open field test, giving the CSS rats a total of at least 8 hours in this room without foot-shock. The room in which the open field and EZM tests take place is then associated with safety for the CSS group, perhaps suppressing any increase in anxiety-like behavior caused by the CSS. In contrast, the acoustic startle test only includes a 5-minute habituation period before the presentation of the acoustic startle stimuli. Perhaps this does not give the CSS rats enough time to form an association of safety with this environment. Alternatively, the acoustic startle response and open field and EZM tests could probe different manifestations of anxiety. Both the open field and EZM tests measure exploratory and risk-taking behavior by observing the rats' approach to the center or open portions of the fields. In contrast, the acoustic startle response is looking at a reflexive pathway that can be modulated by fear and anxiety (Davis et al., 1997). It is possible that our CSS paradigm only affects the reflexive anxiety response and not exploratory behavior. Perhaps a more unpredictable stress paradigm, such as chronic unpredictable stress, would cause a more general increase in anxiety-like behavior in all tasks (Ventura-Silva et al., 2013).

Unsurprisingly, the CSS paradigm caused CSS rats to exhibit fear-behavior in the shock context the day after the last exposure to the foot-shock (**Figure 4.1A**). Interestingly,

the context fear was drastically reduced 6 days after CSS, however there was still a trend toward the CSS group freezing more than the NS rats in the shock context. The BNST is known to be critical for context fear conditioning (Davis and Walker, 2014; Zimmerman and Maren, 2011; Hammack et al., 2015). Importantly, the BNST has also been shown to be an important modulator of the startle reflex. Early studies showed that lesions of the BNST had no effect on fear-potentiated startle, but prevented the gradual increase in baseline startle due to repeated foot-shock (Gewirtz et al., 1998). Therefore, changes observed in the BNST_{ALG} after CSS may, in part, lead to these changes in behavior.

Effect of stress on electrophysiological properties and genetic expression in Type III cells

To our knowledge, no study has examined the effects of chronic stress on intrinsic electrophysiological properties of different cell types in the BNST. Here, we showed that multiple electrophysiological properties of Type III cells were uniquely affected by CSS. There was a 25 % reduction in input resistance in Type III cells after CSS, indicating it will take more current to depolarize Type III cells after CSS (**Figure 4.2A**). Additionally, there was a decrease in the time constant of the membrane in Type III cells from CSS rats. This may be explained by the reduction in input resistance, as the time constant of the membrane is a function of the cell's input resistance. A reduction in input resistance would result in a change in the neuron's observed signal-to-noise ratio; specifically, excitatory input would need to be stronger in order to drive the neuron to action potential threshold. Furthermore, the faster time constant would cause summation of EPSCs to be more difficult, also resulting in a need for more excitatory input to drive the cell. If there was an increase in activity in Type III neurons during CSS, a reduction in input resistance may be one way in

which Type III neurons are maintaining homeostatic control (Gasselin et al., 2015). Interestingly, neurons in the dorsal BNST have been shown to be under tonic GABA inhibition (Egli and Winder, 2003). It is possible that the lower input resistance of Type III cells after CSS is due to an increase in tonic inhibition of these cells, perhaps as a way to prevent this population of CRF neurons from being too active. Alternatively, the input resistance could be lower due to an increase in baseline glutamatergic input. Future studies could examine spontaneous excitatory and inhibitory postsynaptic potentials to determine if there is a change in baseline input to Type III neurons after stress.

In addition to changes in input resistance, Type III neurons exhibited a widening of the action potential waveform and a change in firing rate (**Figure 4.2C-D, 4.3C-D**). In the hippocampus, activity-dependent changes in action potential repolarization have been shown to be driven by a switch from the expression of Kv3 channels to Kv2 channels (Steinert et al., 2011). However, here we saw a change in the rise time of the action potential. Interestingly, the reduction in input resistance was consistent with a homeostatic mechanism to reduce excitability after prolonged activation of Type III cells, however, the widening of the action potential was not; rather, the action potential waveform would be predicted to be narrower after stress (Lee et al., 2015). Regardless of the cause for the wider action potential waveform, this change may have resulted in altered calcium signaling. A longer action potential results in more calcium entry in the dendrites (McCobb and Beam, 1991; Helmchen et al., 1996), potentially acting on calcium-activated effectors. One such class of proteins are potassium channel interacting proteins (KChIPs) found in the dendrites of neurons in the BNST_{ALG} (Rainnie et al., 2014). KChIPs bind calcium and facilitate the transport of Kv4 channels to the plasma membrane (Shibata et al., 2003; Wang et al., 2005;

Chen et al., 2006). Kv4 channels are voltage-gated potassium channels that exhibit rapid inactivation, fast recovery from inactivation, and subthreshold activation, allowing them to modulate action potential waveform, latency to spike, and firing frequency (Malin and Nerbonne, 2001; Shibata et al., 2003; Bourdeau et al., 2011). Knock-down of KChIPs using short interfering RNAs (siRNAs) has been shown to increase the firing rate of interneurons, but not pyramidal cells, in the hippocampus (Bourdeau et al., 2011). Perhaps increased KChIP activation caused the reduction in firing frequency seen in Type III cells after stress (**Figure 4.3C-D**). Importantly, Kv4 channels have also been shown to regulate EPSP conduction from the dendrites to the soma. A change in dendritic expression of Kv4 channels could influence the effectiveness of excitatory activity to drive action potentials. Future studies could examine the change in Kv4 channel activity by measuring the effect of CSS on the magnitude of the I_A current in Type I, Type II, and Type III cells to see if it, too, is specifically changed in the Type III cells. This observed reduction in firing rate in the Type III cells is potentially another way in which the Type III neurons are maintaining homeostatic plasticity after a period of prolonged activation.

Importantly, previous studies have shown that about 95% of Type III cells in the rat BNST express the mRNA for CRF (Dabrowska et al., 2011; 2013a). Here we showed all cell types in the BNST_{ALG} expressed some levels of CRF mRNA; however, the Type III neurons expressed it at higher levels than the Type II cells and were the only cell type that showed increased CRF mRNA expression after CSS (**Figure 4.7A**). The discrepancy between previous studies and the current study is likely due to differences in methodology. Previous scRT-PCR experiments did not include a pre-amplification step prior to performing the PCR (Dabrowska et al., 2011; Hazra et al., 2011; Dabrowska et al., 2013a;

2013b). With our new method, we were able to detect mRNA at much lower levels than before. Importantly, mRNA is not always translated into protein, so the presence of low levels of mRNA does not guarantee that the cell is producing the corresponding protein. However, a switch to higher production of mRNA following CSS suggests the Type III neurons were potentially producing more of the protein. Consistent with our observation, chronic mild stress has been shown to cause a selective increase in CRF mRNA expression in the dorsal BNST but not ventral BNST or central amygdala, and experimental neuropathic pain has been shown to cause an increase in CRF mRNA expression in the ovBNST (Kim et al., 2006; Rouwette et al., 2012). Together, these results suggest that the Type III CRF neurons in the BNST_{ALG} are particularly sensitive to chronic stress. In our data, we saw a small population of Type III neurons in CSS rats that had less CRF mRNA than the rest of the population (**Figure 4.6A**). Perhaps with each stressor, a portion of Type III neurons are recruited into the stress response and begin increasing production of CRF mRNA. If this is true, we would predict that there would be fewer Type III cells with high levels of CRF mRNA after two days of shock stress; this population would grow the longer and more frequent the stressor occurs. Future studies could explore this hypothesis.

In addition to expressing CRF mRNA, Type III neurons expressed the mRNA for the CRF 1 receptor (CRFR1; **Figure 4.6B**). Although there was low expression for CRFR1 mRNA in all cell types in the BNST, Type III cells expressed it at higher levels than Type I and Type II cells. Interestingly, regions of the brain containing CRF neurons are often interconnected and express CRFR1 (Sakanaka et al., 1986; Day et al., 1999; Dabrowska et al., 2011; O'Malley et al., 2014). This suggests that CRF neurons throughout the brain are sensitive to the activity of other CRF neurons. For example, the central amygdala is known

to release CRF in the BNST_{ALG} (Erb et al., 2001; Nakagawa et al., 2005). CRF acts on CRFR1 in the BNST to increase glutamatergic input and anxiety-like behavior (Sahuque et al., 2006; Kash et al., 2008). Although part of the CRF action in the BNST is presynaptic, the expression of CRFR1 mRNA in Type III neurons suggests there could also be a postsynaptic effect on Type III cells. Alternatively, CRFR1 in Type III cells could be localized to axon terminals. Although the projections for the majority of neurons in the ovBNST remain inside the BNST, CRF neurons in the ovBNST are known to project to other areas including the PVN (Dabrowska et al., 2011). Here, CRF may act on presynaptic CRFR1 to modulate neurotransmitter release at target sites.

Interestingly, the majority of the electrophysiological changes observed after stress specifically occurred in the Type III neurons and suggest a reduction in excitability, potentially as a form of homeostatic plasticity after prolonged activation. Stress caused by acute pain in the hind paw of a rat results in an increase in cFos and CRF mRNA expression in the ovBNST (Rouvette et al., 2011). Perhaps Type III neurons, or a portion of Type III neurons, in the ovBNST are being activated with each session of footshock, causing a long-term shift in their electrophysiological properties and genetic expression profile. As discussed previously, the widening of the action potential is the one electrophysiological change that does not correspond with a homeostatic mechanism to reduce excitability. Rather, the longer duration of the action potential leads to more opportunity for calcium to enter the neuron (Cárdenas and Marengo, 2016). Calcium is the crucial signal for the release of vesicles; for fast synaptic transmission, such as the release of GABA, calcium channels are closely associated with the active zone causing fast release of the neurotransmitter. In contrast, large dense core vesicles (LDCV) containing neuropeptides

such as CRF, are further away from calcium channels and require more calcium in order to be released (Kits and Mansvelder, 2000). Perhaps the wider action potentials after stress facilitate the release of more neuropeptide from Type III neurons. However, firing frequency has been shown to be a crucial factor in determining release of LDCVs in adrenal chromaffin cells (Cárdenas and Marengo, 2016), and the Type III neurons have a lower firing rate after stress.

Here, we showed multiple ways in which Type III neurons exhibited a reduction in excitability after CSS. On the other hand, previous work in our lab showed that Type III neurons undergo a more pronounced LTP after chronic restraint stress due to a reduction in expression of STEP (Dabrowska et al., 2013b). Importantly, our scRT-PCR data replicated this observed reduction in STEP expression in Type III cells after CSS (**Figure 4.6C**). STEP is a brain-specific tyrosine phosphatase known to block LTP in the amygdala and BNST (Paul et al., 2007; Dabrowska et al., 2013b). Here, we showed that STEP mRNA was expressed in Type I, Type II, and Type III cells; however, there was only a reduction in STEP expression in the Type III neurons (**Figure 4.6C**). In fact, there was a slight trend toward an increase in STEP mRNA in Type I neurons after CSS. Previously we reported STEP mRNA expression was restricted to Type III cells and STEP-immunoreactivity was restricted to CRF neurons (Dabrowska et al., 2013b), however, similar methodological considerations discussed in regards to the CRF mRNA expression apply here. Significantly, Type III neurons are the only cell type that show an increase in CRF mRNA and reduction in STEP mRNA after CSS. This reduction in STEP expression makes Type III neurons more susceptible to plasticity after stress (Dabrowska et al., 2013b). Moreover, the changes in mRNA expression levels were negatively correlated, such that Type III

neurons with high levels of CRF mRNA expressed low levels of STEP mRNA (**Figure 4.7**), suggesting that reductions in the expression of STEP may precede enhancement of CRF expression.

There are multiple signaling molecules that control the activity of STEP. For example, the phosphatase PP1 activates STEP by dephosphorylating the enzyme, and DARPP-32 inhibits PP1, thereby indirectly inhibiting STEP activity (Greengard, 2001; Goebel-Goody et al., 2012). Conversely, calcineurin inhibits DARPP-32, releasing PP1 inhibition of STEP (Greengard, 2001). Here we looked to see if expression of any of these key regulatory proteins in Type III neurons was affected by stress. As expected, Type III neurons expressed DARPP-32 as well as multiple isoforms of both PP1 and calcineurin, however there was no difference in expression levels between the NS and CSS groups, suggesting expression of STEP was specifically affected by stress manipulations (**Figure 4.8**).

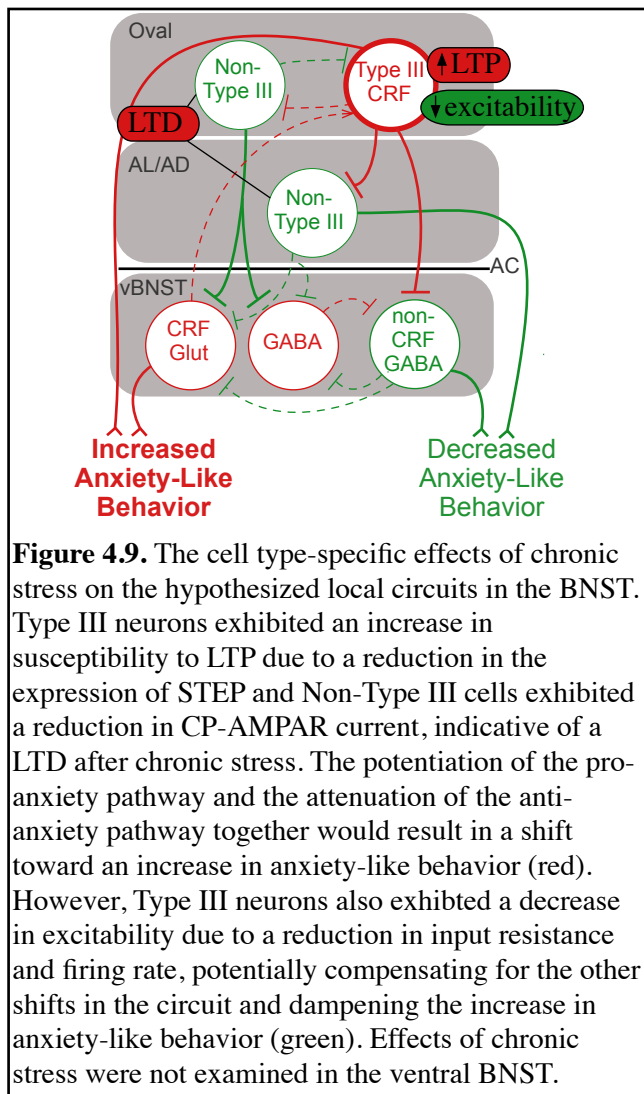
AMPA-to-NMDA ratio

The reduction in STEP expression in the Type III neurons may have caused these neurons to be particularly sensitive to changes in synaptic plasticity. Previous studies have shown that stress can cause changes in synaptic plasticity at glutamatergic synapses in the BNST (McElligott and Winder, 2007; Francesconi et al., 2009; Conrad et al., 2011; Glangetas et al., 2013; Dabrowska et al., 2013b), however, no study to date had specifically examined the effect of chronic stress on the ratio of AMPA to NMDA receptor- dependent currents (AMPA:NMDAR) in the BNST_{ALG}. An increase in the AMPAR:NMDAR is indicative of a strengthening of excitatory synapses and is known to occur in the BNST in response to self-administration of cocaine (Dumont et al., 2005). However, in this study,

we did not observe a change in the AMPAR:NMDAR with CSS (**Figure 4.2A**). Importantly, we were not able to differentiate between cell types in this experiment. In order to accurately measure the AMPAR:NMDAR, the cell must be voltage-clamped at a depolarized potential to ensure the release of the magnesium block of the NMDA receptors. A cesium-gluconate based patch solution was used in order to block potassium channels and prevent cell death at depolarized potentials. Unfortunately, the patch solution also significantly altered the currents that are used to distinguish cell types from one another. Hence, it is possible that a particular cell type does have a change in AMPAR:NMDAR following CSS that was masked by including other cell types in the analysis.

AMPA Rectification and CP-AMPARs

The majority of AMPARs do not pass calcium and display a linear current-voltage (IV) relationship; however, AMPARs lacking the GluA2 subunit, coded by *Gria2*, are permeable to calcium (CP-AMPAR) and inwardly rectifying due to an intracellular polyamine block at depolarized potentials (Cull-Candy et al., 2006). Due to their ability to pass calcium at hyperpolarized potentials, CP-AMPARs have been implicated in NMDA-independent LTD and LTP, homeostatic regulation, and synaptic priming (Cull-Candy et al., 2006; Tukey and Ziff, 2013). A previous study has shown that stress can cause LTD in the BNST by reducing CP-AMPAR-dependent current in mice (McElligott et al., 2010). However, the McElligott study did not address the question of cell type-specificity of this response. Here we tested the relative contribution of CP-AMPARs to the AMPA current of BNST neurons in two ways: indirectly, by measuring the inward rectification of the AMPAR current, and directly with the use of the CP-AMPAR specific antagonist, Naspmp.



First, after measuring the AMPAR:NMDAR, the amplitude of the AMPAR current was measured at voltages ranging from +40 mV to -70 mV, creating an IV plot for the AMPA current. Because whole-cell patch clamp recordings dilute the polyamines necessary to block the CP-AMPA receptors at depolarized potentials, exogenous spermine (100 μM) was included in the cesium-gluconate patch solution (Bellone and Lüscher, 2006; Wiltgen et al., 2010). Spermine is an endogenous polyamine that is a major contributor

to the intracellular block for the CP-AMPA receptors. However, we did not observe any differences in the rectification properties of the AMPA receptors between NS and CSS rats, and the IV plot did not significantly differ from linearity for either group (**Figure 4.4B**). Nevertheless, the ability of the CP-AMPA antagonist, Naspmm to reduce the amplitude of the EPSCs in the BNST demonstrated that there was a significant contribution of CP-AMPA receptors to the AMPA current (**Figure 4.5**). Paradoxically, we did not observe the inward rectification of the AMPA current that is indicative of the presence of CP-AMPA receptors (Cull-Candy et al., 2006). This was potentially due to an incomplete diffusion

of the exogenous spermine or the loss of the polyamine block due to the polyamines permeating the AMPA receptors during the prolonged depolarization at + 40 mV (Koh et al., 1995; Bellone and Lüscher, 2006). For this reason, we were not able to use this experiment to determine if there was a change in the contribution of CP-AMPA receptors to the AMPAR current with stress.

We then directly tested the contribution of CP-AMPA receptors to the AMPAR current with the application of Nasp. The cells were held at -70 mV to ensure the presence of the magnesium block on NMDA receptors and the release of the polyamine block on CP-AMPA receptors (Dingledine et al., 1999). Nasp reduced the amplitude of the EPSCs in all cell types in the BNST, but the sensitivity to Nasp was blunted after CSS, indicating a reduction in the contribution of CP-AMPA receptors to the total AMPAR current after stress (**Figure 4.5A**). This replicated the finding that chronic restraint stress reduced Nasp-sensitivity in the BNST of mice (McElligott et al., 2010). We then built on this observation to show that the effect of stress on CP-AMPA current was not seen equally in all cell types; there was no significant difference in the response to Nasp between the Type III cells from the NS and CSS groups while there was a significant interaction effect of time and stress in the non-Type III cells (**Figure 4.5B-C**). The reduction in CP-AMPA current in the BNST of the mouse was shown to be a result of a LTD mediated by α 1-adrenergic receptors (McElligott et al., 2010). These new findings indicate that only non-Type III cells in the BNST would undergo this LTD after stress, leaving Type III cells just as sensitive to glutamatergic input as they were prior to stress. We have proposed a model of opposing circuits within the BNST in which non-Type III and Type III CRF cells mutually inhibit one another, with Type III cells acting to enhance anxiety-like behavior (Daniel and

Rainnie, 2015). With the loss of CP-AMPA-dependent current, non-Type III cells may be less responsive to glutamatergic input, thereby less able to provide inhibitory input to the Type III CRF neurons. This shift in synaptic strength may mediate, in part, the increase in anxiety-like behavior seen after CSS.

AMPA receptors are composed of two sets of symmetric dimers: generally, a dimer consisting of GluA2 (coded by *Gria2*) with a dimer of either GluA1, GluA3, or GluA4 (coded by genes *Gria1*, *Gria3*, *Gria4* respectively). However, CP-AMPA receptors lack GluA2 entirely, and instead consist only of dimers of GluA1, GluA3, and GluA4 (Cull-Candy et al., 2006). Interestingly, none of the neurons in our sample expressed mRNA for *Gria3* or *Gria4*, although only a small number of cells have been screened for these genes. In contrast, all of the cell types in the BNST expressed mRNA for *Gria1* and *Gria2*. There was no change in *Gria1* expression with stress in any of the three cell types, however, there was a significant effect of stress on the expression of mRNA for *Gria2*. The lack of change in *Gria1* expression with stress in any cell type fits with the lack of change in the AMPAR:NMDAR. Importantly, only Type I and Type II cells showed an increase in *Gria2* mRNA after stress while there was no effect of stress in the Type III cells (**Figure 4.6B**). This suggests more AMPARs in Type I and Type II cells would be able to incorporate GluA2 subunits, thereby making AMPARs impermeable to calcium, and supports the hypothesis that there is a reduction of CP-AMPA receptors in non-Type III cells after CSS.

Differences in expression of NMDA receptor subunits

Unlike AMPA receptor expression, there was not a substantial change in the expression of mRNA for NMDA receptor subunits after stress. NMDA receptors are heterotetramers comprised of two GluN1 subunits and two GluN2 subunits, coded by genes

Grin1 and *Grin2* respectively. All cell types expressed mRNA for *Grin1*. Interestingly, there was a trend toward a significant increase in *Grin1* expression in Type III cells (**Figure 4.6C**; $p = 0.01$). Previously, we have shown that there is an increase in the amount of the GluN1 subunit of the NMDA receptor in the membrane fraction of the BNST after chronic restraint stress (Dabrowska et al., 2013b). Importantly, STEP activity can lead to the internalization of NMDA receptors (Goebel-Goody et al., 2012). Future studies will need to see if the observed increase in *Grin1* expression in Type III cells after stress is replicable before determining its significance.

Although we did not find a change in *Grin2* subtype expression with stress, there were significant differences in the distribution of *Grin2* subunits across cell types. The most common *Grin2* subunit across cell types was *Grin2a* followed by *Grin2b* (**Figure 4.6D-E**). Importantly, STEP acts on the GluN2B subunit of NMDA receptors to promote internalization (Goebel-Goody et al., 2012). *Grin2d*, on the other hand, was only expressed at relatively low levels (**Figure 4.4G**). Interestingly, *Grin2c* was expressed at very different levels in the distinct cell types in the BNST (**Figure 4.4F**). Although expressed in Type I cells, it was only there at very low levels. Type II cells expressed moderate amounts of the mRNA for *Grin2c*, and Type III cells expressed the highest levels. Importantly, GluN2C has been implicated in the stress response, fear acquisition, and major depressive disorder (Karst et al., 2002; Hillman et al., 2011; Chandley et al., 2014) and is not widely expressed in the brain (Thompson et al., 2000). This raises the possibility for GluN2C to be a potential target for therapeutic manipulation. Although there is no GluN2C specific antagonist currently, there is a potentiator selective for the GluN2C and GluN2D subunits (Mullasseril

et al., 2010), suggesting GluN2C containing receptors could be targeted for therapeutic benefit.

NMDA receptors containing GluN1 and GluN2 subunits require the binding of glutamate and glycine to be activated. In contrast, NMDA receptors containing GluN1 and GluN3 subunits only require glycine to be activated but only exhibit a small current (Chatterton et al., 2002; Mohamad et al., 2013). Because of the relatively weak current that GluN3 containing NMDA receptors generate, GluN3 subunits have been regarded as inhibitory subunits in the NMDAR complex. Interestingly, only about 57 % of Type III neurons expressed detectable levels of *Grin3a* mRNA whereas 89 % of Type II neurons expressed it. In Type I cells, only 50 % of cells from NS rats expressed detectable levels of *Grin3a* but 89 % of cells from CSS rats expressed it, and, in Type I cells that expressed *Grin3a*, there was a trend toward an increase in expression after CSS ($p = 0.005$; **Figure 4.6H**). Although GluN3A is mostly thought to be involved in development, adult GluN3A knock-out mice display differences in locomotion, enhanced pain sensation, enhanced object recognition and spatial memory, as well as enhanced LTP in the hippocampus (Mohamad et al., 2013). To our knowledge, no study has examined the role of GluN3A-containing NMDA receptors in the BNST. Future studies could determine if the increase in *Grin3a* mRNA expression in Type I cells after CSS is reproducible and translates to a significant change in GluN3A containing NMDA receptors.

Conclusion

These studies reveal several ways in which chronic stress differentially affects Type I, Type II, and Type III cells in the BNST_{ALG}. Importantly, none of the effects of stress observed were seen in all cell types. We show non-Type III cells undergo a reduction in

CP-AMPA current indicative of LTD after CSS (McElligott and Winder, 2007). This process does not occur in Type III neurons, potentially causing a shift in the balance of glutamatergic input in the BNST_{ALG} to favor the Type III cells. Importantly, we provide evidence here that Type III neurons in the BNST_{ALG} represent a group of CRF neurons particularly sensitive to chronic stress manipulations. The differential effect of stress on Type III neurons compared to the other cells in the BNST suggests Type III cells perform a different role in the circuit than Type I and Type II cells. Type III cells exhibited multiple physiological changes indicative of a reduction in excitability. However, these neurons also showed a significant reduction in STEP mRNA expression and increase in CRF mRNA expression, suggesting they had increased the release of CRF to downstream targets. Whereas most of the electrophysiological changes in Type III neurons are in line with a reduction in excitability, the loss of STEP would result in these neurons being particularly sensitive to future input and synaptic plasticity. These experiments were performed 6 - 9 days after the CSS ended, suggesting the effects of stress are long-lasting. However, we are most likely also capturing slow compensatory responses that act to maintain homeostatic control after a period of chronic stress. Future studies could aim to tease apart the behavioral role of these changes in the circuit and find ways in which to target specific cell types to reduce the long-term effects of chronic stress.

Gene name	Type I		Type II		Type III	
	NS	CSS	NS	CSS	NS	CSS
CRF	13 / 18	11 / 17	31 / 32	24 / 24	25 / 27	22 / 22
CRFR1	15 / 18	17 / 17	31 / 32	24 / 24	26 / 27	22 / 22
STEP	18 / 18	17 / 17	31 / 32	24 / 24	27 / 27	22 / 22
PP1A					27 / 27	22 / 22
PP1B					20 / 20	17 / 18
PP1C					20 / 20	16 / 18
Calcineurin A					27 / 27	22 / 22
Calcineurin B					27 / 27	22 / 22
Calcineurin C					18 / 20	16 / 18
DARPP-32					27 / 27	22 / 22
<i>Gria1</i>	18 / 18	17 / 17	32 / 32	22 / 24	27 / 27	22 / 22
<i>Gria2</i>	18 / 18	17 / 17	31 / 32	24 / 24	25 / 27	22 / 22
<i>Gria3</i>	0/4	0/4	0/7	0/6	0/7	0/6
<i>Gria4</i>	0/4	0/4	0/7	0/6	0/7	0/6
<i>Grin1</i>	18 / 18	17 / 17	32 / 32	24 / 24	26 / 27	22 / 22
<i>Grin2a</i>	18 / 18	17 / 17	32 / 32	24 / 24	27 / 27	22 / 22
<i>Grin2b</i>	18 / 18	17 / 17	31 / 32	22 / 24	26 / 27	22 / 22
<i>Grin2c</i>	3 / 4	4 / 4	6 / 7	5 / 6	7 / 7	6 / 6
<i>Grin2d</i>	4 / 4	4 / 4	5 / 7	5 / 6	7 / 7	4 / 6
<i>Grin3a</i>	9 / 18	16 / 18	28 / 32	22 / 24	16 / 27	12 / 22

Supplementary Table 4.1. Number of neurons that expressed detectable levels of a specific mRNA in each cell type in NS and CSS rats out of the number of neurons screened for that gene.

Chapter 5: Conclusion and future directions

The preceding chapters have examined the complex organization of neurons in the anterolateral group of the BNST (BNST_{ALG}) and how these neurons are differentially affected by stress. By defining cell types based on similar electrophysiological and genetic expression profiles, we can create an experimental construct beyond anatomical location that allows for a more nuanced way of probing the circuit being studied. Here we show that Type III cells in the BNST_{ALG} represent a population of neurons in the oval nucleus (ovBNST) that are particularly sensitive to chronic stress and are likely to use corticotropin releasing factor (CRF) as a neuropeptide. Separating cells in the BNST_{ALG} based on their response to current injection allowed for detection of effects of stress that would otherwise have been washed out in the population average. Future research can aim to use viral-based approaches to selectively define and target more precise cell types in the BNST for manipulation in order to define their role in the circuit. As we begin to gain a better understanding for the ways in which particular cell types are affected by chronic stress (or other manipulations) and the behavioral outcomes of these changes, we can use our knowledge of the differential genetic expression profile of these cell types to pharmacologically target specific parts of the circuit for therapeutic benefit.

The meaning of a cell type is ill-defined; neurons can be classified based on distinct electrophysiological, morphological, genetic, or other phenotypic differences. The motivation behind defining cell types in the BNST is to define groups of neurons that play the same role in a circuit and whose activity results in a particular set of behavioral or physiological outcomes. For example, our current hypothesis is that Type III neurons in the ovBNST of the rat represent a single cell type that promotes anxiety-like behavior, uses GABA and CRF for cell signaling, and is particularly sensitive to stress manipulations.

Importantly, neurons of the same cell type, Type I, II or III, in the BNST have other similarities with one another as well, such as ion channel and serotonin receptor expression profile (Hazra et al., 2011; 2012). This provides further evidence that these neurons represent a functional unit of the circuit. However, as we learn more about these cell types, we may find that a single electrophysiologically defined cell type is actually comprised of multiple cell types classified by differences in genetic expression profile. For example, we have previously shown that there are three distinct subdivisions of Type II neurons based on ion channel and serotonin receptor expression (Hazra et al., 2011; 2012). Perhaps as we learn more about the expression profile of the Type I and Type III cells, we will discover multiple distinct cell types within those classifications as well. Indeed, the expression levels of many genes examined in the Type I cells were found to vary widely and sometimes exhibited a bimodal distribution (**Figure 4.6 – 4.7**), suggesting the possibility that the Type I neurons are a heterogeneous population. Use of single cell RNAseq may help us to better define neuronal cell types in the BNST by providing us with a complete picture of the genetic expression profile of these neurons (Cadwell et al., 2016).

As we showed in **Chapter 2**, these electrophysiologically defined cell types may not exist as such across species. In fact, there could be differences in the appearance of electrophysiological cell types between strains of rats. Importantly, Type I-III neurons were originally described in Sprague-Dawley rats and then confirmed to also exist in similar proportions in Lewis rats, indicating these cell types are not a manifestation of one lab strain (Hammack et al., 2007; Rodriguez-Sierra et al., 2013). However, we see drastic differences in the proportion of cell types in the BNST of mice and rhesus macaques compared to that of rats (**Chapter 2**). Minor changes in the distribution of ion channel

expression relative to cell morphology can have a significant impact on the observed electrophysiological properties of neurons. It is likely that there is conservation of cell types across species if we were to define cell types based on genetic expression profile and perhaps response to stress rather than on electrophysiological properties alone. For example, we have shown that Type III neurons in the BNST of the rat are sensitive to stress manipulations and express more CRF mRNA after chronic stress (**Chapter 4**). In the mouse and primate, Type III-like neurons defined by their electrophysiological properties represent a much higher proportion of neurons in the BNST than seen in the rat (**Chapter 2**). It is unknown if these Type III-like neurons in the mouse and primate BNST play the same functional role in the circuit as the Type III neurons seen in the rat. Just the higher percentage of Type III-like neurons in the mouse and primate BNST suggests that this group of neurons is different than Type III neurons in the rat BNST. Perhaps analysis of single cell mRNA expression profiles of the Type III-like neurons in the mouse and primate would reveal only a subpopulation of these cells closely resemble the Type III neurons in the rat BNST. This kind of comparative analysis of cell types across species is important for gaining a better understanding for how cell types in the human BNST may be organized. Specifically, determining if there is an analogous group of cells in the primate BNST to the Type III neurons in the rat may point to Type III neurons being a candidate target for therapeutic manipulation.

In addition to using GABA, and sometimes glutamate as a neurotransmitter, neurons in the BNST can also express neuropeptides such as CRF, enkephalin, neuropeptide Y, substance P, neurotensin, and many others (Ju et al., 1989; Walter et al., 1991; Day et al., 1999). One goal in defining cell types is identifying groups of neurons

that are more likely to express a particular neuropeptide and thereby have similar downstream effects. Previously, our lab has presented the hypothesis that Type III neurons in the rat BNST represent CRF neurons due to the high percentage of Type III neurons in which CRF mRNA was detected (Dabrowska et al., 2013a; 2013b). In these studies, CRF mRNA was also detected in a smaller percentage of Type I and Type II cells. Here, with improved single cell RT-PCR methods, CRF mRNA was detected in the vast majority of neurons in the BNST. In the rats that had not undergone chronic stress, the amount of CRF mRNA was relatively low, however Type III neurons had more CRF mRNA than Type II cells. Type I cells on the other hand seemed to fall into two populations: most neurons had low levels of CRF mRNA but three cells expressed higher levels of CRF mRNA (**Figure 4.7A**). In the stress group of rats, there was a significant increase in CRF mRNA in the Type III neurons. This suggests that Type III neurons after stress are producing more CRF mRNA to use for cell signaling. However, we have yet to prove that Type III neurons in the BNST are translating the CRF mRNA into CRF protein. We also do not know if the low levels of CRF mRNA in Type I and Type II cells are translated to protein. Future studies could aim to address these concerns using advanced techniques in molecular neuroscience. For example the translational ribosome affinity purification (TRAP) technique allows for tagging ribosomal subunits for analysis of which mRNA sequences are being actively translated into protein (Cook-Snyder et al., 2015). Here, we could use an adeno associated virus (AAV) to deliver a plasmid coding for the expression of a green fluorescent protein (GFP)-tagged L10a ribosomal subunit under a neuronal promoter. We would then record from the GFP tagged neurons in the BNST and classify these cells based on their electrophysiological properties before removing the intracellular contents as if

performing single cell RT-PCR. Then, before amplifying the mRNA, a magnetic GFP antibody could be used to isolate the GFP-tagged L10a ribosomal subunit along with any attached mRNA sequences (Cook-Snyder et al., 2015). Next, single cell RT-PCR would be performed on just the isolated mRNA. This would allow us to specifically measure the mRNA that is being targeted by ribosomes for translation. Using this technique, we could determine if CRF mRNA is being translated in all cell types in the BNST. The purpose of the transcription of mRNA that is not translated into protein is unknown. Perhaps it is more energetically costly for the neuron to block small levels of transcription than it is to transcribe those small levels of mRNA. Alternatively, small levels of mRNA are transcribed in order for the cell to be able to produce the corresponding protein quickly if necessary. Indeed, external stimuli are known to be able to switch the neurotransmitter being used in interneurons in the hypothalamus (Dulcis et al., 2013). Perhaps there is a trigger for neurons that do not translate CRF mRNA to begin expressing the CRF protein. Investigating which cell types translate the mRNA for CRF and under what conditions will be an important step in understanding the role of CRF neurons in the BNST.

Regardless of if Type III neurons are the only CRF neurons in the ovBNST, we provide evidence that the Type III neurons are uniquely sensitive to stress (**Chapter 4**). Interestingly, some of the changes seen in Type III neurons after chronic stress are indicative of an increase in excitability and susceptibility to activation (increase in action potential width, reduction in STEP mRNA expression, increase in CRF mRNA expression), where as others are reflective of a decrease in excitability (reduction in input resistance, time constant, and firing frequency). This suggests the response to chronic stress in Type III cells is complex and possibly involves multiple independent mechanisms, some

of which may result in an increase in anxiety-like behavior and others that may be acting to prevent changes to the circuit and maintain homeostasis. Indeed, the BNST acts as a break on the HPA axis in addition to its role in facilitating the stress response (Ulrich-Lai and Herman, 2009). For example, enkephalin neurons are active in the ovBNST after an immune stressor (Day et al., 1999), and enkephalin is known to attenuate emotional responses to stress (Tanaka et al., 2000). It is possible that these neurons are active after a stressor as a part of a feedback control system to prevent over-activation of the stress response. Interestingly, we have evidence that a subpopulation of Type II neurons express enkephalin (Dabrowska et al., 2013a), suggesting Type II neurons may act in opposition to Type III neurons in the BNST. Future studies could aim to tease apart what responses to stress are causative and act to facilitate the stress response and what responses are compensatory in nature, acting to oppose the over-activity of the HPA axis and anxiety response.

In order to better understand the causative and compensatory changes in the BNST in response to stress, we need to first learn the timeline of these complex changes. Here, we looked at long-term changes (6 – 9 days after the last stressor) after a chronic (7-day) stressor. Future studies could examine the differences in the immediate and long-term effects of stress as well as the differences between acute and chronic stress. The BNST may play a particularly important role in modulating the effects of chronic stress on anxiety-like behavior. For example, an acute stressor, such as one session of footshock, caused an increase in CRF mRNA expression in both the central nucleus of the amygdala (CeA) and the dorsal BNST, whereas 19 days of chronic mild stress only caused an increase in CRF mRNA levels in the dorsal BNST and not the CeA (Funk et al., 2006; Kim et al.,

2006). Here we showed an increase in CRF mRNA in Type III cells of the ovBNST after a chronic stressor, however, there are some Type III neurons that express low levels of CRF mRNA similar to that of Type III neurons from non-stressed controls. Furthermore, the same neurons that exhibited an increase in CRF mRNA expression showed a significant reduction in expression of STEP mRNA. Perhaps an acute stressor would cause an increase in CRF mRNA expression in a subset of Type III neurons, and with each new stressor, more Type III neurons would upregulate transcription of CRF mRNA. In addition to an increase in CRF mRNA after footshock, there is an increase in the amount of mRNA expression for the immediate early gene, *c-fos* in the dBNST (Funk et al., 2006). We could hypothesize that some of the neurons with *c-fos* mRNA expression after an acute stressor are the same neurons increasing CRF mRNA and reducing expression of STEP mRNA. To test this, we could use the Tet-Tag system (Reijmers et al., 2007; Zhang et al., 2015). Here, AAV in the BNST could be used to deliver the genes for Tetracycline activator (tTA) under the control of the *c-fos* promoter and GFP under the control of the TetO promoter. In this system, when transcription of *c-fos* mRNA is triggered in a neuron, tTA would also be expressed and would activate transcription of GFP. The TetO promoter can be blocked by adding doxycycline into the rat's food in order to temporally control the activation of the system. Using this system, we could "tag" neurons in the BNST activated by acute stress and those activated by acute stress after a history of chronic stress. If our hypothesis is correct, Type III GFP-tagged neurons after an acute stressor would also have elevated levels of CRF mRNA and reduced levels of STEP mRNA. Furthermore, the number of Type III GFP-tagged neurons would increase with a history of chronic stress. Using this system, we could also explore the activation of other cell types in the BNST, such as Type

II enkephalin neurons after acute stress with and without a history of chronic stress. We would expect both Type III and non-Type III cells to also be activated after acute stress, however their activation may be compromised after a history of chronic stress due to the loss of CP-AMPARs (**Chapter 4**). By tracking changes in activation of neurons after acute and chronic stress, we may be able to better understand why chronic stress can lead to long-term changes in anxiety behavior.

In addition to using the Tet-Tag system to study which neurons are activated after a stressor with and without a history of chronic stress, we can use the same system to probe the roles of these neurons in the behavioral output of the nucleus by placing the gene for channel rhodopsin (ChR2) under the TetO promoter. A recent study used this technique to show that activating neurons in the dentate gyrus that were activated during a positive experience reduced depressive symptoms (Ramirez et al., 2015). Perhaps, if an acute stressor activates more neurons in the BNST involved in opposing the stress response than promoting the stress response, optogenetic activation of neurons activated by an acute stressor would cause a reduction in anxiety-like behavior. In contrast, chronic stress causes Type III CRF neurons to be more susceptible to activation due to the reduction in STEP mRNA. Therefore, optogenetic activation of neurons activated by an acute stressor after a history of chronic stress would cause an increase in anxiety-like behavior. The neurons activated after an acute stressor in the BNST can be thought of as an “engram” for the stress response: after an acute stressor the engram may be carried in a mixture of Type I-III cells, however after an acute stressor with a history of chronic stress, the engram may be carried more heavily in the Type III neurons. Interestingly, memory engram cells in the hippocampus are known to have more spontaneous excitatory synaptic activity than cells

not a part of the memory engram (Ryan et al., 2015). We have observed that Type III neurons in the BNST exhibit more spontaneous excitatory post synaptic potentials than Type I and II cells at basal conditions. Future studies could also determine if there is a change in spontaneous synaptic activity in Type III cells after a history of chronic stress. These experiments would help to identify when in the stress response the opposing circuits of the BNST are activated.

Another important future direction of the field is to begin to examine individual variability in how the BNST responds to stress. Indeed, inter-individual variations in basal anxiety behavior have been shown to be mediated by the BNST in the rat (Duvarci et al., 2009). Furthermore, the BNST has been shown to be more active in a threat monitoring task in humans with higher levels of trait anxiety (Somerville et al., 2010), and there is considerable variability among individuals in the fiber tracks from the BNST to the brainstem, potentially resulting in differences in the way the BNST modulates behavioral and physiological responses (Krüger et al., 2015). In addition to differences in trait anxiety, there are individual variations in the emotional response after stress. Post traumatic stress disorder (PTSD) is an extreme example of these differences: importantly, people may experience the same trauma, but only some develop PTSD while others exhibit resiliency (Highland et al., 2015). In our experiment described in **Chapter 4**, there was a large amount of variability in anxiety-like behavior in rats that went through the chronic stress manipulation (**Figure 4.1**). Future studies should aim to determine if these individual differences are manifested in the electrophysiological and genetic response of neurons in the BNST. Perhaps individuals more resilient to the behavioral effects of chronic stress exhibit a weaker causative response to stress in the BNST. In contrast, resilient individuals

may show stronger compensatory responses in the BNST after chronic stress. Having a better understanding of the cause of individual differences in response to stress will help focus our thinking for the treatment of disorders such as PTSD and generalized anxiety disorder (GAD). Perhaps we can develop treatments aimed at magnifying compensatory mechanisms that are already in place in the brain. Alternatively, treatments could aim to attenuate the causative mechanisms. Anxiety disorders are highly individualized so we should begin to try to understand the neurobiological basis behind these differences.

In addition to individual differences, it is becoming more apparent that research on affective and anxiety disorders needs to focus on gender differences. It is well documented that women are more susceptible to depression, anxiety, and eating disorders than men (Palanza, 2001; Sloan and Kornstein, 2003; Risbrough and Stein, 2006). The BNST is sexually dimorphic making it a prime target for studying the basis of gender bias in affective and anxiety disorders (Allen and Gorski, 1990; Stefanova et al., 1998). One study has shown that there are gender differences in CRF expression after stress between male and female rats with prenatal alcohol exposure (Uban et al., 2013). Importantly, stress hormones can act in the BNST to affect anxiety and fear behavior (Toufexis, 2007). The National Institute of Health has recently recognized the disparity in the research using female subjects and has made strong recommendations to labs to begin including female subjects in all studies. Future studies should extend the study of cell type organization in the BNST and the effects of stress to include female subjects. The gender bias of affective and anxiety disorders, sexual dimorphisms of the BNST, and the sensitivity of the BNST to sex hormones strongly suggests that the BNST is a research area ripe for studying gender differences as they pertain to mental health.

The BNST has been described as one of the most complex regions of the mammalian brain (Larriva-Sahd, 2006). Over the past 20 years, there have been more than twice as many papers published on the BNST than the 20 years prior, and our understanding of this complex region has grown commensurately. However, there is still a lot of research to be done to catch up to the level of understanding of more commonly studied regions such as the amygdala and hippocampus. The data presented in this dissertation extends our knowledge of cell types in the rat BNST defined by their anatomical location, electrophysiological and genetic profile, and differences in response to chronic stress (**Chapters 3-4**). Additionally, we begin to compare cell types of the rat BNST to those seen in the BNST of the mouse and rhesus macaque to gain a better understanding of how these organizational properties translate between species (**Chapter 2**). The BNST lies at the intersection of many processes beyond those involved in stress and anxiety including pain perception, reproductive regulation, aggression, regulation of food and water intake, appetitive behavior, and maternal behavior. For this reason, research building upon our understanding of the circuits within this nucleus can have far-reaching implications for increasing our knowledge of how the brain controls behavior.

Literature Cited

- Abrams JK, Johnson PL, Hay-Schmidt A, Mikkelsen JD, Shekhar A, Lowry CA (2005) Serotonergic systems associated with arousal and vigilance behaviors following administration of anxiogenic drugs. *Neuroscience* 133:983–997.
- Alheid GF, Heimer L (1988) New perspectives in basal forebrain organization of special relevance for neuropsychiatric disorders: the striatopallidal, amygdaloid, and corticopetal components of substantia innominata. *NSC* 27:1–39.
- Allen LS, Gorski RA (1990) Sex difference in the bed nucleus of the stria terminalis of the human brain. *J Comp Neurol* 302:697–706.
- Alvarez RP, Chen G, Bodurka J, Kaplan R, Grillon C (2011) Phasic and sustained fear in humans elicits distinct patterns of brain activity. *NeuroImage* 55:389–400.
- Alves FHF, Crestani CC, Gomes FV, Guimarães FS, Correa FMA, Resstel LBM (2010) Cannabidiol injected into the bed nucleus of the stria terminalis modulates baroreflex activity through 5-HT_{1A} receptors. *Pharmacol Res* 62:228–236.
- Amat J, Baratta MV, Paul ED, Bland ST, Watkins LR, Maier SF (2005) Medial prefrontal cortex determines how stressor controllability affects behavior and dorsal raphe nucleus. *Nat Neurosci* 8:365–371.
- Amat J, Tamblyn JP, Bland ST, Amat P, Foster AC, Watkins LR, Maier SF (2004) Microinjection of urocortin 2 into the dorsal raphe nucleus activates serotonergic neurons and increases extracellular serotonin in the basolateral amygdala. *NSC* 129:509–519.
- Andero R, Dias BG, Ressler KJ (2014) A role for Tac2, NkB, and Nk3 receptor in normal and dysregulated fear memory consolidation. *Neuron* 83:444–454.
- Aston-Jones G, Delfs JM, Druhan J, Zhu Y (1999) The bed nucleus of the stria terminalis. A target site for noradrenergic actions in opiate withdrawal. *Ann N Y Acad Sci* 877:486–498.
- Avery SN, Clauss JA, Winder DG, Woodward N, Heckers S, Blackford JU (2014) BNST neurocircuitry in humans. *NeuroImage* 91:311–323.
- Bali A, Randhawa PK, Jaggi AS (2015) Stress and opioids: role of opioids in modulating stress-related behavior and effect of stress on morphine conditioned place preference. *Neuroscience & Biobehavioral Reviews* 51:138–150.
- Bangasser DA (2013) Sex differences in stress-related receptors: “micro” differences with “macro” implications for mood and anxiety disorders. *Biol Sex Differ* 4:2.

- Banihashemi L, Rinaman L (2006) Noradrenergic Inputs to the Bed Nucleus of the Stria Terminalis and Paraventricular Nucleus of the Hypothalamus Underlie Hypothalamic-Pituitary-Adrenal Axis But Not Hypophagic or Conditioned Avoidance Responses to Systemic Yohimbine. *Journal of Neuroscience* 26:11442–11453.
- Barrett JN, Crill WE (1974) Specific membrane properties of cat motoneurons. *J Physiol (Lond)* 239:301–324.
- Bellone C, Lüscher C (2006) Cocaine triggered AMPA receptor redistribution is reversed in vivo by mGluR-dependent long-term depression. *Nat Neurosci* 9:636–641.
- Bota M, Sporns O, Swanson LW (2012) Neuroinformatics analysis of molecular expression patterns and neuron populations in gray matter regions: the rat BST as a rich exemplar. *Brain Research* 1450:174–193.
- Bourdeau ML, Laplante I, Laurent CE, Lacaille J-C (2011) KChIP1 modulation of Kv4.3-mediated A-type K(+) currents and repetitive firing in hippocampal interneurons. *Neurosci* 176:173–187.
- Bowers LK, Swisher CB, Behbehani MM (2003) Membrane and synaptic effects of corticotropin-releasing factor on periaqueductal gray neurons of the rat. *Brain Research* 981:52–57.
- Brischoux F, Chakraborty S, Brierley DI, Ungless MA (2009) Phasic excitation of dopamine neurons in ventral VTA by noxious stimuli. *Proc Natl Acad Sci USA* 106:4894–4899.
- Budygin EA, Park J, Bass CE, Grinevich VP, Bonin KD, Wightman RM (2012) Aversive stimulus differentially triggers subsecond dopamine release in reward regions. *Neuroscience* 201:331–337.
- Burghardt NS, Bauer EP (2013) Acute and chronic effects of selective serotonin reuptake inhibitor treatment on fear conditioning: implications for underlying fear circuits. *Neuroscience* 247:253–272.
- Burghardt NS, Sullivan GM, McEwen BS, Gorman JM, LeDoux JE (2004) The selective serotonin reuptake inhibitor citalopram increases fear after acute treatment but reduces fear with chronic treatment: a comparison with tianeptine. *BPS* 55:1171–1178.
- Cadwell CR, Palasantza A, Jiang X, Berens P, Deng Q, Yilmaz M, Reimer J, Shen S, Bethge M, Tolias KF, Sandberg R, Tolias AS (2016) Electrophysiological, transcriptomic and morphologic profiling of single neurons using Patch-seq. *Nat Biotechnol* 34:199–203.
- Campsall KD, Mazerolle CJ, De Repentigny Y, Kothary R, Wallace VA (2002) Characterization of transgene expression and Cre recombinase activity in a panel of

- Thy-1 promoter-Cre transgenic mice. *Dev Dyn* 224:135–143.
- Carboni E, Silvagni A, Rolando MT, Di Chiara G (2000) Stimulation of in vivo dopamine transmission in the bed nucleus of stria terminalis by reinforcing drugs. *J Neurosci* 20:RC102.
- Cárdenas, A. M. & Marengo, F. How the stimulus defines the dynamics of vesicle pool recruitment, fusion mode and vesicle recycling in neuroendocrine cells. *J Neurochem.* n/a–n/a (2016). doi:10.1111/jnc.13565
- Cecchi M, Capriles N, Watson SJ, Akil H (2007) Beta1 adrenergic receptors in the bed nucleus of stria terminalis mediate differential responses to opiate withdrawal. *Neuropsychopharmacology* 32:589–599.
- Cecchi M, Khoshbouei H, Javors M, Morilak DA (2002) Modulatory effects of norepinephrine in the lateral bed nucleus of the stria terminalis on behavioral and neuroendocrine responses to acute stress. *NSC* 112:13–21.
- Chandley MJ, Szebeni A, Szebeni K, Crawford JD, Stockmeier CA, Turecki G, Kostrzewa RM, Ordway GA (2014) Elevated gene expression of glutamate receptors in noradrenergic neurons from the locus coeruleus in major depression. *Int J Neuropsychopharmacol* 17:1569–1578.
- Chatterton JE, Awobuluyi M, Premkumar LS, Takahashi H, Talantova M, Shin Y, Cui J, Tu S, Sevarino KA, Nakanishi N, Tong G, Lipton SA, Zhang D (2002) Excitatory glycine receptors containing the NR3 family of NMDA receptor subunits. *Nature* 415:793–798.
- Chen C-P, Lee L, Chang L-S (2006) Effects of metal-binding properties of human Kv channel-interacting proteins on their molecular structure and binding with Kv4.2 channel. *Protein J* 25:345–351.
- Choi DC, Furay AR, Evanson NK, Ostrander MM, Ulrich-Lai YM, Herman JP (2007) Bed nucleus of the stria terminalis subregions differentially regulate hypothalamic-pituitary-adrenal axis activity: implications for the integration of limbic inputs. *J Neurosci* 27:2025–2034.
- Commons KG, Connolley KR, Valentino RJ (2003) A neurochemically distinct dorsal raphe-limbic circuit with a potential role in affective disorders. *Neuropsychopharmacology* 28:206–215.
- Conrad KL, Louderback KM, Gessner CP, Winder DG (2011) Stress-induced alterations in anxiety-like behavior and adaptations in plasticity in the bed nucleus of the stria terminalis. *Physiology & Behavior* 104:248–256.
- Conrad KL, Winder DG (2011) Altered anxiety-like behavior and long-term potentiation in the bed nucleus of the stria terminalis in adult mice exposed to chronic social isolation, unpredictable stress, and ethanol beginning in adolescence. *Alcohol*

45:585–593.

- Cook-Snyder DR, Jones A, Reijmers LG (2015) A retrograde adeno-associated virus for collecting ribosome-bound mRNA from anatomically defined projection neurons. *Front Mol Neurosci* 8:56.
- Crestani CC, Alves FHF, Gomes FV, Resstel LB, Correa FM, Herman JP (2013) Mechanisms in the bed nucleus of the stria terminalis involved in control of autonomic and neuroendocrine functions: a review. *Curr Neuropharmacol* 11:141–159.
- Crestani CC, Alves FHF, Resstel LBM, Corrêa FM de A (2006) The bed nucleus of the stria terminalis modulates baroreflex in rats. *Neuroreport* 17:1531–1535.
- Crestani CC, Alves FHF, Tavares RF, Corrêa FMA (2009) Role of the bed nucleus of the stria terminalis in the cardiovascular responses to acute restraint stress in rats. *Stress* 12:268–278.
- Cull-Candy S, Kelly L, Farrant M (2006) Regulation of Ca²⁺-permeable AMPA receptors: synaptic plasticity and beyond. *Current Opinion in Neurobiology* 16:288–297.
- Cummings S, Elde R, Ells J, Lindall A (1983) Corticotropin-releasing factor immunoreactivity is widely distributed within the central nervous system of the rat: an immunohistochemical study. *Journal of Neuroscience* 3:1355–1368.
- Dabrowska J, Hazra R, Ahern TH, Guo J-D, McDonald AJ, Mascagni F, Muller JF, Young LJ, Rainnie DG (2011) Neuroanatomical evidence for reciprocal regulation of the corticotrophin-releasing factor and oxytocin systems in the hypothalamus and the bed nucleus of the stria terminalis of the rat: Implications for balancing stress and affect. *Psychoneuroendocrinology* 36:1312–1326.
- Dabrowska J, Hazra R, Guo J-D, Dewitt S, Rainnie DG (2013a) Central CRF neurons are not created equal: phenotypic differences in CRF-containing neurons of the rat paraventricular hypothalamus and the bed nucleus of the stria terminalis. *Front Neurosci* 7:156.
- Dabrowska J, Hazra R, Guo J-D, Li CC, Dewitt S, Xu J, Lombroso PJ, Rainnie DG (2013b) Striatal-enriched protein tyrosine phosphatase-STEPs toward understanding chronic stress-induced activation of corticotrophin releasing factor neurons in the rat bed nucleus of the stria terminalis. *Biol Psychiatry* 74:817–826.
- Daniel SE, Rainnie DG (2015) Stress Modulation of Opposing Circuits in the Bed Nucleus of the Stria Terminalis. *Neuropsychopharmacology* 41:103–125.
- Davis M, Walker DL (2014) Role of bed nucleus of the stria terminalis and amygdala AMPA receptors in the development and expression of context conditioning and sensitization of startle by prior shock. *Brain Struct Funct* 219:1969–1982.

- Davis M, Walker DL, Lee Y (1997) Amygdala and bed nucleus of the stria terminalis: differential roles in fear and anxiety measured with the acoustic startle reflex. *Philos Trans R Soc Lond, B, Biol Sci* 352:1675–1687.
- Day HEW, Curran EJ, Watson SJ, Akil H (1999) Distinct neurochemical populations in the rat central nucleus of the amygdala and bed nucleus of the stria terminalis: evidence for their selective activation by interleukin-1beta. *J Comp Neurol* 413:113–128.
- Day HEW, Masini CV, Campeau S (2004) The pattern of brain c-fos mRNA induced by a component of fox odor, 2,5-dihydro-2,4,5-trimethylthiazoline (TMT), in rats, suggests both systemic and processive stress characteristics. *Brain Research* 1025:139–151.
- Day HEW, Vittoz NM, Oates MM, Badiani A, Watson SJ, Robinson TE, Akil H (2002) A 6-hydroxydopamine lesion of the mesostriatal dopamine system decreases the expression of corticotropin releasing hormone and neurotensin mRNAs in the amygdala and bed nucleus of the stria terminalis. *Brain Research* 945:151–159.
- Dingledine R, Borges K, Bowie D, Traynelis SF (1999) The glutamate receptor ion channels. *Pharmacol Rev* 51:7–61.
- Dong HW, Petrovich GD, Swanson LW (2001a) Topography of projections from amygdala to bed nuclei of the stria terminalis. *Brain Res Brain Res Rev* 38:192–246.
- Dong HW, Petrovich GD, Watts AG, Swanson LW (2001b) Basic organization of projections from the oval and fusiform nuclei of the bed nuclei of the stria terminalis in adult rat brain. *J Comp Neurol* 436:430–455.
- Dong HW, Swanson LW (2004) Organization of axonal projections from the anterolateral area of the bed nuclei of the stria terminalis. *J Comp Neurol* 468:277–298.
- Dulcis D, Jamshidi P, Leutgeb S, Spitzer NC (2013) Neurotransmitter switching in the adult brain regulates behavior. *Science* 340:449–453.
- Dumont EC, Mark GP, Mader S, Williams JT (2005) Self-administration enhances excitatory synaptic transmission in the bed nucleus of the stria terminalis. *Nat Neurosci* 8:413–414.
- Dumont EC, Williams JT (2004) Noradrenaline triggers GABA_A inhibition of bed nucleus of the stria terminalis neurons projecting to the ventral tegmental area. *J Neurosci* 24:8198–8204.
- Duvarci S, Bauer EP, Pare D (2009) The bed nucleus of the stria terminalis mediates inter-individual variations in anxiety and fear. *J Neurosci* 29:10357–10361.
- Egli RE, Kash TL, Choo K, Savchenko V, Matthews RT, Blakely RD, Winder DG

- (2004) Norepinephrine Modulates Glutamatergic Transmission in the Bed Nucleus of the Stria Terminalis. *Neuropsychopharmacology*.
- Egli RE, Winder DG (2003) Dorsal and ventral distribution of excitable and synaptic properties of neurons of the bed nucleus of the stria terminalis. *Journal of Neurophysiology* 90:405–414.
- Ehrlich DE, Ryan SJ, Rainnie DG (2012) Postnatal development of electrophysiological properties of principal neurons in the rat basolateral amygdala. *J Physiol (Lond)* 590:4819–4838.
- Eiler WJA, Seyoum R, Foster KL, Mailey C, June HL (2003) D1 dopamine receptor regulates alcohol-motivated behaviors in the bed nucleus of the stria terminalis in alcohol-preferring (P) rats. *Synapse* 48:45–56.
- Erb S, Hitchcott PK, Rajabi H, Mueller D, Shaham Y, Stewart J (2000) Alpha-2 adrenergic receptor agonists block stress-induced reinstatement of cocaine seeking. *Neuropsychopharmacology* 23:138–150.
- Erb S, Salmaso N, Salmaso N, Rodaros D, Stewart J (2001) A role for the CRF-containing pathway from central nucleus of the amygdala to bed nucleus of the stria terminalis in the stress-induced reinstatement of cocaine seeking in rats. *Psychopharmacology* 158:360–365.
- Erb S, Stewart J (1999) A role for the bed nucleus of the stria terminalis, but not the amygdala, in the effects of corticotropin-releasing factor on stress-induced reinstatement of cocaine seeking. *J Neurosci* 19:RC35.
- Fendt M, Siegl S, Steiniger-Brach B (2005) Noradrenaline transmission within the ventral bed nucleus of the stria terminalis is critical for fear behavior induced by trimethylthiazoline, a component of fox odor. *J Neurosci* 25:5998–6004.
- Feng G, Mellor RH, Bernstein M, Keller-Peck C, Nguyen QT, Wallace M, Nerbonne JM, Lichtman JW, Sanes JR (2000) Imaging neuronal subsets in transgenic mice expressing multiple spectral variants of GFP. *Neuron* 28:41–51.
- Forray MI, Bustos G, Gysling K (1999) Noradrenaline inhibits glutamate release in the rat bed nucleus of the stria terminalis: in vivo microdialysis studies. *J Neurosci Res* 55:311–320.
- Forray MI, Gysling K, Andrés ME, Bustos G, Araneda S (2000) Medullary noradrenergic neurons projecting to the bed nucleus of the stria terminalis express mRNA for the NMDA-NR1 receptor. *Brain Res Bull* 52:163–169.
- Fox AS, Shelton SE, Oakes TR, Converse AK, Davidson RJ, Kalin NH (2010) Orbitofrontal cortex lesions alter anxiety-related activity in the primate bed nucleus of stria terminalis. *J Neurosci* 30:7023–7027.

- Francesconi W, Berton F, Repunte-Canonigo V, Hagihara K, Thurbon D, Lekic D, Specio SE, Greenwell TN, Chen SA, Rice KC, Richardson HN, O'Dell LE, Zorrilla EP, Morales M, Koob GF, Sanna PP (2009) Protracted withdrawal from alcohol and drugs of abuse impairs long-term potentiation of intrinsic excitability in the juxtacapsular bed nucleus of the stria terminalis. *J Neurosci* 29:5389–5401.
- Freedman LJ, Cassell MD (1994) Distribution of dopaminergic fibers in the central division of the extended amygdala of the rat. *Brain Research* 633:243–252.
- Funk D, Li Z, Lê AD (2006) Effects of environmental and pharmacological stressors on c-fos and corticotropin-releasing factor mRNA in rat brain: Relationship to the reinstatement of alcohol seeking. *Neurosci* 138:235–243.
- Gardner KL, Thiruvikraman KV, Lightman SL, Plotsky PM, Lowry CA (2005) Early life experience alters behavior during social defeat: focus on serotonergic systems. *NSC* 136:181–191.
- Gasselin C, Inglebert Y, Debanne D (2015) Homeostatic regulation of h-conductance controls intrinsic excitability and stabilizes the threshold for synaptic modification in CA1 neurons. *J Physiol (Lond)* 593:4855–4869.
- Georges F, Aston-Jones G (2001) Potent regulation of midbrain dopamine neurons by the bed nucleus of the stria terminalis. *J Neurosci* 21:RC160.
- Georges F, Aston-Jones G (2002) Activation of ventral tegmental area cells by the bed nucleus of the stria terminalis: a novel excitatory amino acid input to midbrain dopamine neurons. *J Neurosci* 22:5173–5187.
- Gewirtz JC, McNish KA, Davis M (1998) Lesions of the bed nucleus of the stria terminalis block sensitization of the acoustic startle reflex produced by repeated stress, but not fear-potentiated startle. *Progress in Neuropsychopharmacology & Biological Psychiatry* 22:625–648.
- Glangetas C, Girard D, Groc L, Marsicano G, Chaouloff F, Georges F (2013) Stress switches cannabinoid type-1 (CB1) receptor-dependent plasticity from LTD to LTP in the bed nucleus of the stria terminalis. *J Neurosci* 33:19657–19663.
- Goebel-Goody SM, Baum M, Paspalas CD, Fernandez SM, Carty NC, Kurup P, Lombroso PJ (2012) Therapeutic implications for striatal-enriched protein tyrosine phosphatase (STEP) in neuropsychiatric disorders. *Pharmacol Rev* 64:65–87.
- Gomes FV, Alves FHF, Guimarães FS, Correa FMA, Resstel LBM, Crestani CC (2013) Cannabidiol administration into the bed nucleus of the stria terminalis alters cardiovascular responses induced by acute restraint stress through 5-HT1A receptor. *European Neuropsychopharmacology* 23:1096–1104.
- Gomes FV, Reis DG, Alves FHF, Correa FM, Guimaraes FS, Resstel LB (2012) Cannabidiol injected into the bed nucleus of the stria terminalis reduces the

- expression of contextual fear conditioning via 5-HT_{1A} receptors. *Journal of Psychopharmacology* 26:104–113.
- Gomes FV, Resstel LBM, Guimarães FS (2011) The anxiolytic-like effects of cannabidiol injected into the bed nucleus of the stria terminalis are mediated by 5-HT_{1A} receptors. *Psychopharmacology* 213:465–473.
- Grahn RE, Will MJ, Hammack SE, Maswood S, McQueen MB, Watkins LR, Maier SF (1999) Activation of serotonin-immunoreactive cells in the dorsal raphe nucleus in rats exposed to an uncontrollable stressor. *Brain Research* 826:35–43.
- Gray TS, Magnuson DJ (1992) Peptide immunoreactive neurons in the amygdala and the bed nucleus of the stria terminalis project to the midbrain central gray in the rat. *Peptides* 13:451–460.
- Greengard P (2001) The neurobiology of slow synaptic transmission. *Science* 294:1024–1030.
- Grillon C, Levenson J, Pine DS (2007) A single dose of the selective serotonin reuptake inhibitor citalopram exacerbates anxiety in humans: a fear-potentiated startle study. *Neuropsychopharmacology* 32:225–231.
- Guo J-D, Hammack SE, Hazra R, Levita L, Rainnie DG (2009) Bi-directional modulation of bed nucleus of stria terminalis neurons by 5-HT: molecular expression and functional properties of excitatory 5-HT receptor subtypes. *Neuroscience* 164:1776–1793.
- Guo J-D, Rainnie DG (2010) Presynaptic 5-HT_{1B} receptor-mediated serotonergic inhibition of glutamate transmission in the bed nucleus of the stria terminalis. *Neuroscience* 165:1390–1401.
- Hale MW, Stamper CE, Staub DR, Lowry CA (2010) Urocortin 2 increases c-Fos expression in serotonergic neurons projecting to the ventricular/periventricular system. *Experimental Neurology* 224:271–281.
- Hammack SE, Guo J-D, Hazra R, Dabrowska J, Myers KM, Rainnie DG (2009) The response of neurons in the bed nucleus of the stria terminalis to serotonin: implications for anxiety. *Progress in Neuro-Psychopharmacology and Biological Psychiatry* 33:1309–1320.
- Hammack SE, Mania I, Rainnie DG (2007) Differential expression of intrinsic membrane currents in defined cell types of the anterolateral bed nucleus of the stria terminalis. *Journal of Neurophysiology* 98:638–656.
- Hammack SE, Richey KJ, Schmid MJ, LoPresti ML, Watkins LR, Maier SF (2002) The role of corticotropin-releasing hormone in the dorsal raphe nucleus in mediating the behavioral consequences of uncontrollable stress. *J Neurosci* 22:1020–1026.

- Hammack SE, Roman CW, Lezak KR, Kocho-Shellenberg M, Grimmig B, Falls WA, Braas K, May V (2010) Roles for pituitary adenylate cyclase-activating peptide (PACAP) expression and signaling in the bed nucleus of the stria terminalis (BNST) in mediating the behavioral consequences of chronic stress. *J Mol Neurosci* 42:327–340.
- Hammack SE, Schmid MJ, LoPresti ML, Der-Avakian A, Pellymounter MA, Foster AC, Watkins LR, Maier SF (2003) Corticotropin releasing hormone type 2 receptors in the dorsal raphe nucleus mediate the behavioral consequences of uncontrollable stress. *J Neurosci* 23:1019–1025.
- Hammack SE, Todd TP, Kocho-Schellenberg M, Bouton ME (2015) Role of the bed nucleus of the stria terminalis in the acquisition of contextual fear at long or short context-shock intervals. *Behavioral Neuroscience* 129:673–678.
- Hasue RH, Shammah-Lagnado SJ (2002) Origin of the dopaminergic innervation of the central extended amygdala and accumbens shell: a combined retrograde tracing and immunohistochemical study in the rat. *J Comp Neurol* 454:15–33.
- Haubensak W, Kunwar PS, Cai H, Ciocchi S, Wall NR, Ponnusamy R, Biag J, Dong HW, Deisseroth K, Callaway EM, Fanselow MS, Lüthi A, Anderson DJ (2010) Genetic dissection of an amygdala microcircuit that gates conditioned fear. *Nature* 468:270–276.
- Hazra R, Guo J-D, Dabrowska J, Rainnie DG (2012) Differential distribution of serotonin receptor subtypes in BNST(ALG) neurons: modulation by unpredictable shock stress. *Neuroscience* 225:9–21.
- Hazra R, Guo J-D, Ryan SJ, Jasnow AM, Dabrowska J, Rainnie DG (2011) A transcriptomic analysis of type I-III neurons in the bed nucleus of the stria terminalis. *Mol Cell Neurosci* 46:699–709.
- Hedlund PB (2009) The 5-HT₇ receptor and disorders of the nervous system: an overview. *Psychopharmacology* 206:345–354.
- Heisler LK, Zhou L, Bajwa P, Hsu J, Tecott LH (2007) Serotonin 5-HT_{2C} receptors regulate anxiety-like behavior. *Genes Brain Behav* 6:491–496.
- Helmchen F, Imoto K, Sakmann B (1996) Ca²⁺ buffering and action potential-evoked Ca²⁺ signaling in dendrites of pyramidal neurons. *Biophys J* 70:1069–1081.
- Highland KB, Costanzo M, Jovanovic T, Norrholm SD, Ndiongue R, Reinhardt B, Rothbaum B, Roy MJ (2015) Biomarkers of post-deployment resilience among military service members. *Neurobiol Stress* 2:62–66.
- Hillman BG, Gupta SC, Stairs DJ, Buonanno A, Dravid SM (2011) Behavioral analysis of NR2C knockout mouse reveals deficit in acquisition of conditioned fear and working memory. *Neurobiol Learn Mem* 95:404–414.

- Hott SC, Gomes FV, Fabri DRS, Reis DG, Crestani CC, Correa FMA, Resstel LBM (2012) Both α 1- and β 1-adrenoceptors in the bed nucleus of the stria terminalis are involved in the expression of conditioned contextual fear. *Br J Pharmacol* 167:207–221.
- Hubert GW, Muly EC (2014) Distribution of AMPA receptor subunit *glur1* in the bed nucleus of the stria terminalis and effect of stress. *Synapse* 68:194–201.
- Jalabert M, Aston-Jones G, Herzog E, Manzoni O, Georges F (2009) Role of the bed nucleus of the stria terminalis in the control of ventral tegmental area dopamine neurons. *Progress in Neuro-Psychopharmacology and Biological Psychiatry* 33:1336–1346.
- Janitzky K, Janitzky K, D Hanis W, Kröber A, Kröber A, Schwegler H, Schwegler H (2014) TMT predator odor activated neural circuit in C57BL/6J mice indicates TMT-stress as a suitable model for uncontrollable intense stress. *Brain Research* 1599:1–8.
- Jasnow AM, Davis M, Huhman KL (2004) Involvement of Central Amygdala and Bed Nucleus of the Stria Terminalis Corticotropin-Releasing Factor in Behavioral Responses to Social Defeat. *Behavioral Neuroscience* 118:1052–1061.
- Jennings JH, Sparta DR, Stamatakis AM, Ung RL, Pleil KE, Kash TL, Stuber GD (2013) Distinct extended amygdala circuits for divergent motivational states. *Nature* 496:224–228.
- Ju G, Swanson LW, Simerly RB (1989) Studies on the cellular architecture of the bed nuclei of the stria terminalis in the rat: II. Chemoarchitecture. *J Comp Neurol* 280:603–621.
- Kalin NH, Shelton SE, Fox AS, Oakes TR, Davidson RJ (2005) Brain regions associated with the expression and contextual regulation of anxiety in primates. *BPS* 58:796–804.
- Karst H, Nair S, Velzing E, Rumpff-van Essen L, Slagter E, Shinnick-Gallagher P, Joëls M (2002) Glucocorticoids alter calcium conductances and calcium channel subunit expression in basolateral amygdala neurons. *Eur J Neurosci* 16:1083–1089.
- Kash TL, Nobis WP, Matthews RT, Winder DG (2008) Dopamine enhances fast excitatory synaptic transmission in the extended amygdala by a CRF-R1-dependent process. *J Neurosci* 28:13856–13865.
- Kent JM, Coplan JD, Gorman JM (1998) Clinical utility of the selective serotonin reuptake inhibitors in the spectrum of anxiety. *BPS* 44:812–824.
- Kim S-J, Park S-H, Choi S-H, Moon B-H, Lee K-J, Kang SW, Lee M-S, Choi S-H, Chun B-G, Shin K-H (2006) Effects of repeated tianeptine treatment on CRF mRNA expression in non-stressed and chronic mild stress-exposed rats. *NP* 50:824–833.

- Kim S-Y, Adhikari A, Lee SY, Marshel JH, Kim CK, Mallory CS, Lo M, Pak S, Mattis J, Lim BK, Malenka RC, Warden MR, Neve R, Tye KM, Deisseroth K (2013) Diverging neural pathways assemble a behavioural state from separable features in anxiety. *Nature* 496:219–223.
- Kirby LG, Rice KC, Valentino RJ (2000) Effects of corticotropin-releasing factor on neuronal activity in the serotonergic dorsal raphe nucleus. *Neuropsychopharmacology* 22:148–162.
- Kits KS, Mansvelder HD (2000) Regulation of exocytosis in neuroendocrine cells: spatial organization of channels and vesicles, stimulus-secretion coupling, calcium buffers and modulation. *Brain Res Brain Res Rev* 33:78–94.
- Koh DS, Burnashev N, Jonas P (1995) Block of native Ca(2+)-permeable AMPA receptors in rat brain by intracellular polyamines generates double rectification. *J Physiol (Lond)* 486 (Pt 2):305–312.
- Krawczyk M, Georges F, Sharma R, Mason X, Berthet A, Bézard E, Dumont EC (2011a) Double-dissociation of the catecholaminergic modulation of synaptic transmission in the oval bed nucleus of the stria terminalis. *Journal of Neurophysiology* 105:145–153.
- Krawczyk M, Sharma R, Mason X, Debacker J, Jones AA, Dumont EC (2011b) A switch in the neuromodulatory effects of dopamine in the oval bed nucleus of the stria terminalis associated with cocaine self-administration in rats. *J Neurosci* 31:8928–8935.
- Krüger O, Shiozawa T, Kreifelts B, Scheffler K, Ethofer T (2015) Three distinct fiber pathways of the bed nucleus of the stria terminalis to the amygdala and prefrontal cortex. *Cortex* 66:60–68.
- Kudo T, Uchigashima M, Miyazaki T, Konno K, Yamasaki M, Yanagawa Y, Minami M, Watanabe M (2012) Three types of neurochemical projection from the bed nucleus of the stria terminalis to the ventral tegmental area in adult mice. *J Neurosci* 32:18035–18046.
- Larriva-Sahd J (2006) Histological and cytological study of the bed nuclei of the stria terminalis in adult rat. II. Oval nucleus: extrinsic inputs, cell types, neuropil, and neuronal modules. *J Comp Neurol* 497:772–807.
- Lee KY, Royston SE, Vest MO, Ley DJ, Lee S, Bolton EC, Chung HJ (2015) N-methyl-D-aspartate receptors mediate activity-dependent down-regulation of potassium channel genes during the expression of homeostatic intrinsic plasticity. *Mol Brain* 8:4.
- Lee Y, Davis M (1997) Role of the hippocampus, the bed nucleus of the stria terminalis, and the amygdala in the excitatory effect of corticotropin-releasing hormone on the

- acoustic startle reflex. *Journal of Neuroscience* 17:6434–6446.
- Leri F, Flores J, Rodaros D, Stewart J (2002a) Blockade of stress-induced but not cocaine-induced reinstatement by infusion of noradrenergic antagonists into the bed nucleus of the stria terminalis or the central nucleus of the amygdala. *J Neurosci* 22:5713–5718.
- Leri F, Flores J, Rodaros D, Stewart J (2002b) Blockade of stress-induced but not cocaine-induced reinstatement by infusion of noradrenergic antagonists into the bed nucleus of the stria terminalis or the central nucleus of the amygdala. *J Neurosci* 22:5713–5718.
- Levita L, Hammack SE, Mania I, Li XY, Davis M, Rainnie DG (2004) 5-hydroxytryptamine_{1A}-like receptor activation in the bed nucleus of the stria terminalis: electrophysiological and behavioral studies. *NSC* 128:583–596.
- Liang KC, Chen HC, Chen DY (2001) Posttraining infusion of norepinephrine and corticotropin releasing factor into the bed nucleus of the stria terminalis enhanced retention in an inhibitory avoidance task. *Chin J Physiol* 44:33–43.
- Livak KJ, Schmittgen TD (2001) Analysis of relative gene expression data using real-time quantitative PCR and the 2(-Delta Delta C(T)) Method. *Methods*, 25:402–408.
- Lowry CA (2002) Functional subsets of serotonergic neurones: implications for control of the hypothalamic-pituitary-adrenal axis. *Journal of Neuroendocrinology* 14:911–923.
- Macey DJ, Smith HR, Nader MA, Porrino LJ (2003) Chronic cocaine self-administration upregulates the norepinephrine transporter and alters functional activity in the bed nucleus of the stria terminalis of the rhesus monkey. *J Neurosci* 23:12–16.
- Mainen ZF, Sejnowski TJ (1996) Influence of dendritic structure on firing pattern in model neocortical neurons. *Nature* 382:363–366.
- Makino S, Gold PW, Schulkin J (1994) Effects of corticosterone on CRH mRNA and content in the bed nucleus of the stria terminalis; comparison with the effects in the central nucleus of the amygdala and the paraventricular nucleus of the hypothalamus. *Brain Research* 657:141–149.
- Malin SA, Nerbonne JM (2001) Molecular heterogeneity of the voltage-gated fast transient outward K⁺ current, I(Af), in mammalian neurons. *J Neurosci* 21:8004–8014.
- Mansari El M, Guiard BP, Chernoloz O, Ghanbari R, Katz N, Blier P (2010) Relevance of norepinephrine-dopamine interactions in the treatment of major depressive disorder. *CNS Neurosci Ther* 16:e1–e17.
- Mantsch JR, Vranjkovic O, Twining RC, Gasser PJ, McReynolds JR, Blacktop JM

- (2014) Neurobiological mechanisms that contribute to stress-related cocaine use. *Neuropharmacology* 76 Pt B:383–394.
- Marcinkiewicz CA, Dorrier CE, Lopez AJ, Kash TL (2015) Ethanol induced adaptations in 5-HT_{2c} receptor signaling in the bed nucleus of the stria terminalis: Implications for anxiety during ethanol withdrawal. *NP* 89:157–167.
- Martin EI, Ressler KJ, Jasnow AM, Dabrowska J, Hazra R, Rainnie DG, Nemeroff CB, Owens MJ (2010) A Novel Transgenic Mouse for Gene-Targeting Within Cells That Express Corticotropin-Releasing Factor. *BPS* 67:1212–1216.
- Massi L, Elezgarai I, Puente N, Reguero L, Grandes P, Manzoni OJ, Georges F (2008) Cannabinoid Receptors in the Bed Nucleus of the Stria Terminalis Control Cortical Excitation of Midbrain Dopamine Cells In Vivo. *Journal of Neuroscience* 28:10496–10508.
- McCobb DP, Beam KG (1991) Action potential waveform voltage-clamp commands reveal striking differences in calcium entry via low and high voltage-activated calcium channels. *Neuron* 7:119–127.
- McDonald AJ (1991) Topographical organization of amygdaloid projections to the caudatoputamen, nucleus accumbens, and related striatal-like areas of the rat brain. *Neurosci* 44:15–33.
- McElligott ZA, Klug JR, Nobis WP, Patel S, Grueter BA, Kash TL, Winder DG (2010) Distinct forms of G_q-receptor-dependent plasticity of excitatory transmission in the BNST are differentially affected by stress. *Proc Natl Acad Sci USA* 107:2271–2276.
- McElligott ZA, Winder DG (2007) α 1-Adrenergic Receptor-Induced Heterosynaptic Long-Term Depression in the Bed Nucleus of the Stria Terminalis Is Disrupted in Mouse Models of Affective Disorders. *Neuropsychopharmacology* 33:2313–2323.
- Meloni EG, Gerety LP, Knoll AT, Cohen BM, Carlezon WA (2006) Behavioral and anatomical interactions between dopamine and corticotropin-releasing factor in the rat. *J Neurosci* 26:3855–3863.
- Meltzer HY, Arvanitis L, Bauer D, Rein W, Meta-Trial Study Group (2004) Placebo-controlled evaluation of four novel compounds for the treatment of schizophrenia and schizoaffective disorder. *Am J Psychiatry* 161:975–984.
- Mengod G, Villaró MT, Landwehrmeyer GB, Martinez-Mir MI, Niznik HB, Sunahara RK, Seeman P, O'Dowd BF, Probst A, Palacios JM (1992) Visualization of dopamine D₁, D₂ and D₃ receptor mRNAs in human and rat brain. *Neurochem Int* 20 Suppl:33S–43S.
- Michaeli A, Yaka R (2010) Dopamine inhibits GABA(A) currents in ventral tegmental area dopamine neurons via activation of presynaptic G-protein coupled inwardly-rectifying potassium channels. *Journal of Neuroscience* 165:1159–1169.

- Miczek KA, Nikulina E, Kream RM, Carter G, Espejo EF (1999) Behavioral sensitization to cocaine after a brief social defeat stress: c-fos expression in the PAG. *Psychopharmacology* 141:225–234.
- Mnie-Filali O, Faure C, Lambás-Señas L, Mansari El M, Belblidia H, Gondard E, Etiévant A, Scarna H, Didier A, Berod A, Blier P, Haddjeri N (2011) Pharmacological blockade of 5-HT₇ receptors as a putative fast acting antidepressant strategy. *Neuropsychopharmacology* 36:1275–1288.
- Mohamad O, Song M, Wei L, Yu SP (2013) Regulatory roles of the NMDA receptor GluN3A subunit in locomotion, pain perception and cognitive functions in adult mice. *J Physiol (Lond)* 591:149–168.
- Molineux ML, Fernandez FR, Mehaffey WH, Turner RW (2005) A-type and T-type currents interact to produce a novel spike latency-voltage relationship in cerebellar stellate cells. *J Neurosci* 25:10863–10873.
- Motzkin JC, Philippi CL, Oler JA, Kalin NH, Baskaya MK, Koenigs M (2015) Ventromedial prefrontal cortex damage alters resting blood flow to the bed nucleus of stria terminalis. *Cortex* 64:281–288.
- Mullasseril P, Hansen KB, Vance KM, Ogden KK, Yuan H, Kurtkaya NL, Santangelo R, Orr AG, Le P, Vellano KM, Liotta DC, Traynelis SF (2010) A subunit-selective potentiator of NR2C- and NR2D-containing NMDA receptors. *Nat Commun* 1:90–98.
- Muly EC, Senyuz M, Khan ZU, Guo J-D, Hazra R, Rainnie DG (2009) Distribution of D1 and D5 dopamine receptors in the primate and rat basolateral amygdala. *Brain Struct Funct* 213:375–393.
- Nakagawa T, Yamamoto R, Fujio M, Suzuki Y, Minami M, Satoh M, Kaneko S (2005) Involvement of the bed nucleus of the stria terminalis activated by the central nucleus of the amygdala in the negative affective component of morphine withdrawal in rats. *Neuroscience* 134:9–19.
- Nobis WP, Kash TL, Silberman Y, Winder DG (2011) β -Adrenergic receptors enhance excitatory transmission in the bed nucleus of the stria terminalis through a corticotrophin-releasing factor receptor-dependent and cocaine-regulated mechanism. *Biol Psychiatry* 69:1083–1090.
- Nguyen, A. Q., Cruz, Dela, J. A. D., Sun, Y., Holmes, T. C. & Xu, X. Genetic cell targeting uncovers specific neuronal types and distinct subregions in the bed nucleus of the stria terminalis. *J. Comp. Neurol.* (2015). doi:10.1002/cne.23954
- Oler JA, Fox AS, Shelton SE, Christian BT, Murali D, Oakes TR, Davidson RJ, Kalin NH (2009) Serotonin transporter availability in the amygdala and bed nucleus of the stria terminalis predicts anxious temperament and brain glucose metabolic activity. *J*

- Neurosci 29:9961–9966.
- O'Malley D, Julio-Piepera M, Dinan TG, Cryan JF (2014) Strain differences in stress-induced changes in central CRF1 receptor expression. *Neurosci Lett* 561:192–197.
- Onaka T, Yagi K (1998) Role of noradrenergic projections to the bed nucleus of the stria terminalis in neuroendocrine and behavioral responses to fear-related stimuli in rats. *Brain Research* 788:287–293.
- Palanza P (2001) Animal models of anxiety and depression: how are females different? *Neuroscience & Biobehavioral Reviews* 25:219–233.
- Park J, Bucher ES, Budygin EA, Wightman RM (2015) Norepinephrine and dopamine transmission in 2 limbic regions differentially respond to acute noxious stimulation. *Pain* 156:318–327.
- Park J, Bucher ES, Fontillas K, Owesson-White C, Ariansen JL, Carelli RM, Wightman RM (2013) Opposing catecholamine changes in the bed nucleus of the stria terminalis during intracranial self-stimulation and its extinction. *Biol Psychiatry* 74:69–76.
- Park J, Kile BM, Wightman RM (2009) In vivo voltammetric monitoring of norepinephrine release in the rat ventral bed nucleus of the stria terminalis and anteroventral thalamic nucleus. *Eur J Neurosci* 30:2121–2133.
- Park J, Wheeler RA, Fontillas K, Keithley RB, Carelli RM, Wightman RM (2012) Catecholamines in the bed nucleus of the stria terminalis reciprocally respond to reward and aversion. *Biol Psychiatry* 71:327–334.
- Paul S, Olausson P, Venkitaramani DV, Ruchkina I, Moran TD, Tronson N, Mills E, Hakim S, Salter MW, Taylor JR, Lombroso PJ (2007) The striatal-enriched protein tyrosine phosphatase gates long-term potentiation and fear memory in the lateral amygdala. *BPS* 61:1049–1061.
- Paxinos G, Huang X.F., and Toga A.W. (2000) *The Rhesus Monkey Brain in Stereotaxic Coordinates*. Academic Press.
- Petit JM, Luppi PH, Peyron C, Rampon C, Jouvet M (1995) VIP-like immunoreactive projections from the dorsal raphe and caudal linear raphe nuclei to the bed nucleus of the stria terminalis demonstrated by a double immunohistochemical method in the rat. *Neurosci Lett* 193:77–80.
- Peyron C, Petit JM, Rampon C, Jouvet M, Luppi PH (1998) Forebrain afferents to the rat dorsal raphe nucleus demonstrated by retrograde and anterograde tracing methods. *NSC* 82:443–468.
- Pêgo JM, Morgado P, Pinto LG, Cerqueira JJ, Almeida OFX, Sousa N (2008) Dissociation of the morphological correlates of stress-induced anxiety and fear. *Eur J*

Neurosci 27:1503–1516.

Phelix CF, Liposits Z, Paull WK (1992) Serotonin-CRF interaction in the bed nucleus of the stria terminalis: a light microscopic double-label immunocytochemical analysis. *Brain Res Bull* 28:943–948.

Phelix CF, Liposits Z, Paull WK (1994) Catecholamine-CRF synaptic interaction in a septal bed nucleus: afferents of neurons in the bed nucleus of the stria terminalis. *Brain Res Bull* 33:109–119.

Pleil KE, Lowery-Gionta EG, Crowley NA, Li C, Marcinkiewicz CA, Rose JH, McCall NM, Maldonado-Devinci AM, Morrow AL, Jones SR, Kash TL (2015) Effects of chronic ethanol exposure on neuronal function in the prefrontal cortex and extended amygdala. *Neuropharmacology* 99:735–749.

Poulin J-F, Arbour D, Laforest S, Drolet G (2009) Neuroanatomical characterization of endogenous opioids in the bed nucleus of the stria terminalis. *Progress in Neuropsychopharmacology & Biological Psychiatry* 33:1356–1365.

Preuss TM (1995) Do rats have prefrontal cortex? The rose-woolsey-akert program reconsidered. *J Cogn Neurosci* 7:1–24.

Radley JJ, Gosselink KL, Sawchenko PE (2009) A Discrete GABAergic Relay Mediates Medial Prefrontal Cortical Inhibition of the Neuroendocrine Stress Response. *J Neurosci* 29:7330–7340.

Rainnie DG, Hazra R, Dabrowska J, Guo J-D, Li CC, Dewitt S, Muly EC (2014) Distribution and functional expression of Kv4 family α subunits and associated KCHIP β subunits in the bed nucleus of the stria terminalis. *J Comp Neurol* 522:609–625.

Ramirez S, Liu X, MacDonald CJ, Moffa A, Zhou J, Redondo RL, Tonegawa S (2015) Activating positive memory engrams suppresses depression-like behaviour. *Nature* 522:335–339.

Reijmers LG, Perkins BL, Matsuo N, Mayford M (2007) Localization of a stable neural correlate of associative memory. *317:1230–1233*.

Risbrough VB, Stein MB (2006) Role of corticotropin releasing factor in anxiety disorders: a translational research perspective. *Hormones and Behavior* 50:550–561.

Robinson OJ, Overstreet C, Allen PS, Pine DS, Grillon C (2012) Acute Tryptophan Depletion Increases Translational Indices of Anxiety but not Fear: Serotonergic Modulation of the Bed Nucleus of the Stria Terminalis. *37:1963–1971*.

Rodaros D, Caruana DA, Amir S, Stewart J (2007) Corticotropin-releasing factor projections from limbic forebrain and paraventricular nucleus of the hypothalamus to the region of the ventral tegmental area. *NSC* 150:8–13.

- Rodríguez-Sierra OE, Turesson HK, Pare D (2013) Contrasting distribution of physiological cell types in different regions of the bed nucleus of the stria terminalis. *Journal of Neurophysiology* 110:2037–2049.
- Rouwette T, Vanelderen P, de Reus M, Loohuis NO, Giele J, van Egmond J, Scheenen W, Scheffer GJ, Roubos E, Vissers K, Kozicz T (2012) Experimental neuropathy increases limbic forebrain CRF. *Eur J Pain* 16:61–71.
- Ryan SJ, Ehrlich DE, Jasnow AM, Daftary S, Madsen TE, Rainnie DG (2012) Spike-Timing Precision and Neuronal Synchrony Are Enhanced by an Interaction between Synaptic Inhibition and Membrane Oscillations in the Amygdala Menendez de la Prida L, ed. *PLoS ONE* 7:e35320.
- Ryan SJ, Ehrlich DE, Rainnie DG (2014) Morphology and dendritic maturation of developing principal neurons in the rat basolateral amygdala. *Brain Struct Funct*.
- Ryan TJ, Roy DS, Pignatelli M, Arons A, Tonegawa S (2015) Memory. Engram cells retain memory under retrograde amnesia. *Science* 348:1007–1013.
- Sahuque LL, Kullberg EF, Mcgeehan AJ, Kinder JR, Hicks MP, Blanton MG, Janak PH, Olive MF (2006) Anxiogenic and aversive effects of corticotropin-releasing factor (CRF) in the bed nucleus of the stria terminalis in the rat: role of CRF receptor subtypes. *Psychopharmacology* 186:122–132.
- Sakanaka M, Shibasaki T, Lederis K (1986) Distribution and efferent projections of corticotropin-releasing factor-like immunoreactivity in the rat amygdaloid complex. *Brain Research* 382:213–238.
- Savasta M, Dubois A, Scatton B (1986) Autoradiographic localization of D1 dopamine receptors in the rat brain with [³H]SCH 23390. *Brain Research* 375:291–301.
- Scibilia RJ, Lachowicz JE, Kilts CD (1992) Topographic nonoverlapping distribution of D1 and D2 dopamine receptors in the amygdaloid nuclear complex of the rat brain. *Synapse* 11:146–154.
- Shaham Y, Highfield D, Delfs J, Leung S, Stewart J (2000) Clonidine blocks stress-induced reinstatement of heroin seeking in rats: an effect independent of locus coeruleus noradrenergic neurons. *Eur J Neurosci* 12:292–302.
- Shalev U, Morales M, Hope B, Yap J, Shaham Y (2001) Time-dependent changes in extinction behavior and stress-induced reinstatement of drug seeking following withdrawal from heroin in rats. *Psychopharmacology* 156:98–107.
- Shibata R, Misonou H, Campomanes CR, Anderson AE, Schrader LA, Doliveira LC, Carroll KI, Sweatt JD, Rhodes KJ, Trimmer JS (2003) A fundamental role for KChIPs in determining the molecular properties and trafficking of Kv4.2 potassium channels. *Journal of Biological Chemistry* 278:36445–36454.

- Shin J-W, Geerling JC, Loewy AD (2008) Inputs to the ventrolateral bed nucleus of the stria terminalis. *J Comp Neurol* 511:628–657.
- Silberman Y, Matthews RT, Winder DG (2013) A corticotropin releasing factor pathway for ethanol regulation of the ventral tegmental area in the bed nucleus of the stria terminalis. *J Neurosci* 33:950–960.
- Sink KS, Davis M, Walker DL (2013) CGRP antagonist infused into the bed nucleus of the stria terminalis impairs the acquisition and expression of context but not discretely cued fear. *Learn Mem* 20:730–739.
- Sink KS, Walker DL, Yang Y, Davis M (2011) Calcitonin gene-related peptide in the bed nucleus of the stria terminalis produces an anxiety-like pattern of behavior and increases neural activation in anxiety-related structures. *J Neurosci* 31:1802–1810.
- Sloan DME, Kornstein SG (2003) Gender differences in depression and response to antidepressant treatment. *Psychiatr Clin North Am* 26:581–594.
- Somerville LH, Whalen PJ, Kelley WM (2010) Human bed nucleus of the stria terminalis indexes hypervigilant threat monitoring. *Biol Psychiatry* 68:416–424.
- Soto D, Coombs ID, Kelly L, Farrant M, Cull-Candy SG (2007) Stargazin attenuates intracellular polyamine block of calcium-permeable AMPA receptors. *Nat Neurosci* 10:1260–1267.
- Staub DR, Spiga F, Lowry CA (2005) Urocortin 2 increases c-Fos expression in topographically organized subpopulations of serotonergic neurons in the rat dorsal raphe nucleus. *Brain Research* 1044:176–189.
- Stefanova N, Bozhilova-Pastirova A, Ovtsharoff W (1998) Sex and age differences of neurons expressing GABA-immunoreactivity in the rat bed nucleus of the stria terminalis. *Int J Dev Neurosci* 16:443–448.
- Steinert JR, Robinson SW, Tong H, Haustein MD, Kopp-Scheinflug C, Forsythe ID (2011) Nitric oxide is an activity-dependent regulator of target neuron intrinsic excitability. *Neuron* 71:291–305.
- Stokes PE, Holtz A (1997) Fluoxetine tenth anniversary update: the progress continues. *Clin Ther* 19:1135–1250.
- Straube T, Mentzel H-J, Miltner WHR (2007) Waiting for spiders: brain activation during anticipatory anxiety in spider phobics. *NeuroImage* 37:1427–1436.
- Sugino K, Hempel CM, Miller MN, Hattox AM, Shapiro P, Wu C, Huang ZJ, Nelson SB (2005) Molecular taxonomy of major neuronal classes in the adult mouse forebrain. *Nat Neurosci* 9:99–107.
- Sullivan GM, Apergis J, Bush DEA, Johnson LR, Hou M, Ledoux JE (2004) Lesions in

the bed nucleus of the stria terminalis disrupt corticosterone and freezing responses elicited by a contextual but not by a specific cue-conditioned fear stimulus. *Neuroscience* 128:7–14.

- Tanaka M, Yoshida M, Emoto H, Ishii H (2000) Noradrenaline systems in the hypothalamus, amygdala and locus coeruleus are involved in the provocation of anxiety: basic studies. *European Journal of Pharmacology* 405:397–406.
- Thompson CL, Drewery DL, Atkins HD, Stephenson FA, Chazot PL (2000) Immunohistochemical localization of N-methyl-D-aspartate receptor NR1, NR2A, NR2B and NR2C/D subunits in the adult mammalian cerebellum. *Neurosci Lett* 283:85–88.
- Toufexis D (2007) Region- and Sex-Specific Modulation of Anxiety Behaviours in the Rat. *Journal of Neuroendocrinology* 19:461–473.
- Tropea D, Capsoni S, Tongiorgi E, Giannotta S, Cattaneo A, Domenici L (2001) Mismatch between BDNF mRNA and protein expression in the developing visual cortex: the role of visual experience. *Eur J Neurosci* 13:709–721.
- Tukey DS, Ziff EB (2013) Ca²⁺-permeable AMPA (-Amino-3-hydroxy-5-methyl-4-isoxazolepropionic Acid) Receptors and Dopamine D1 Receptors Regulate GluA1 Trafficking in Striatal Neurons. *Journal of Biological Chemistry* 288:35297–35306.
- Tureson HK, Rodriguez-Sierra OE, Pare D (2013) Intrinsic connections in the anterior part of the bed nucleus of the stria terminalis. *Journal of Neurophysiology* 109:2438–2450.
- Uban KA, Comeau WL, Ellis LA, Galea LAM, Weinberg J (2013) Basal regulation of HPA and dopamine systems is altered differentially in males and females by prenatal alcohol exposure and chronic variable stress. *Psychoneuroendocrinology* 38:1953–1966.
- Ulrich-Lai YM, Herman JP (2009) Neural regulation of endocrine and autonomic stress responses. *Nat Rev Neurosci* 10:397–409.
- Valjent E *et al.* (2005) Regulation of a protein phosphatase cascade allows convergent dopamine and glutamate signals to activate ERK in the striatum. *Proceedings of the National Academy of Sciences* 102:491–496.
- Valjent E, Pages C, Herve D, Girault J-A, Caboche J (2004) Addictive and non-addictive drugs induce distinct and specific patterns of ERK activation in mouse brain. *Eur J Neurosci* 19:1826–1836.
- Van Bockstaele EJ, Peoples J, Valentino RJ (1999) A.E. Bennett Research Award. Anatomic basis for differential regulation of the rostralateral peri-locus coeruleus region by limbic afferents. *BPS* 46:1352–1363.

- Vandesompele J, De Preter K, Pattyn F, Poppe B, Van Roy N, De Paepe A, Speleman F: Accurate normalization of real-time quantitative RT-PCR data by geometric averaging of multiple internal control genes. *Genome Biol* 2002
- Ventura-Silva AP, Melo A, Ferreira AC, Carvalho MM, Campos FL, Sousa N, Pêgo JM (2013) Excitotoxic lesions in the central nucleus of the amygdala attenuate stress-induced anxiety behavior. *Front Behav Neurosci* 7:32.
- Vranjkovic O, Hang S, Baker DA, Mantsch JR (2012) β -adrenergic receptor mediation of stress-induced reinstatement of extinguished cocaine-induced conditioned place preference in mice: roles for β 1 and β 2 adrenergic receptors. *J Pharmacol Exp Ther* 342:541–551.
- Vyas A, Bernal S, Chattarji S (2003) Effects of chronic stress on dendritic arborization in the central and extended amygdala. *Brain Research* 965:290–294.
- Walker DL, Davis M (1997) Double dissociation between the involvement of the bed nucleus of the stria terminalis and the central nucleus of the amygdala in startle increases produced by conditioned versus unconditioned fear. *Journal of Neuroscience* 17:9375–9383.
- Walker DL, Davis M (2008) Role of the extended amygdala in short-duration versus sustained fear: a tribute to Dr. Lennart Heimer. *Brain Struct Funct* 213:29–42.
- Walker DL, Miles LA, Davis M (2009) Selective participation of the bed nucleus of the stria terminalis and CRF in sustained anxiety-like versus phasic fear-like responses. *Progress in Neuropsychopharmacology & Biological Psychiatry* 33:1291–1308.
- Walter A, Mai JK, Lanta L, Görös T (1991) Differential distribution of immunohistochemical markers in the bed nucleus of the stria terminalis in the human brain. *J Chem Neuroanat* 4:281–298.
- Wang X, Bao J, Zeng X-M, Liu Z, Mei Y-A (2005) Elevation of intracellular Ca^{2+} modulates A-currents in rat cerebellar granule neurons. *J Neurosci Res* 81:530–540.
- Watts AG, Kelly AB, Sanchez-Watts G (1995) Neuropeptides and thirst: the temporal response of corticotropin-releasing hormone and neurotensin/neuromedin N gene expression in rat limbic forebrain neurons to drinking hypertonic saline. *Behavioral Neuroscience* 109:1146–1157.
- Weller KL, Smith DA (1982) Afferent connections to the bed nucleus of the stria terminalis. *Brain Research* 232:255–270.
- Wiltgen BJ, Royle GA, Gray EE, Abdipranoto A, Thangthaeng N, Jacobs N, Saab F, Tonegawa S, Heinemann SF, O'Dell TJ, Fanselow MS, Vissel B (2010) A role for calcium-permeable AMPA receptors in synaptic plasticity and learning. *PLoS ONE* 5.

- Yang C-H, Huang C-C, Hsu K-S (2012) A critical role for protein tyrosine phosphatase nonreceptor type 5 in determining individual susceptibility to develop stress-related cognitive and morphological changes. *J Neurosci* 32:7550–7562.
- Yassa MA, Hazlett RL, Stark CEL, Hoehn-Saric R (2012) Functional MRI of the amygdala and bed nucleus of the stria terminalis during conditions of uncertainty in generalized anxiety disorder. *J Psychiatr Res* 46:1045–1052.
- Zhang Z, Ferretti V, Güntan İ, Moro A, Steinberg EA, Ye Z, Zecharia AY, Yu X, Vyssotski AL, Brickley SG, Yustos R, Pillidge ZE, Harding EC, Wisden W, Franks NP (2015) Neuronal ensembles sufficient for recovery sleep and the sedative actions of $\alpha 2$ adrenergic agonists. *Nat Neurosci* 18:553–561.
- Zimmerman JM, Maren S (2011) The bed nucleus of the stria terminalis is required for the expression of contextual but not auditory freezing in rats with basolateral amygdala lesions. *Neurobiol Learn Mem* 95:199–205.